THE
PHYSICAL REVIEW
A Journal of Experimental and Theoretical Physics Established by E. L. Nichols in 1893

VOL. 53, NO. 9 MAY 1, 1938 SECOND SERIES

The Rate of Production of Very Large Cosmic-Ray Bursts as a Function of Lead Shielding Thickness

WILLIAM P. JESSE
Ryerson Laboratory, University of Chicago, Chicago, Illinois

AND

RICHARD L. DOAN
Phillips Petroleum Company, Bartlesville, Oklahoma

(Received March 15, 1938)

Experiments have been performed at Chicago with two Compton-Bennett cosmic-ray meters to determine the frequency of occurrence of very large bursts (120 to more than 1000 particles) as a function of lead shielding thickness. The thickness of lead for optimum burst rate was found on both meters to be in the neighborhood of 3 centimeters. This is larger than the optimum for showers and small bursts, a fact which is in qualitative agreement with the theory of Carlson and Oppenheimer. Quantitatively, the maximum determined experimentally is of the same order of magnitude as that predicted by the theory though lower.

DURING the past few years many experiments have been performed on the effect of shielding upon cosmic-ray showers and small bursts. Much less work has been done where very large bursts are involved. It has, therefore, seemed worth while to report here in brief some experiments carried out at intervals during the past two years upon very large cosmic-ray bursts. These results are in general agreement with the work on showers and small bursts and are principally of interest because the bursts measured are probably as large as any which have been thus systematically studied.

The measurements were made at Chicago with two type C cosmic-ray meters of the Carnegie Institution of Washington which have been described in detail elsewhere.[1] The meters were both placed in a shop building directly under the roof in such a position that no side wall was less than fifteen feet from the instrument and the roof was at no point closer than twenty feet. The roof was a thin one of slate supported by steel girders. The ionization chamber of each instrument consisted of a spherical chamber 35 cm in diameter, the walls of which were $\frac{1}{2}$ inch (1.25 cm) steel. These chambers were filled with argon at a pressure of approximately fifty atmospheres. The lower hemisphere of the ionization chamber was at all times submerged in lead shot: the upper was covered with a succession of hemispherical caps, each of $\frac{1}{8}$ in. (0.32 cm) thickness. For any given shielding thickness, the number of bursts occurring during a given interval of time was read from the recording tape and hence the average burst rate could be computed.

The results for meter No. 4 and meter No. 6 are given in Table I. The smallest burst which

[1] A. H. Compton, E. O. Wollan and R. D. Bennett, Rev. Sci. Inst. **5**, 415 (1934).

could be definitely distinguished from a random fluctuation on the trace was arbitrarily taken as one giving a sharp displacement of 1 millimeter. This corresponds to the formation of 23×10^6 ion pairs within the chamber. Above this minimum, bursts were observed ranging in magnitude up to a few scattered ones giving over 400×10^6 ion pairs. In Table I, the number of bursts observed in each size range is indicated and below it in parenthesis the rate of occurrence in bursts per hour. The small number of bursts counted within each size range precludes any great accuracy for the distribution curve of the number of bursts with size of burst. This distribution is, however, in agreement with previous work[2, 3] on the same type meter. The total burst count and burst rate, including bursts of all sizes, are given in the last column. The burst rates for this column are plotted in Fig. 1 against the shielding thickness of lead. The statistical uncertainty, indicated by the length of the vertical lines through the points, is rather large. In addition, because of the scattered points, there is some uncertainty in the drawing of the curve for meter No. 4. Both curves are observed to have a maximum in the neighborhood of 3 cm of lead. The curve for meter No. 6, however, lies throughout somewhat above that for meter No. 4. The explanation for this is not apparent. The effect, however, has been observed before with two similar meters.[2]

TABLE I. *Summary of data.*

Thickness of Lead cm	Hours	Distribution of burst size in ion pairs produced					
		$23-45\times10^6$	$45-68\times10^6$	$68-90\times10^6$	$90-113\times10^6$	over 113×10^6	Total
Meter No. 6							
0	422	21 (0.050)	14 (0.033)	1 (0.002)	1 (0.002)	0 (0.00)	36 (0.085)
0.95	210	15 (0.071)	10 (0.048)	4 (0.019)	1 (0.005)	0 (0.00)	30 (0.143)
1.90	165	21 (0.127)	11 (0.067)	1 (0.006)	1 (0.006)	3 (0.02)	37 (0.224)
2.5	216	30 (0.139)	14 (0.065)	3 (0.014)	4 (0.018)	3 (0.014)	54 (0.25)
2.9	219	32 (0.146)	14 (0.065)	7 (0.032)	5 (0.023)	6 (0.028)	64 (0.292)
3.2	240	28 (0.117)	23 (0.096)	2 (0.008)	3 (0.012)	3 (0.012)	59 (0.246)
3.8	66	7 (0.106)	4 (0.06)	1 (0.015)	1 (0.015)	3 (0.045)	16 (0.242)
10.7	752	70 (0.093)	27 (0.036)	7 (0.009)	2 (0.003)	3 (0.004)	109 (0.145)
Meter No. 4							
0	314	3 (0.01)	2 (0.006)	4 (0.013)	1 (0.003)	0	10 (0.032)
0.95	381	14 (0.037)	9 (0.024)	4 (0.105)	3 (0.008)	4 (0.01)	34 (0.089)
1.90	364	21 (0.058)	10 (0.027)	2 (0.005)	2 (0.005)	3 (0.008)	38 (0.104)
2.9	488	60 (0.123)	28 (0.057)	12 (0.025)	4 (0.008)	5 (0.01)	109 (0.223)
3.8	504	41 (0.081)	18 (0.036)	8 (0.016)	2 (0.004)	4 (0.008)	73 (0.145)
10.7	290	18 (0.062)	13 (0.045)	3 (0.01)	3 (0.01)	3 (0.01)	40 (0.138)

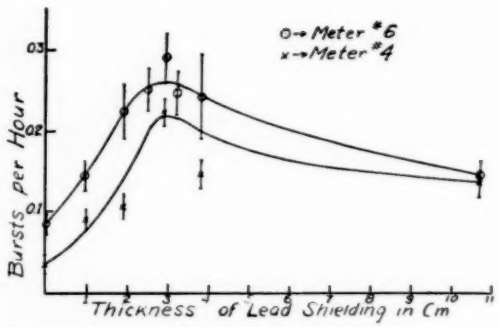

FIG. 1. Curve showing relation between burst rate and thickness of lead shielding for bursts of all sizes observed.

If the number of ions produced by a particle per centimeter path in air at atmospheric pressure is taken as 60 ion pairs per centimeter,[4] then from the geometry of the system the ionization produced by each shower particle traversing the chamber is computed to be in the neighborhood of 100,000 ion pairs. This is at best only an approximation. Hence for our minimum burst size we have about 230 particles traversing the chamber. For the largest bursts observed the number of particles is of the order of 4000.

DISCUSSION

In comparing these results with the results obtained by others, we meet with the usual difficulty that the geometry of the systems used by various experimenters is quite different. In addition to this, the fact that the wall of our

[2] R. L. Doan, Phys. Rev. **49**, 107 (1935).
[3] D. Heyworth and Ralph D. Bennett, Phys. Rev. **50**, 589 (1936).
[4] W. F. G. Swann, Phys. Rev. **44**, 961 (1933).

ionization chamber was quite thick (1.25 cm of iron) presents an added complication in the comparison. The effect of this wall thickness on the burst production observed might be twofold. First, we add an additional thickness of shielding material. This would probably amount to an equivalent thickness of only a few millimeters of lead, the exact value depending upon the form of the law[5] used to represent the relative burst frequency in iron and in lead. Second, an additional uncertainty would also be introduced by the possibility of lead-iron transition phenomena. These effects have been discussed by others[6] but the exact correction in the present experiments cannot be accurately evaluated. It might be pointed out that such phenomena may possibly be present as a disturbing factor, to a greater or less degree, in any experiments where the wall of the ionization chamber is of a different material from the shielding material. No attempt has been made to correct the data for either of these two effects.

The results of the present experiment are in good agreement with earlier[2, 3] less quantitative experiments on the type C meter. The curve in Fig. 1 is also in agreement with the results of Carmichael[7] for bursts of comparable size (160–720 particles). Nie,[8] however, for about the same range of burst sizes finds an optimum shielding thickness of between 4 and 5 centimeters of lead. Finally, the present maximum at about 3 centimeters of lead is definitely larger than the maximum below 2 centimeters found by others[9, 10] for showers of only two or three particles and of about 2 centimeters found for small bursts[11] consisting of 30 particles or less. This increase in the optimum thickness of shielding with the size of the burst has already been noted experimentally by the authors cited within the region of showers and small bursts, and is qualitatively in agreement with the multiplicative theory of showers of Carlson and Oppenheimer.[12] Because of the large uncertainties both in theory and experiment, it is impossible to make an exact quantitative comparison between the theoretical prediction and the present experimental value for the optimum lead thickness. Suffice it to say, that for a burst of 450 particles, about the mean size of the bursts observed above, a thickness in the neighborhood of 4 centimeters would be expected. This is of the same order of magnitude though larger than the present experimental result.

The authors wish to express their thanks to Professor A. H. Compton for placing at their disposal the facilities for this work and for his continued interest in it. They also wish to thank the Carnegie Institution of Washington for the use of the meters employed for the experiments.

[5] W. M. Nielsen and J. E. Morgan, Phys. Rev. **52**, 568 (1937).
[6] C. G. Montgomery, D. D. Montgomery, W. F. G. Swann, Phys. Rev. **47**, 512 (1935).
[7] H. Carmichael, Proc. Roy. Soc. **154**, 223 (1936).
[8] H. Nie, Zeits. f. Physik **99**, 453 (1936).
[9] D. K. Froman and J. C. Stearns, Phys. Rev. **52**, 382 (1937).
[10] M. A. Starr, Phys. Rev. **53**, 6 (1938).
[11] R. T. Young, Phys. Rev. **52**, 559 (1937).
[12] J. F. Carlson and J. R. Oppenheimer, Phys. Rev. **51**, 217 (1937).

A New Analysis of Cosmic Radiation Including the Hard Component*

L. W. NORDHEIM
Duke University, Durham, North Carolina

(Received February 19, 1938)

A representation of all known data on cosmic-ray intensities in their dependence on geomagnetic latitude and on altitude, respectively, depth below sea level, has been obtained on the following assumptions: 1. A soft component consisting of electrons which follow the Bethe-Heitler theory up to the highest energies with a primary distribution E^{-n} (E=energy, n between 3 and 2). 2. A hard component of different nature which in addition to normal ionization is absorbed by a discontinuous process leading also to the production of numerous secondaries with a cross section inversely proportional to E for high energies. The primary distribution in energy is about the same form as for the soft component, and also the absolute numbers of hard and soft primaries are of the same order of magnitude. This picture is furthermore well compatible with the observed secondary and transition effects, especially the Rossi transition curves for showers, and their occurrence below thick layers of heavy material and underground.

I. THE DUALISTIC NATURE OF COSMIC RADIATION

DURING the last years it has become more and more clear that there are two distinct components in the cosmic radiation, the hard and the soft one. They both have electronic charge (positive and negative) but are distinguished by their penetrating power through heavy material, for instance, lead. The soft component is absorbed in a few cm of this material and produces secondaries (showers) in profusion, whilst the hard component can pass through one meter without being reduced by more than about 50 percent. The soft component can be well accounted for by the assumption that it consists of electrons (and photons) which behave according to the theory of radiation.

It is indicated by the following facts that the hard rays cannot possibly consist of electrons of a different, higher energy range for which the theory does not hold any more:

1. The ionization-curvature measurements of Anderson and Neddermeyer[1] and others which seem to show (though it can hardly be taken as definitely proven) the existence of radiating and nonradiating particles of the same curvature.

2. The good representation of many shower phenomena by the "multiplication theory" as worked out by Carlson and Oppenheimer[2] and Bhabha and Heitler[3] which demand the validity of the theoretical formula for radiative effects to very high energies (even in lead) together with the observation that only a small fraction of all ionizing rays produce showers.[4]

3. The absence of equilibrium between the two components as found by Rossi[5] and Auger and others[6] and discussed by Heitler.[7]

4. The absorption curves at high altitudes and different latitudes, as will be discussed in Section II.

In view of this situation the question arises whether it is possible to arrive at a complete description of all the cosmic-ray phenomena by ascribing to the hard component a definite set of properties. The following attempt seems, as a whole, to give a simple picture of the majority of the observed facts without being in contradiction to any particular detail.

It should be realized, however, that such a phenomenological approach can only be of a preliminary nature until a definite theory has been found which connects the high energy phenomena with our other knowledge of the laws of physics. Until this is accomplished it is not possible to prove the uniqueness of a particular picture as at least two functions, *viz.* the primary distribution and the absorption and secondary effects in dependence of energy, can be adjusted

* A report on this paper has already been given at the Indianapolis Meeting of the American Physical Society, December 30, 1937.

[1] Anderson and Neddermeyer, Phys. Rev. **50**, 263 (1936); **51**, 884 (1937).

[2] Carlson and Oppenheimer, Phys. Rev. **51**, 220 (1937).

[3] Bhabha and Heitler, Proc. Roy. Soc. **A159**, 432 (1937).

[4] This point is made particularly clear by the extensive investigation of Starr, Phys. Rev. **53**, 6 (1938).

[5] Rossi, *La radiation cosmique* (Hermann, Paris, 1935).

[6] Auger, Ehrenfest and Leprince Ringuet, J. de phys. et rad. **7**, 58 (1936).

[7] Heitler, Proc. Roy. Soc. **A161**, 261 (1937).

to give the desired results. It is, therefore, not surprising that previous attempts have failed so far to converge, and also the present one should not be taken as more than a working hypothesis which might possibly lead to a better understanding of the connections between the observed phenomena.

In the next section we give firstly a discussion of the high altitude measurements in order to be able to separate off the contribution of the soft component.

II. Discussion of the High Altitude Data

The hypothesis of two different components in the cosmic radiation, one of which consists of electrons and photons behaving according to theory, is strongly supported by the intensity *versus* altitude data at different geomagnetic latitudes.

Figure 6 (full lines) contains the observational results as available to the author. Curves I and II have been taken from the ionization curves of Bowen, Millikan and Neher[8] (B.M.N.) at geomagnetic latitudes $\lambda = 3°$ and 38° converted to vertical incidence by the well-known Gross[9] transformation

$$V(x) = I(x) - x(dI(x)/dx), \qquad (1)$$

where x is the depth below the top of the atmosphere (in mass units), I the intensity for all-around incidence (as obtained by an ionization chamber) and $V(x)$ the corresponding vertical intensity. Curve III is the one measured by Pfotzer[10] with a counter telescope at $\lambda = 49°$. The units are those used by B.M.N.[8] Pfotzer's data have been expressed in approximately the same units by multiplying his values by a factor 2.7 which gives the correct latitude effect at a pressure of 6 to 7 m H_2O.[11]

The minimum energy for vertical incidence at a latitude λ is given by Stoermer's formula

$$E_{\min} = 18 \cos^4 \lambda \cdot 10^9 \text{ ev}. \qquad (2)$$

Hence curve I represents the effect of uncharged primary radiation and of charged primaries above about 18 billion electron volts. II includes the charged primaries down to 6.7 and III to 3.1 billion electron volts.

As the percentage of the soft component increases strongly with altitude[6] it is suggestive to compare the observations first with the results which would follow from a suitable primary electron distribution alone. Such a comparison[12] is given in Fig. 1. The full line gives the difference between the curves II and III of Fig. 6 corresponding to the energy range "C" from 3 to 6.7×10^9 ev, and the barbed line the difference between I and II, the energy range "B" from 6.7 to 18×10^9 ev. The dotted curves are calculated from a primary electronic distribution which behaves essentially like $E^{-2.8}$ (E = energy) in the range from 3 to 18×10^9 ev. The details of the calculation are given in the Appendix. The calculated values are the same as for the soft component in Table III for the corresponding energy ranges multiplied by 1.35. For the upper part of the curves the agreement is quite good and certainly within the limits of accuracy of observation and theory. The relative heights of the peaks can, of course, be adjusted by the choice of a corresponding primary distribution so that the only check on theory is given by the shape of the curves which is not very sensitive against a change of the primary distribution within the intervals. One sees that the position of the maxima is given correctly in both energy ranges and that the curves for interval "C" are steeper and narrower than for interval "B." Below about 4 m H_2O both the theoretical curves fall off much

[8] Millikan, Neher and Haynes, Phys. Rev. **50**, 992 (1936); Bowen, Millikan and Neher (B.M.N.) Phys. Rev. **52**, 80 (1937).

[9] Gross, Zeits. f. Physik **83**, 217 (1933).

[10] Pfotzer, Zeits. f. Physik **102**, 23, 41 (1936).

[11] This factor gives a latitude effect of ~10 percent at 6.7 m H_2O between $\lambda = 49°$ (Pfotzer curve) and $\lambda = 38°$ (transformed B.M.N. curve at Fort Sam Houston). It should be emphasized that the data contained in Fig. 6 cannot be considered as too accurate. The transformation (1) magnifies any error of the original measurements, especially when the second term involving a differentiation becomes larger than the first one; this is the case for all $x > 4$ m H_2O whilst for smaller x the measurements themselves are necessarily less certain. The assumption of uniform all around incidence on which (1) is based is furthermore not quite correct owing to the complicated nature of the geomagnetic effect, but it seems not to be worth while at the present stage to attempt a more elaborate discussion. Though the points of B.M.N. follow a much smoother curve than those of Pfotzer, curves I and II are not inherently better than III. The difference III–II, of course, is still less certain owing to the empirical conversion of the units.

[12] A similar comparison with nearly the same results has already been made by B.M.N. (reference 8). The argument is repeated here as our conclusions are somewhat different from theirs and in order to obtain data which are needed later.

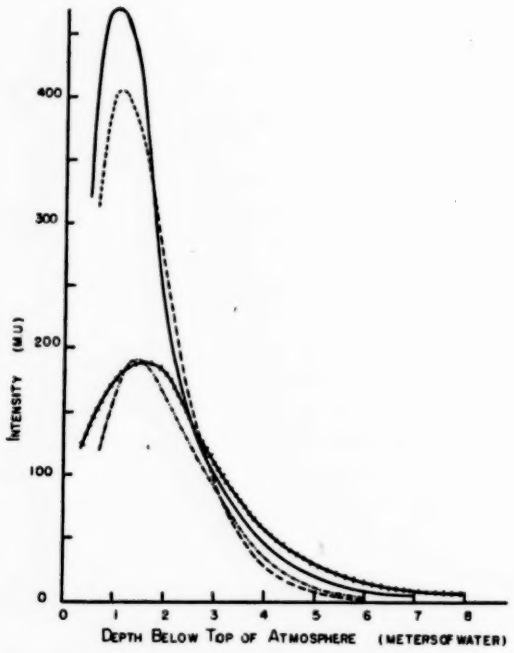

FIG. 1. Field sensitive vertical intensities (dashed, and dot-dashed curves, calculated from primary electron distribution; solid and barbed curves, observed).

more rapidly than the observed ones. According to theory there is no perceptible influence farther down than 6 m H_2O whilst a marked geomagnetic effect is known to reach down to sea level (10 m H_2O) and even somewhat below. This discrepancy cannot be removed, at least not in a simple way, by the assumption of a failure or break-down of the theory. The fit at small depths is equally good and the disagreement for larger depths is equally pronounced for both intervals so that the long tail of the empirical data cannot be ascribed to a break-down at high energies. A "stretching" of the curves along the abscissa (corresponding to a change in the constants of the formulae of radiation theory) to obtain more intensity at lower depths would make the upper regions entirely too broad and shift the maxima too far down. Fig. 1 in conjunction with the observations mentioned in Section I suggests thus strongly a practically quantitative validity of radiation theory up to at least 18×10^9 ev *plus the existence of a separate component of higher penetrating power.*

If we then adopt this interpretation we have, of course, to reduce somewhat the amount of soft radiation in the upper reaches of the atmosphere. We can further conclude that the hard component alone is responsible for the geomagnetic effect at sea level, that it also increases strongly with elevation and that it is still responsible for the greater part of the geomagnetic effect up to about 4 m H_2O.

A few remarks should be added about the third interval "A" pertaining to curve I, Fig. 6, i.e., primary energies over 18×10^9 ev and contributions from uncharged radiation (neutral particles and γ-rays). For this practically every law of absorption at low depths can be obtained by a suitable choice of the primary distribution. The observed absorption coefficient of 0.5 m^{-1} H_2O for the soft component which near sea level is nonfield-sensitive would be given by a primary electronic distribution proportional to $E^{-2.3}$ at high energies, as shown by the author, and a smooth combination of this with an initial $E^{-2.8}$ law for lower energies accounts for practically every property of the soft component.[13, 7] It should be mentioned, however, that according to this view the rest of the soft component near sea level is due to electrons of primary energies of about 10^{12} ev and over. It is quite possible, and even probable that the radiation theory which seems to hold well up to some 10^{10} ev will have to be modified in this region. For instance, the finite mass of the atomic nuclei and their recoil momenta in radiative processes would have to be taken into account. The same final absorption law might therefore be due to a more rapidly decreasing primary distribution together with smaller radiation probabilities at these extremely high energies.

III. General Properties of the Hard Component

We consider now a number of facts pertaining to the hard component, which seem to allow some significant conclusions.

1. The apparent absorption of the hard rays is nearly proportional to the mass of the traversed layers, certainly not to Z^2.

2. At sea level about 70 percent of the total radiation belongs to the hard group. The fraction caused by it may even be somewhat higher as it also produces some soft radiation (showers) by

[13] Nordheim, Phys. Rev. **51**, 1110 (1937).

secondary processes. The large majority of the more energetic rays over 10^9 ev is certainly hard (i.e., they do not radiate appreciably).

3. The energy distribution at sea level has been measured by Blackett.[14] He finds an about equal number of positives and negatives. Leaving out the particles below 5.10^8 ev the number of which is not very accurately determined and which seem to be mostly electrons, the center of gravity of Blackett's distribution lies around 3×10^9 ev with a slow tailing off at high energies. The particles with energies above 10^{10} ev form about 10 percent, the ones above 20×10^9 ev (not deflected by his magnetic field) about 5 percent of the total. According to 2, we can take these figures as representative for the hard component alone.

4. The geomagnetic effect at sea level shows that 80 to 85 percent of the total, and therefore, (when allowance is made for a field-insensitive contribution due to the soft component) that around 70 percent of the hard rays are not influenced by the magnetic field of the earth. This means, that so much of it must be due to primaries over 18×10^9 ev (or neutral radiation). On the other hand, the geomagnetic effect at sea level extends up to 50° latitude which means that primaries of 3×10^9 ev must already be able, with some probability, to penetrate through the atmosphere.

From 3 and 4 it seems necessary to conclude that also the majority of the hard rays at sea level are not the primaries themselves but of secondary nature.[15] Though the majority of the rays is due to primaries over 18×10^9 ev their average energy at sea level is of the order of 3×10^9 ev. This difference of about 15×10^9 ev cannot be due to a continuous slowing down process as this would be in contradiction to the extension of the geomagnetic effect to 50°; and it would furthermore be difficult to reconcile such a large energy loss with the great penetrating power of the hard component after having come down to sea level. The degeneration of the high primary energies must be effected by a discontinuous process, leading to very extended straggling.

Further indications for the largely secondary nature of the hard rays at sea level are given by the following observations. The east-west effect[15] shows that the majority of the field sensitive rays are due to positive primaries whilst Blackett[14] has found no significant deviation from a half-and-half division. The absorption curves of the hard component in lead interposed between counters seem to be practically the same at all latitudes and also below a thick layer of rock[16] (of about 60 m water equivalent) which means that their energy distribution must be nearly the same under these different conditions. Lastly the existence of a long range secondary radiation has directly been proved by the transition effects for showers under thick layers of heavy material (second maximum of the Rossi curve) and the transition effect air to water or rock as will be discussed in Section IV.

As a last significant fact we take the continuation of the absorption curves to depths below sea level, investigated extensively by Ehmert[17] and Wilson.[18] It is found that the intensity as a function of depth is very well given by simple power laws over very large ranges. For the first 20 m water equivalent below sea level a transition effect[19] apparently takes place. From about 20 m to 250 m (Ehmert's end point) both Ehmert's and Wilson's data follow very closely the function x^{-n} where x is the total mass of the layer above including the atmosphere and the exponent lies between 1.8 and 2 (Ehmert gives 1.87). From 250 m to about 1500 m

[14] Blackett, Proc. Roy. Soc. **A159**, 1 (1937).

[15] Also in case that part of the hard rays were due to an uncharged primary radiation they had to be classified, of course, as secondaries. There is, however, no other evidence in favor of such an assumption which would only make the picture more complicated. On the other hand, a considerable fraction of the hard radiation, larger than indicated by the geomagnetic effect at sea level alone, must be due to charged primaries, as the east-west effect persists even at the equator, and also the simple geomagnetic effect increases considerably at moderate altitudes, where the soft component should still not be appreciably field sensitive. For data on the east-west effect compare Johnson, Phys. Rev. **48**, 287 (1935).

[16] Measurements by Morgan and Nielsen, now in progress.

[17] Ehmert, Zeits. f. Physik **106**, 751 (1937).

[18] Wilson, Phys. Rev. **53**, 337 (1938). The author is greatly indebted to Professor Compton and Dr. Wilson for kind communication of their data.

[19] This transition effect could formally be made to disappear by ascribing to the atmosphere a water equivalent of about 15 m instead of the 10 m according to its mass; i.e. with this assumption the $\sim x^{-2}$ law would hold immediately from sea level on. Such an interpretation seems, however, to be unlikely as there is no significant deviation between Ehmert's measurements in water and Wilson's in rock, and it would be difficult to understand, why there should be a considerable difference between air and water, but none between water and rock.

(Wilson's end point) the exponent is somewhat higher (about 2.4) corresponding to a more rapid decrease. Some single points by Barnothy and Forró[20] fall in between the extrapolated $x^{-1.87}$ curve and Wilson's observations.

These results are the more surprising in view of the discontinuous absorption mechanism discussed above. From this one would have expected an exponential type law but the observations do not show the least resemblance to the latter as the apparent absorption coefficient

$$\kappa = -1/V(dV/dx)$$

(V = intensity) changes from 0.1 m^{-1} H_2O near sea level to about 0.003 m^{-1} at a depth of about 1000 m H_2O. Such a slow absorption and apparent hardening of the radiation can, however, result also from a discontinuous absorption mechanism, provided the absorption cross section decreases with energy. The combination of such a behavior with a suitable primary distribution tailing off slowly to high energies might, of course, produce any kind of absorption curve. When we admit, however, that the validity of simple power laws over such large ranges is more than a mere coincidence, we can limit the possibilities so far, as to give at least a model for the observed behavior without too much arbitrariness. This shall be attempted in the next section where various schemes will be discussed.

The absorption law described above constitutes a rather strong argument against a hypothesis put forward by Heisenberg[21] that the cosmic radiation is brought down to the greatest depths by neutrinos. According to his ideas, the neutrinos, generated themselves as secondaries in the atmosphere and higher strata of the surface of the earth, would be distributed over a comparatively narrow energy band, and their absorption by conversion into ionizing tertiaries should consequently follow an exponential law.

IV. The Absorption Law for the Hard Component

We try now to bring the qualitative considerations of Section III—which seem to be well founded—into a quantitative form, which necessarily will be much more uncertain.

The hard rays firstly lose energy by normal ionization, an effect which certainly must be taken into account, when treating the penetration to great depths. At a distance x from the top of the atmosphere the energy of a ray of initial energy E will be

$$E(x) = E_0 - \beta x, \tag{3}$$

where β is the specific energy loss. β can be considered as a constant since the density of ionization seems to be practically independent of energy.

We furthermore were led to assume an absorption coefficient $\kappa(E)$ dependent on energy. The chance for a primary of energy E_0 to survive down to a depth x will then be given by an attenuation factor

$$A(E_0, x) = \exp\left[-\int_0^x \kappa(E_0 - \beta z)dz\right]$$

$$= \exp\left[-\int_{E_0-\beta x}^{E_0} \kappa(E)dE/\beta\right] \tag{4}$$

and the number of rays of energy E from a primary distribution $N(E_0, 0)$ will be

$$N(E, x) = N(E+\beta x, 0)$$

$$\times \exp\left[-\int_0^x \kappa(E+\beta z)dz\right]. \tag{5}$$

The energy lost in the absorption processes will reappear through the production of secondary radiation which, as it seems, is very important. We can obtain an estimate of this effect on the basis of the following assumptions.

1. The secondaries have a shorter range than the primaries so that they can be considered to be in equilibrium with the primary beam. This appears to be well justified in our case where we have an absorption coefficient decreasing with increasing energy. (It is, however, absolutely wrong for electrons and photons.) 2. The dissipation of the primary energies is ultimately always effected by ionizing particles all of the same ionizing power β, regardless of their nature. This too seems to be very nearly correct as the fraction of heavy ionizing tracks and of actual nuclear disintegrations in the cosmic radiation seems to be quite small.

[20] Barnothy and Forró, Zeits. f. Physik **104**, 744 (1937).
[21] Heisenberg, Zeits. f. Physik **101**, 533 (1936).

With these two assumptions the number $S(E)$ of secondaries in equilibrium with a primary beam of energy E will be simply the energy lost by absorption from the primary bundle over the energy loss of a single ray by ionization, i.e.,

$$S(E)=E\kappa(E)/\beta. \tag{6}$$

This formula will hold also in case the secondaries are of different nature (hard and soft rays). It is irrelevant whether the secondaries are emitted singly or in bundles. Eq. (6) will also remain correct in case of further multiplication of the secondaries (even with nonionizing links) if only the total conversion of energy takes place in a short enough distance. Of course, it is not possible to give a more detailed discussion of transition effects between different materials without more specific statements regarding the production of secondaries.

With these assumptions the total number of rays penetrating to a depth x becomes

$$Z(x)=\int_{E=0}^{\infty} N(E+\beta x)\exp\left[-\int_0^x \kappa(E+\beta z)dz\right]\times(1+E\kappa(E)/\beta)dE. \tag{7}$$

$Z(x)$ is empirically found to be close to x^{-2} (see Section III). Such a behavior can be obtained from (7) in various ways, as there are two adjustable functions ($N(E_0)$ and $\kappa(E)$).

The following cases may be noted.

(a) If the absorption is neglected ($\kappa=0$), i.e., if only ionization is present, a primary distribution $N(E_0)dE_0\sim E^{-n}dE$ will give a $Z(x)\sim x^{-(n-1)}$.

(b) If the energy loss through ionization is neglected ($\beta=0$), a power law for the absorption coefficient $\kappa(E)=\kappa_s E^{-s}$ together with a power law $N(E_0)=E_0^{-n}$ will give asymptotically

$$Z(x)\sim x^{-(n-1)/s}.$$

(c) For the combination of the two effects a *simple* solution is possible only for

$$\kappa=\kappa_1/E, \tag{8}$$

i.e., an absorption coefficient inversely proportional to energy. This gives for the attenuation factor (4)

$$A=\exp\left[-\int_0^x \kappa_1/(E+\beta z)dz\right]=(E/(E+\beta x))^{\sigma};\qquad(\sigma=\kappa_1/\beta) \tag{4a}$$

and for $N(E_0)=CE_0^{-n}$

$$Z(x)=\frac{C}{(\beta x)^{n-1}}\frac{(\sigma+1)!(n-2)!}{(\sigma+n-1)!}. \tag{7a}$$

For $n=3$ this would be

$$Z(x)=C/(x^2\beta^2(\kappa_1/\beta+2)). \tag{7b}$$

The law (8) is practically the only one which combines the previously deduced qualitative features without being too complicated or artificial and seems, therefore, to be very suitable for a discussion of the hard component. But (8) would give rise to very large cross sections at low energies. To avoid this singularity we make the further assumption that the absorption cross section becomes constant below a certain energy β_0, i.e.

$$\kappa(E)=\begin{cases}\kappa_1/\beta_0 & \text{for } E<\beta_0,\\ \kappa_1/E & \text{for } E>\beta_0.\end{cases} \tag{8a}$$

This law should not be taken too literally. It means simply that below a certain energy β_0 the behavior of the hard rays can be represented by a sort of average absorption coefficient which might well conceal a more complicated dependence on energy while above β_0 a definite tendency to decrease with energy is present. The change in the low energy region does not influence the asymptotic behavior at large depths.

For the practical application of the above hypothesis we define an influence function $I(E_0, x)$ giving the number of rays (primaries and secondaries) at a depth x, due to primaries of initial energy E_0. Using (7) and (8a) we obtain

$$I(E_0x)=\begin{cases}N(E_0,0)((E_0-\beta x)/E_0)^{\sigma}(1+\sigma) & \text{for } \beta_0<E_0-\beta x,\\ N(E_0,0)\left(\dfrac{\beta_0}{E_0}\right)^{\sigma}\exp\left[-\sigma\left(1-\dfrac{E_0-\beta x}{\beta_0}\right)\right]\left\{1+\dfrac{\sigma(E_0-\beta x)}{\beta_0}\right\} & \text{for } E_0-\beta x<\beta_0<E_0,\\ N(E_0,0)\exp\left[-(\kappa_1/\beta_0)x\right]\{1+(\sigma(E_0-\beta x))/\beta_0\} & \text{for } \beta x<E_0<\beta_0.\end{cases} \tag{9}$$

The total intensity due to primary energies above a given E_{min} becomes

$$Z(x)=\int_{E_{min}}^{\infty} I(E, x)dE. \tag{10}$$

By proper choice of E_{min} (compare (2)) we can evaluate also the geomagnetic effect. In (9) β represents the specific energy loss through ionization, β_0 the critical energy in (8a) where the law of absorption changes, and $\sigma=\kappa_1/\beta$ the average number of secondaries in equilibrium with a high energy primary.

V. Numerical Representation of Cosmic-Ray Intensities at all Latitudes and Altitudes

With the hypotheses about the hard component discussed in the preceding section their primary distribution for medium and high energies is already determined by the absorption curve below sea level as CE^{-n} with n between[22] 2.8 and 3. We extrapolate this distribution also to low energies as the simplest possible assumption. To obtain numerical agreement with the data and units given in Section II we take

$$N(E_0, 0)=(10/E_0)^{2.8} \tag{11}$$

(E_0 in billion electron volts). The absorption curve below sea level is then taken care of automatically.[23] To adjust the two available constants in the absorption law (8a) we use the geomagnetic effect at sea level. The following values have finally been assumed

energy loss through ionization
$\beta_0=0.3\times10^9$ ev/m H_2O
critical energy at which absorption law changes $\beta_0=9\times10^9$ ev
absorption coefficient below β_0; $\kappa_0=0.5$/m H_2O (12)
absorption coefficient above β_0; $\kappa(E)=\kappa_1/E=4.5/E$ (E in 10^9 ev)
from this the average number σ of secondaries for $E>\beta_0$; $\sigma=\kappa_1/\beta=15$.

Fig. 2 shows the influence curves (9) calculated for the values (11) and (12) for the depths $x=10$ (sea level), 5 and 2 m H_2O. The insert gives the geomagnetic effect at sea level obtained by integrating the influence curve from the corresponding minimum energies (2) on. It has been made[24] to be 20 percent between the equator and the plateau reached at $\lambda=50°$. (A contribution of 2 in our units for the soft component which is independent of latitude at sea level has been added to the total.)

The calculated curve gives very well the type of the observed effect. The smallness of the effect is due to the greater penetrating power and larger ratio of secondaries to primaries of high energy, the pronounced beginning at 50° to a large number of primaries of low energy together with a comparatively high absorption coefficient. The beginning of the plateau at 50° is, of course, due to our choice of β with which just 3×10^9 ev are required for a vertical traversal of the atmosphere. The irregularity at $\lambda=30°$ (from the dip in the influence curve) comes from the break in the functional behavior (8a) of the absorption coefficient. It could be removed, of course, by rounding off (8a). As a matter of fact, such an irregularity in the geomagnetic effect seems actually to exist, though, of course, the interpretation by the change in the absorption coefficient is highly doubtful. We have given no experimental points for comparison as the geomagnetic effect has not been measured very exactly with counters (i.e., vertical incidence). Also the observations with ionization chambers (which give a somewhat smaller value) show large fluctuations due to seasonal and local influences[25] (irregularities in the earth magnetic field).

[22] According to the observations of Wilson (reference 18) the absorption exponent changes to slightly higher values below 250 m H_2O. From this follows a somewhat stronger falling off of the energy distribution at extremely high energies. It is not necessary, to take this into consideration for the discussion of the behavior of the cosmic radiation in the atmosphere, as about 60×10^9 ev are required from the ionization losses alone before a ray can penetrate to these depths.

[23] The transition effect air underground (water or rock) mentioned in Section III might be due to any of the following causes or a combination of them: (a) deviation of the primary distribution from (11) at lower energies. A change of the exponent to 2.5 below $\sim15\times10^9$ ev would be sufficient. (b) The values of the constants in (8a) in different media might be different. A change in the product $\kappa_1\beta$ (compare (7b)) by about 30 percent would be sufficient. (c) Inadequacy of the assumption of equilibrium between primaries and secondaries, i.e., the secondaries at a given depth would already be created in a higher stratum with greater primary intensity. (d) Change of counting efficiency due to the surroundings by dense material. It seems not possible, at present, to decide between these possibilities.

[24] This corresponds to the figure given by Johnson and Read, Phys. Rev. **51**, 557 (1937).

[25] Compton and Turner, Phys. Rev. **52**, 799 (1937).

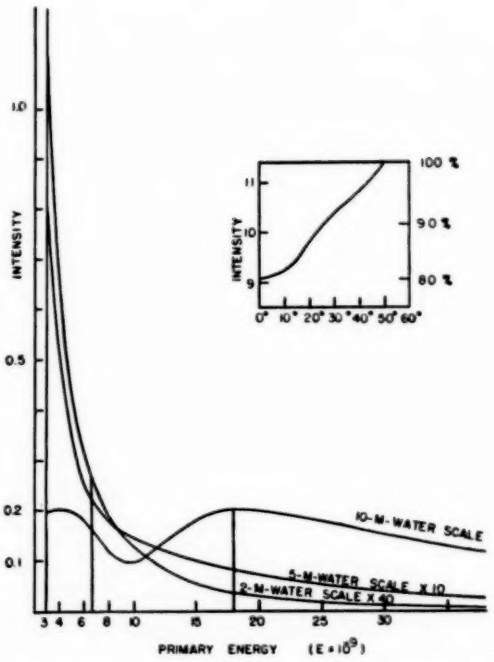

FIG. 2. Influence curves for the hard component. Insert, geomagnetic effect at sea level.

With the constants thus determined the intensity of the hard component can be calculated for all latitudes and altitudes. This has been done by drawing the influence curves (9) for various depths (some of which are shown in Fig. 2) and numerical integration. For the long drawn out high energy tail a suitable transformation has first been made. The obtained values are just of the kind required by the high altitude analysis in Section II.

For the soft component the distribution previously determined from Pfotzer's data[7, 13] were used as described in the appendix. Its form is nearly the same as for the hard component, i.e., an initial $E^{-2.8}$ law, which only falls off more slowly at high energies, the exponent being -2.3 in the region over 10^{11} ev.

The relative numbers of hard and soft primaries can be seen from the first column ($x=0$) of Table III in the appendix. They are of the same order of magnitude with the electrons slightly predominant.

The results of these calculations are shown in Figs. 3 to 6. The first three give the energy ranges "A," "B," "C" of Section II with the contribution of hard component alone, the sum of the hard and soft components as calculated (dotted lines), and the observational data (full lines). It is seen that the hard component too shows a strong increase with altitude especially in the low energy range. A synopsis of the results is given in Fig. 6. The fit is extremely good and certainly within the accuracy of theory and experiment. At very high altitudes the calculated values fall somewhat below the observed ones. An additional soft primary γ-radiation (of energy below 3×10^9 ev) of small intensity would just account for the differences shown in all three curves but as all the data, the experimental as well as the theoretical ones, are least certain in this region, its reality can hardly be taken as proven. The numbers of particles outside the atmosphere before the secondary effects set in are given in Table III. They are much smaller than at the intensity maxima, in qualitative agreement with the recent observations of Curtiss and others.[26]

The data observed in the balloon flights of B.M.N. and Pfotzer are, of course, less accurate at low altitudes as their apparatus are adapted to the high intensities farther up. They can be used only to about 6 to 7 m H_2O. From 5 to 6 m down to sea-level ionization chamber measurements have been given by B.M.N.[27] and Regener and Hoerlin.[28] From a Gross transformation of their curves (which does not give very accurate results in this region) the author finds a ratio of between 3.5 and 4 for the vertical intensities between 10 m and 6.7 m H_2O in good agreement with the calculated figures. (Compare Table III.) On the other hand, Auger and others[6] report a ratio of not more than 2 as measured by counter telescopes. The reason for this disagreement is not clear. It might be due to a change in efficiency of the counter set used. Further precision measurements both with counters and unshielded ionization chambers at small and moderate altitudes would, therefore, be very desirable.

[26] Curtiss, Astin, Stockmann, Brown and Korff, Phys. Rev. **53**, 23 (1938). The value of about 1/150 of the maximal ionization reported by these authors seems, however, to be far too low. It is to be noticed that the maximum intensity at our latitudes is, at least, twice as high as near the equator and this difference has to be accounted for by charged primaries. This would require the production of approximately 75 secondaries per primary in about 2 m H_2O which can neither be obtained from radiative multiplication nor any other known effect.

[27] Bowen, Millikan and Neher, Int. Conf. Phys. London 1934.

[28] Regener and Hoerlin, Int. Conf. Physics, London 1934; Hoerlin, Zeits. f. Physik **102**, 652 (1936).

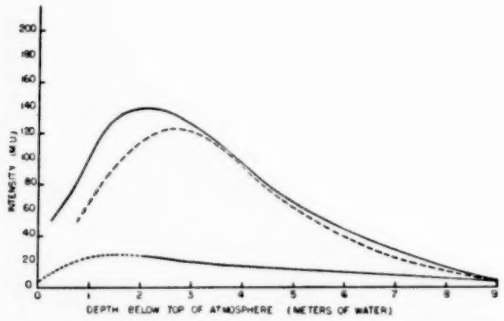

FIG. 3. Vertical intensity due to primaries over 18×10^9 ev. (Range "A.")

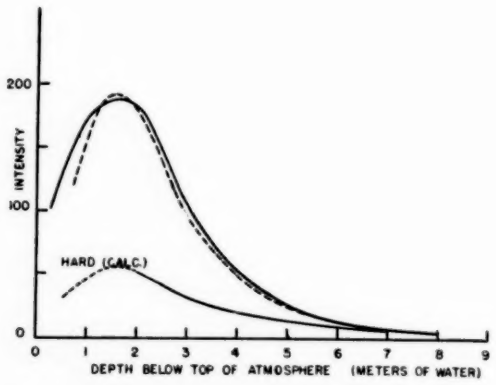

FIG. 4. Vertical intensity due to primaries between 6.7 and 18×10^9 ev. (Range "B.")

A discussion of the measurements obtained with shielded ionization chambers would be possible only with a more detailed knowledge of the secondary processes of the hard component which seem to be of quite an involved nature (see following section). The general results for a shielded chamber in comparison to an unshielded one, i.e., a much less rapid increase of ionization with altitude (due to stronger absorption of the soft component in the shield) and an at least as high latitude effect at moderate altitudes are in qualitative agreement with our picture.[29]

Our formulae give thus a very good representation of the cosmic-ray intensities at all latitudes, altitudes and depths and also of the relative influence of the hard and soft components. They allow us to retain fully the multiplication theory of showers and explain therefore the general parallelism[30] between the intensities of showers and the soft component as already pointed out by Heitler[7] and the author.[13]

Some remarks should be added on how far the assumed constants could be varied without destroying the agreement with experience. With the power law (11) for the primary distribution and the geomagnetic effect at sea level the constants are actually fixed within rather narrow limits. The comparatively high value for the absorption constant κ_1 in (8a) (and with that the high value for the average number of secondaries σ) is necessary to account for the smallness of the geomagnetic effect near sea level. The high value for β_0 has then to be taken in order to keep the absorption coefficient for primaries of low and medium energy sufficiently down to give them a chance to penetrate through the atmosphere. With this the amount of hard radiation in the atmosphere is completely determined. Only the constant β for the linear energy loss could be changed in rather wide limits. It has been found that all calculated intensities remain the same within a few percent for all values of β between 0.2 and 0.4×10^9 ev/m H_2O (the assumed value was 0.3) provided the other constants (κ_1, β_0) are kept fixed. ($\sigma=\kappa_1/\beta$ has, of course, to be changed accordingly.)

However, one has to remember that the primary distribution (11) is made necessary by the absorption curve underground only for energies[31] above 15 to 20×10^9 ev. A less pronounced increase in the number of primaries below this energy would lead to smaller values for κ_1, σ and β_0 and a somewhat smaller geomagnetic effect from the hard component at moderate altitudes. It would furthermore offer an explanation for the transition effect air-underground (compare

[29] The filtering of part of the soft component will increase the geomagnetic effect below 5 m H_2O. The absorption of the hard component in the shield will tend to decrease the geomagnetic effect. The balance of these two effects might produce an apparent insensitivity of the geomagnetic effect against thickness of shielding as reported by some observers.

[30] The showers produced by the hard component certainly play an insignificant role in the upper atmosphere. At sea level, however, we estimate that between 1/4 and 1/2 of the soft rays and showers are actually generated by the hard component (which are included in our figures for the latter). The small latitude effect for showers as reported recently by Neher and Pickering, Phys. Rev. **52**, 111 (1938) might be well due to this portion. The absence of an exact parallelism of their curve to the one for single rays (if it really exists) cannot be taken as an argument against our view as the shower production of the hard rays might well depend on energy.

[31] The maximum of the influence curve for a depth x occurs at the energy $E_{max}=\beta\kappa\sigma/n$ (n = exponent in primary distribution) and the greatest contribution comes from energies $>E_{max}$.

reference 22). These features would facilitate the representation of the observational data.[32] We have, however, refrained from introducing such modifications in order not to make too many hypotheses *ad hoc*.

VI. The Secondary Effects of the Hard Component

We have, so far, not attempted any detailed description of the absorption mechanism of the hard rays. From our general discussion we deduced a number $\sigma=15$ of secondaries[33] in equilibrium with energetic hard primaries, and it remains to be seen whether such a high value is compatible with our other knowledge. It allows firstly a natural explanation of Blackett's energy spectrum.[14] Practically all the rays below 10 to 15×10^9 ev will be secondaries according to our view and the ratio of rays below and above this is of the order 10 to 1. The greater part of the total intensities at sea level and underground is then carried down by the rays of high energy which are accompanied by a secondary spectrum which does not depend much on the primary energies and is therefore nearly the same everywhere. The low value of the ionization near the top of the atmosphere is also an indication for a high number of secondaries, though only of a qualitative nature.

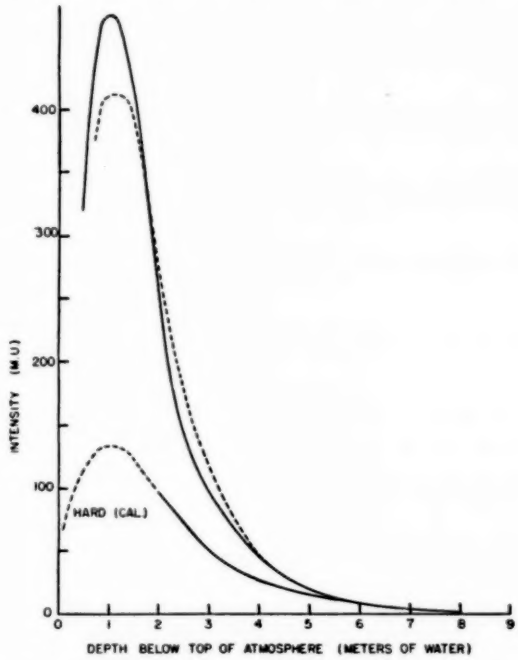

FIG. 5. Vertical intensity due to primaries between 3 and 6.7×10^9 ev. (Range "C.")

As for the chance of a direct observation of the secondary processes we note first that our maximum absorption coefficient (holding for the majority of observable rays) is of the order of 0.5 m^{-1} H_2O. This means that such an event should happen in the average after traversing a layer of about 200 g/cm^2, i.e., for instance, about 20 cm of lead. These processes will be in most cases indistinguishable from electronic processes (forks or showers) and the above figure seems to be low enough to account for the small ratio of showers to single rays observed in cloud chambers.

The hard rays have to be responsible also for the showers observed below thick layers of heavy material, i.e. the tail end of the Rossi curves, and for showers underground. These showers seem to be in general also of electronic nature as shown by

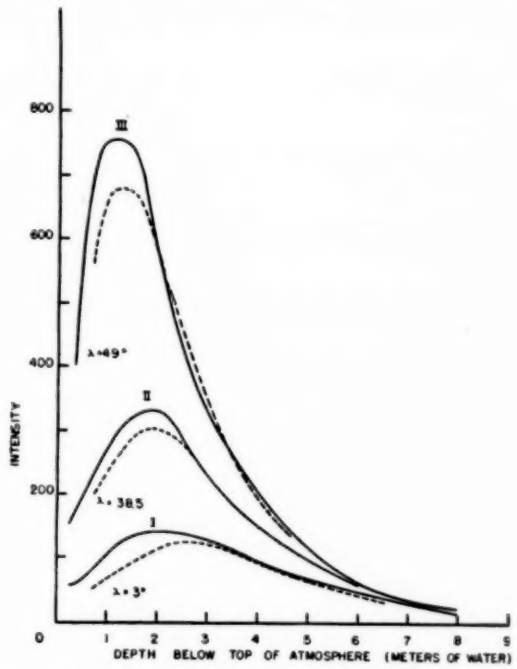

FIG. 6. Vertical intensity in the atmosphere at different latitudes; full lines observed, dotted lines calculated.

[32] B.M.N. (Abstract, Phys. Rev. **53**, 329, (1938)) have reported that their newly measured absorption curves at $\lambda=50°$ and 60° show only a very small difference even at high altitudes. This would indicate definitely a limitation of the primary distribution at lower energies.

[33] This figure has to be taken as entirely provisional. It could well be lowered for the following reasons. (a) change in the primary distribution as discussed at the end of last section. (b) not all absorbed energy goes into production of normally ionizing rays. (c) the average linear energy loss is higher than assumed.

the transition effects between different materials.[34] To explain this it is only necessary to assume that in some of the absorption processes at least one electron or photon can be produced which automatically will appear as a shower if it is energetic enough. Since the number of soft particles in equilibrium with the hard component (as found at some meters underground when the rest of the effect of soft primaries has apparently already been filtered out) seems to be of the order 10 to 20 percent, about the same fraction[35] of the absorbed energy should go into production of soft radiation following from the argument in Section IV.

This picture of a composite effect of a hard secondary radiation of average range of about 200 g/cm² and a soft one corresponding to electronic nature, finds considerable support in the recent experiments of Bothe and Schmeiser.[36] They find the "second maximum" of the Rossi transition curve to come out much more markedly[37] for showers of small angular divergence so that its existence is now beyond doubt. Such a maximum can only be due to a transition effect of rays of corresponding range which agrees remarkably well with our absorption coefficient for the less energetic hard rays. On the other hand, the final shower rays, also emerging from the region of this second maximum are highly absorbable, i.e., they are of "soft" nature.

The absorption mechanism of the hard component is, thus, certainly of a rather complex nature. It seems to be premature to attempt a detailed analysis of these secondary effects. We therefore leave it open whether the absorption mechanism consists in the emission of single rays, bundles or even explosion phenomena, whether the emission of hard and soft radiation occurs in the same or different events, and whether the nuclear disintegration processes sometimes observed in the cloud chamber are representative of its nature or belong to a different category.

The chief point of the foregoing considerations was to show the compatibility of our analysis with the observed effects and it seems even that it offers an explanation of many of them in a very natural way.

VII. Conclusions

The picture at which we finally arrive might be summarized as follows: There are two different components, electrons (always accompanied by photons) which behave according to the theory of radiation, and hard rays. The latter are absorbed by a discontinuous mechanism in which both hard rays and soft ones are emitted. Their absorption coefficient is more or less constant up to energies of some billion electron volts and decreases thereafter with energy. The primary distributions of both kinds are very similar[38] and nearly a power law E^{-n} with n between 2 and 3. Also the absolute numbers of hard and soft primaries are nearly the same. As a matter of fact, with only slight deviations from the assumed simple form of the absorption laws or with small changes in the observed intensity curves, even an exact coincidence between the

[34] Morgan and Nielsen, Phys. Rev. **52**, 564 (1937) have shown that the effects of thin plates of Pb under thick plates of Fe and *vice versa* conform very well to the predictions of Carlson and Oppenheimer (reference 2). The absence of the first Rossi maximum for showers underground or below thick layers of light material (concrete, ice) is simply an effect of geometry. The multiplication distance in these materials (40 cm in H_2O) is still small enough so that all soft radiation (electrons and photons) will already appear in bundles in contrast to air with a free path of several hundred meters. This difference, therefore, constitutes an argument for and not against the multiplication theory of showers.

[35] According to Ehmert and Wilson (references 17 and 18) the proportion of showers to single rays increases somewhat when going to very great depths. This might be due to a dependence of shower production on energy as the average energy of the rays will increase with depth.

[36] Bothe and Schmeiser, Naturwiss. **25**, 669, 834 (1937). For the proof of existence of a hard secondary radiation compare also Maass, Ann. d. Physik **27**, 507 (1936).

[37] That this second maximum is, in general, so little pronounced must be caused by the fact that the absorption coefficient is apparently very nearly proportional to the mass of the material so that the distribution of the hard rays does not change very much when going to another medium.

[38] This similarity of the two distributions is somewhat surprising as they have been derived from quite different arguments, for the electrons from the high altitude data (shape of the absorption curve and geomagnetic effect) and for the hard component from the absorption measurements underground. The two distributions might even be exactly the same within the limits of error of our determination. This likeness is suggestive perhaps of a common origin. It also seems rather certain that the distribution must fall off rather slowly with energy, i.e. not exponentially but with a power law. E^{-3} would still be possible according to our analysis though we obtain a somewhat better fit with $E^{-2.8}$. As from ordinary processes one would expect rather a Maxwellian kind of distribution, a power law might point to a cosmological origin.

two primary distributions might be effected.[39]

The given figures and tables show that it is possible to obtain on these lines a more or less quantitative description of the intensities of both components at all depths, altitudes and latitudes, and at least a qualitative understanding of the Rossi transition curves.

In judging the success of this attempt, it should be borne in mind that throughout the simplest possible assumptions have been made, and complications such as irregularities in the primary distributions and in the behavior of the absorption coefficient have been avoided. Though the qualitative features seem in most cases to be well founded, the numerical details will in course of time certainly need considerable readjustment, and it might well be that some of the facts which we accepted as fundamental will turn out to be a premature generalization.

With all due reserve as to the final meaning of our speculations a few general remarks might be added. This analysis does not say anything about the nature of the hard particles. We only have to conclude that their mass must be large compared to the mass of an electron as otherwise they would radiate strongly[40] and the energy loss through radiation would increase with energy, in contrast to the behavior of our absorption coefficient. A mass of about a hundred times the electronic mass, as suggested by some recent observations,[41] would be amply sufficient while a protonic nature seems only to be excluded by the ionization curvature measurements of Anderson,[1] Street and Stevenson,[42] and the failure to find slow protons in sufficient amount in the cosmic radiation.[43]

In view of the experimental uncertainty about the hard component two other possible interpretations should be mentioned. It is also compatible with our present knowledge that the primaries belonging to the hard rays are of a different nature than the secondary rays observed near sea level. To be more specific they might be protons to which the absorption coefficient κ_1/E might belong. They, in turn, would generate a new particle to which belongs our average absorption coefficient at lower energies. Or else the hard rays might be created by electrons of high energy in addition to ordinary radiative processes in which case most of them would come from the upper region of the atmosphere where the electronic intensity is highest.[44] From the point of simplicity, however, it seemed to be desirable, to discuss the hard rays as they appear, i.e., as a definite separate primary group.

Appendix: Numerical Data

The calculation of the contribution of the soft component has been carried out in the same way as by Heitler.[7] The total number of electrons (negatives and positives) with an energy larger than E, due to a primary electron of energy E_0 after traversing a layer of thickness l, can be represented by a function $Z(l, y)$, where $y=\log E_0/E$, tabulated in Table I.

Some new values have been added to those given by Heitler, part of which have been calculated, the others having been obtained by logarithmic interpolation. For the atmosphere the unit for l is 280 m standard air = 0.35 m water equivalent. The final energy E has to be chosen so that there is no appreciable multiplication below it, i.e., for air $E=0.15\times10^9$ ev.

Our adopted primary distribution for the soft component is listed in Table II, also in a logarithmic energy scale. The total number of rays at depth l, coming from a certain

[39] The number of primaries (column $x=0$ in Table III) is not very exactly determined by our procedure and might easily be in error by a factor of order 2. In using the Bhabha-Heitler influence function $Z(l, y)$ (compare Table I) the low energy electrons with $E<0.15\times10^9$ ev have been neglected. As the distribution in energy of the soft rays does not change much with altitude (with the exception of the very highest layers) the inclusion of these rays of low energy will approximately give a constant factor to the soft total and the number of primaries should be reduced accordingly. The number of hard rays, on the other hand, depends essentially on the average number of secondaries σ which is also rather uncertain (comp. footnote 33) and a lower value of σ would require a higher number of primaries. Both these effects would work in the direction of equalizing the two primary distributions.

[40] Though the energy loss through radiation cannot contribute much to the absorption coefficient it might possibly be responsible for some of the shower production.

[41] Street and Stevenson, Phys. Rev. **52**, 1003 (1937); Nishima, Takeuchi and Ichimiya, Phys. Rev. **52**, 1198 (1937).

[42] Street and Stevenson, Phys. Rev. **51**, 1005 (1937) (A).

[43] Montgomery, Montgomery, Ramsay and Swann, Phys. Rev. **50**, 403 (1936).

[44] This point of view has recently been strongly advocated by B.M.N., Phys. Rev. **53**, 217 (1938). The arguments used by these authors are, however, very similar to some in this paper and entirely compatible with our analysis. This shows again the impossibility to prove the uniqueness of a phenomenological picture as long as the physical laws regarding the hard component are unknown (note added after completion of the manuscript).

TABLE I. *Influence function for electrons $Z(l, y)$.*

l \ y	3	3.5	4	4.5	5	6	7	8	9	10	11	12	13
2	2.1	2.6	3.4	4.4	5.8	10	17	21	26	31	33	34	
3	2.7	3.6	5.0	6.9	8.9	15	26	43	63	76	89	96	
4	2.4	3.6	5.4	7.9	12	22	38	59	84	140	190	250	
5	2.2	3.2	4.9	7.4	13	25	51	98	160	250	360	550	
6	1.3	2.2	4.0	7.2	13	27	66	120	220	370	620	1000	
7	0.9	1.7	3.2	6.2	12	32	68	140	300	540	830	1400	
8.5	0.43	1.0	2.2	4.7	9.3	29	73	170	400	830	1600	2800	
10	0.22	0.63	1.5	3.5	6.6	24	76	200	500	1150	2200	4100	
11.5	0.1	0.28	0.78	1.9	4.1	18	61	180	540	1250	3000	6000	
13	0.05	0.15	0.40	1.0	2.6	12	46	160	480	1300	3500	8300	
15	0.02	0.06	0.17	0.49	1.2	6.4	27	100	360	1150	3200	9300	
17	0.008	0.02	0.07	0.20	0.53	3.1	17	71	260	910	2800	7800	
19	0.003	0.008	0.03	0.08	0.21	1.5	8.7	40	170	650	2100	6000	17000
22		0.002	0.006	0.019	0.056	0.45	3.0	16	73	310	1050	3000	8100
25			0.001	0.004	0.015	0.14	0.95	5.6	30	140	500	1600	4900
29					0.002	0.023	0.21	1.5	8.5	42	180	700	2300

TABLE II. *Primary electronic distribution $F(y)dy = F(E_0)dE_0/E_0$.*

y	3	3.5	4	4.5	5	6	7	8	9	10	11	12	13
E_0 in 10^9 ev	3	5	8.2	13.5	22	60	165	450	1200	3300	9000	2.5×10^4	6.7×10^4
$F(y)$	250	89	33	12.8	5.0	0.87	0.22	0.062	17×10^{-3}	4.7×10^{-3}	1.3×10^{-3}	3.6×10^{-4}	1×10^{-5}

TABLE III. *Cosmic-ray intensities for the different latitude intervals at various depths.*

DEPTH BELOW TOP OF ATMOSPHERE IN m H_2O		0	2	3.3	5	6.7	10
Interval A ($\lambda=0°$)	soft	2.2	90	97	49	18	2
$E_0>18$ 10^9 ev	hard	1.9	22.5	18	14	11	7.1
	total	4.1	112.5	115	63	29	9.1
Interval B	soft	24	125	62	10	0.5	—
$6.7>E_0>18$ 10^9 ev	hard	9.5	53	29	13	7	1.6
	total	33.5	178	91	23	7.5	1.6
Interval C	soft	96	93	48	5	0.3	—
$3>E_0>6.7$ 10^9 ev	hard	37	95	42	16	6.4	0.7
	total	133	188	90	21	6.7	0.7
Intensity at $\lambda=49°$	soft	122.2	308	207	64	18.8	2
	hard	48.4	170.5	89	43	24.4	9.4
	total	170.6	478.5	296	107	43.2	11.4

interval of primary energies, is then

$$N(l)=\int_{y_1}^{y_2}F(y)Z(l, y)dy. \tag{13}$$

To the limits of our intervals A, B, C correspond the values

A: $E=18\times10^9$ ev corresponding to $y=4.75$,
B: $E=6.7\times10^9$ ev corresponding to $y=3.75$,
C: $E=3\times10^9$ ev corresponding to $y=3$.

The integrals (13) have been evaluated graphically. Table III shows some of our final results from which the Figs. 3 to 6 have been drawn. It gives the calculated intensities for the soft and hard component separately for the three intervals at various depths below the atmosphere. The values for $x=0$ give, of course, the number of primaries. A small fraction (perhaps 15 percent) of the figures for the hard group will actually be soft rays, though produced by hard primaries and in equilibrium with them. For instance, 1.4 of the 9.4 for the "hard" component at sea level ($x=10$) might be electrons, which brings the percentage of highly absorbable rays up to about 30 percent as observed. At 6.7 m H_2O corresponding to an elevation of 3500 m, perhaps 3.5 of the hard intensity of 24.4 might be soft and the percentage of the soft rays is then about 50 percent as it should be. The increase of the total intensity between sea level and 3500 m is from 11.4 to 43.2 that is 1 to 3.8 in agreement with the values deduced from ionization chamber measurements. Thus our formulae give also the correct behavior for the intensities of the hard and soft component in the range between sea level and 3500 m altitude, which is not covered by the data summarized in Figs. 3–6.

Fast Neutrons

M. L. Pool
Mendenhall Laboratory of Physics, Ohio State University, Columbus, Ohio
(Received February 28, 1938)

The distribution of fast neutrons about the Li+D source has been investigated by means of radioactivity induced in silver (24.5 min.) and aluminum (14.8 hr.). The observations are roughly in agreement with a distribution calculated from statistical considerations. The maximum neutron energy is 20.8 Mev. An increase in the deuteron energy results in an increase in the neutron energy as measured by the $n-3n$ reaction of scandium and the $n-2n$ reactions of silver and copper. The intermediate nucleus, Be^9, formed by the deuteron bombardment of lithium must have a life short compared to 10^{-12} sec. A number of materials when bombarded with high energy detuerons yield neutrons of sufficient energy to produce the $n-2n$ reaction in silver. Only the neutrons from lithium can produce the $n-3n$ reaction in scandium. Neutrons of somewhat less energy are required for the $n-2n$ copper reaction and of appreciably less for the $n-2n$ silver reaction. When scandium is bombarded with fast neutrons, reactions of the type $n-3n$, $n-2n$, $n-\alpha$, $n-p$ and $n-\gamma$ take place in the following percentages, 24.0, 27.8, 20.6, <0.5, and 27.0, respectively.

Introduction

THE fast neutrons from the Li+D reaction have been used largely to discover new induced radioactive periods in the various elements. This use has been very successful and is of special interest because these neutrons are very proficient in the production of the $n-2n$ type of disintegration.[1, 2]

In this paper, however, known radioactive periods are used to indicate the distribution of these high energy neutrons about the lithium source, the dependence, if any, of the neutron energies on the bombarding deuteron energy and finally the potentialities of other fast neutron sources. Branching ratios for the disintegration products from scandium are also presented.

Fast Neutron Yield

The metallic lithium to be bombarded with deuterons was securely fastened upon a water cooled copper plate. Directly behind the copper plate was placed weighed samples of Cu, Sc, Ag, Al and Dy. These samples were all irradiated at the same time with neutrons obtained from bombarding the lithium with 5.7 Mev deuterons produced by the cyclotron at the University of Michigan. Other sets of samples were given similar treatments but with deuterons of lower energies. Aluminum foils were used to decrease the energy of the deuterons.

The intensities of radioactivity induced in four sets of samples are shown in Fig. 1. All the curves were arbitrarily put through the point 4 on the intensity scale. The rise in intensity of the dysprosium activity (strong 2.5-hr. slow neutron period) with increase of deuteron energy probably indicates the rise in the slow neutron background which, in turn, is a measure of the increase in the total number of Li+D disintegrations taking place. The rise in intensity in excess of the dysprosium rise would indicate the influence of the increased number of faster neutrons.

From the curves it is inferred that faster neutrons are required to produce the 10 min. period in copper than the 24.5 min. period in silver. Both periods are the result of an $n-2n$ type of reaction. The energy of neutrons required to produce the 4.0 hr. period in scandium, an $n-3n$ type of reaction,[3] is probably a little more than that required to produce the 10 min. copper period. Sagane reports that neutrons of more than 12 Mev are required to produce the 10 min. copper activity.[4] The 12.8-hr. copper activity which is produced by both fast and slow neutrons is shown and was measured from the same copper samples that gave the 10 min. period. The $n-\alpha$ type of reaction responsible for the 14.8-hr. period in aluminum apparently takes place as readily with neutrons of quite low energy as with those of much higher energy.

[1] M. L. Pool, J. M. Cork and R. L. Thornton, Phys. Rev. **52**, 239 (1937).
[2] F. A. Heyn, Physica **4**, 160 (1937).
[3] M. L. Pool, J. M. Cork and R. L. Thornton, Phys. Rev. **52**, 41 (1937).
[4] R. Sagane, Phys. Rev. **53**, 212 (1938).

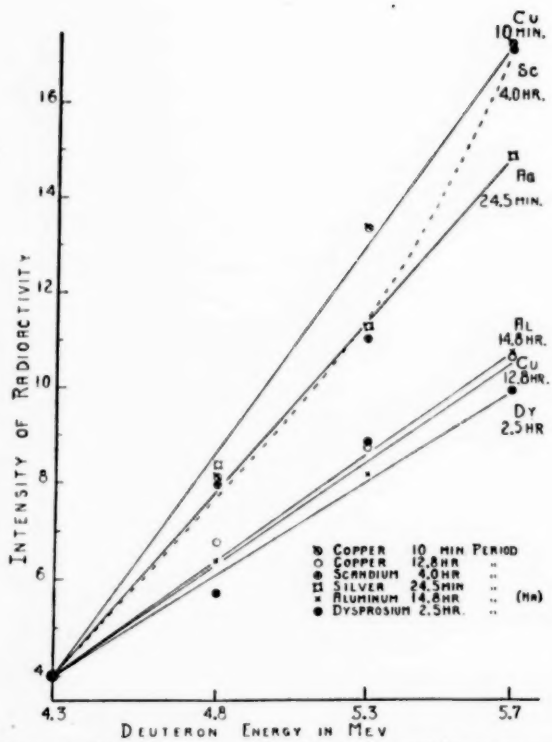

FIG. 1. Intensity of radioactivity induced by neutrons from the Li+D reaction *versus* energy of bombarding deuterons.

The extra energy acquired by the neutrons must be derived from the kinetic energy of the impinging deuterons. For this to happen it is necessary that the intermediate nucleus Be^9 at the time of its disintegration be in motion through the lithium metal. A 5.7 Mev deuteron gives a velocity of about 5×10^7 cm/sec. to Be^9. To bring this nucleus to rest in the metal a time of 10^{-11} to 10^{-12} sec. is required according to a simple calculation based upon estimated range-energy relations.[5] The life of Be^9 must therefore be short compared to 10^{-12} sec.

DISTRIBUTION OF FAST NEUTRONS

Strips of silver and aluminum 1 by 13 cm were bent in an arc of about 2.9 cm radius. The centers of the circular strips coincided with the region of the metallic lithium most strongly bombarded by deuterons of about 6 Mev. If the neutrons ejected from the lithium source had spherical symmetry in energy and number, then the radioactivity induced in each centimeter length of the 13 cm strips would be of the same intensity. The intensities however were found not to be the same. The asymmetry is shown by a polar plot in Fig. 2.

As may be seen the induced radioactivity in the direction of motion of the deuterons is definitely greater than in the direction at right angles and suggests therefore a marked forward throw of the neutrons resulting from the transmutation of the lithium. The 24.5-min. period of silver (Ag^{106}) and the 14.8-hr. period of aluminum (Na^{24}) are known to be produced by only fast neutrons and are not induced by slow neutrons or stray deuterons. Since the asymmetry of the silver radioactivity is greater than that of the aluminum it is concluded that the fast neutrons responsible for the production of the silver activity have a greater asymmetrical distribution than those responsible for the aluminum activity.

Inquiry may be made concerning what energy distribution might be expected of the transmutation products when the intermediate nucleus transforms according to

$$Li^7+D^2\rightarrow Be^9\rightarrow Be^8+n. \qquad (1)$$

Stephens using a 0.91 Mev deuteron beam obtained neutrons coming off at 90° which produced alpha-particle recoils in a helium filled cloud chamber.[6] His results are shown in Fig. 3 and may be interpreted as consistent with the above reaction. For a 6 Mev deuteron beam the

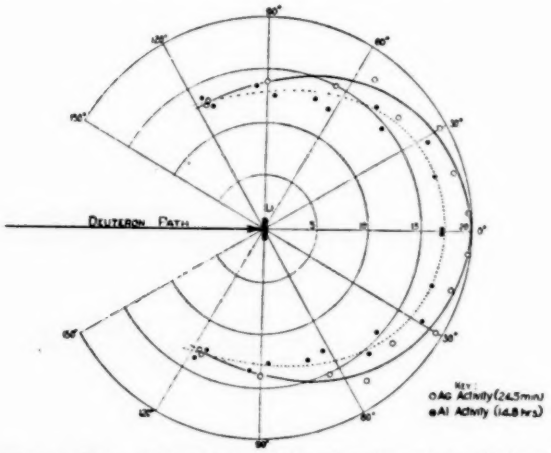

FIG. 2. Polar plot of intensities of radioactivity induced in samples of silver (Ag^{106}, 24.5 min.) and aluminum (Na^{24}, 14.8 hr.) placed symmetrically about the Li+D source of fast neutrons.

[5] F. Kirchner, H. Neuert and O. Laaff, Ann. d. Physik **30**, 527 (1937).

[6] W. E. Stephens, Phys. Rev. **53**, 223 (1938).

neutrons are calculated to be ejected in about equal numbers at right angles and in the forward direction with energies of 17.3 and 20.8 Mev respectively. Since fast neutrons over a wide range of energies seem about equally efficient in producing the $n-\alpha$ reaction in aluminum, the above-mentioned two groups of neutrons should induce in the aluminum approximately equal radioactivity, and give, therefore, a symmetrical intensity distribution. However, asymmetry is observed. This suggests that reaction (1) does not play the dominant role in this experiment.

The asymmetry is easily accounted for provided the transmutation takes place according to

$$\mathrm{Li}^7+\mathrm{D}^2\rightarrow\mathrm{Be}^9\rightarrow\mathrm{He}^4+\mathrm{He}^4+n^1. \qquad (2)$$

For this type of reaction a statistical treatment of the neutron energy distribution may be made by assuming for the two alpha-particles and neutron, equal elements in phase space are equally probable. The treatment of this three-body problem is similar to that given by Fokker, Kloosterman and Belinfante on the energy distribution between the products of the transmutation of boron atoms into three alpha-particles.[7] In our problem it is of particular interest to calculate the number of neutrons, having energies between E and $E+dE$, that are ejected parallel $N_{0°}$ and at right angles $N_{90°}$ to the 6 Mev deuteron beam.

The results are expressed in the following equations where E is the energy of the neutron in Mev:

$$N_{0°}=(17.3+0.77E^{\frac{1}{2}}-E)(E)^{\frac{1}{2}},$$
$$N_{90°}=(17.3-E)(E)^{\frac{1}{2}}.$$

These equations are plotted in Fig. 3. The maximum energy expected for the forward neutrons is 20.8 Mev. The neutron distribution curve for zero energy deuteron bombardment is also shown and may be compared with the distribution observed by Bonner and Brubaker by means of proton recoils in a cloud chamber placed at right angles to an 0.85 Mev deuteron beam.[8] They observed that about 95 percent of the reactions were of type (2). The agreement between theory and experiment and between the experiments themselves is not good but some of

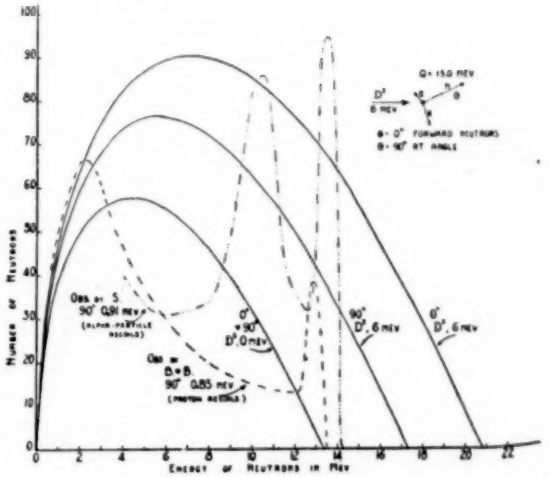

FIG. 3. Calculated energy distribution of neutrons in the directions parallel and at right angles to the impinging deuteron beam. Observations of Bonner and Brubaker (B and B) and Stephens (S) are also shown.

the discrepancy may be attributed to the uncertain cross section for high energy neutron interactions. It may be necessary also to introduce into the theoretical treatment, factors other than those of pure chance as has already been suggested by Cockcroft and Lewis[9] in connection with the break up of B^{10}.

The ratio of the calculated total number of forward neutrons to the total number of right angle neutrons is 1.8. The observed ratios of the intensity of the radioactivity in silver and aluminum in these two directions are 1.43 and 1.35, respectively. The observed asymmetry in the intensity of the radioactivity is therefore easily accounted for on the hypothesis of type (2) reaction.

Other Fast Neutron Sources

A number of materials were bombarded with 6.3 Mev deuterons and the intensities of the fast neutron induced radioactive periods in Ag, Cu, Al and Sc were measured. Table I summarizes the results.

As is seen the Li+D reaction furnishes the best source of fast neutrons. Again the $n-3n$ reaction in scandium appears to require more energetic neutrons than does the $n-2n$ reaction in copper. The $n-2n$ reaction in silver is next in

[7] A. D. Fokker, H. D. Kloosterman and F. J. Belinfante, Physica **1**, 705 (1934).

[8] T. W. Bonner and W. M. Brubaker, Phys. Rev. **48**, 742 (1935).

[9] J. D. Cockcroft and W. B. Lewis, Proc. Roy. Soc. **154**, 254 (1936).

TABLE I. *Intensities of radioactivities induced by neutrons from various sources.*

NEUTRONS FROM	24.5 MIN. Ag $n-2n$	10 MIN. Cu $n-2n$	5 MIN. Cu $n-y$	14.8 HR. Al $n-\alpha$	4 HR. Sc $n-3n$
Li+D	100	100	—	57.5	100
B+D	11.5	12	66	100	—
CaF_2+D	3.15	—	71	59.5	—
Ag+D	2.15	—	20	38	—
Fe+D	1.9	—	12	44	—
Al+D	1.75	—	22	73	—
Be+D	—	—	100	57.5	—

order and the $n-\alpha$ reaction in aluminum requires the least energy.

The maximum energy of the neutrons in the forward direction from the Be+D reaction is calculated to be about 10 Mev. Since the $n-2n$ reaction in silver does not take place with these neutrons, it is inferred that more than 10 Mev neutrons are required to remove two neutrons from silver. There must, however, be neutrons with energies greater than this value released from Al, Fe, Ag, CaF_2 and B when they are bombarded by 6.3 Mev deuterons. It is interesting to note that neutrons from the B+D reaction seem very efficient in producing the $n-\alpha$ reaction in aluminum.

It is also interesting that deuteron bombardment of aluminum produces neutrons which are energetic enough to then produce quite strongly the $n-\alpha$ reaction in aluminum. This tandem reaction probably accounts for at least some of the long radioactive periods observed in aluminum when given extensive bombardment with high energy deuterons.[10] Likewise, neutrons from the Ag+D reaction are capable of producing, although weakly, the $n-2n$ type of reaction in silver.

BRANCHING RATIOS

Since an appreciable quantity of scandium was used in the above experiments, six samples that showed strong radioactivity were chosen to be observed over a period of a few months for the purpose of calculating the branching ratios or relative rates of formation of the disintegration products. Two of the samples were followed in their chemical separations (K, Ca, Sc). The samples had been irradiated from one to four hours with neutrons from a lithium target bombarded with about 6.0 μA of 6.3 Mev deuterons.

[10] M. L. Pool and J. M. Cork, Phys. Rev. **51**, 383 (1937).

TABLE II. *Percent of various radioactive nuclei formed in the transmutation of* Sc^{45} and V^{51} *when bombarded by high energy neutrons.*

NUCLEUS BOMBARDED	TYPE OF REACTION	NUCLEUS FORMED	RADIOACTIVE PERIOD	% OF SUCH NUCLEI FORMED
$_{21}Sc^{45}$	$n-3n$	Sc^{43}	4.0 hr.	24.0
	$n-2n$	Sc^{44}	52 hr.	27.8
	$n-\alpha$	K^{42}	12.4 hr.	20.6
	$n-p$	Ca^{45}	2.4 hr.	< 0.5
	$n-y$	Sc^{46}	85 da.	27.0
$_{23}V^{51}$	$n-3n$	V^{49}	33 min.	0
	$n-2n$	V^{50}	3.7 hr.	3
	$n-\alpha$	Sc^{48}	41 hr.	32
	$n-p$	Ti^{51}	2.8 min.	65

Table II shows a summary of the results and expresses in the last column the relative rates of formation of the various radioactive transmutation products as the percent of such nuclei formed. It is noticed that scandium is transmuted most of the time according to the $n-2n$ type of reaction. The $n-p$ reaction is very weak which is consistent with the findings of Walke.[11] However, his observations that the number of $n-3n$ reactions is nearly twice that of the $n-2n$ reactions is not confirmed. As observed from the six samples in this research the ratio of the number of the former reactions to the latter is more nearly 6/7.

It was thought that possibly the branching ratios for the neighboring odd nucleus $_{23}V^{51}$ would be similar to those for $_{21}Sc^{45}$. Tentative values were obtained and are shown also in Table II. As may be seen, no similarity is apparent.

ACKNOWLEDGMENTS

The author is very grateful to Professor J. M. Cork and Dr. R. L. Thornton of the University of Michigan for the opportunity of working in their laboratory with the cyclotron. Professor B. S. Hopkins of the department of chemistry at the University of Illinois kindly loaned the author a quantity of his dysprosium that is of high purity. Professor Quill of the department of chemistry at Ohio State University supplied the large quantity of scandium used. Professor L. H. Thomas suggested using the statistical treatment for the energy distribution of the neutrons. The author is also grateful to have been the recipient of the Elizabeth Clay Howald Scholarship for 1936–37.

[11] Harold Walke, Phys. Rev. **52**, 669 (1937).

Formation of an Excited He^3 in the Disintegration of Deuterium by Deuterons

T. W. BONNER
Rice Institute, Houston, Texas

(Received March 14, 1938)

The energy distribution of the neutrons from the reaction $H^2+H^2\rightarrow He^3+n^1+Q_1$ has been studied. Two homogeneous neutron groups with energies of 1.08 and 2.50 Mev have been observed at 90° to the 0.11 Mev deuterons. The emission of 1.08 Mev neutrons has been found to be approximately 1/10 as likely as the emission of 2.50 Mev neutrons. The corresponding values of Q_1 are $Q_1^0=3.29\pm0.08$ Mev and $Q_1^1=1.40\pm0.11$ Mev. The low energy group results when the He^3 is left excited to a level of 1.89 ± 0.11 Mev. The mass of He^3 has been calculated from the value of Q_1^0 and the mass-spectrographic value of $H^2=2.01473$. The result is He^3 3.01700. This result indicates that H^3 may spontaneously disintegrate into He^3 with the emission of an electron.

THE neutrons produced in the disintegration of deuterium by deuterons were at first thought to be monoenergetic. This was concluded on the basis of the experiments of Dee[1] and those of Bonner and Brubaker.[2] These experiments indicated that at least most of the neutrons had an energy of about 2.5 Mev. Later experiments by the writer,[3] undertaken primarily to study neutron-proton scattering, gave a first indication that there probably was a second lower energy group with considerably less intensity than the high energy group. The purpose of the present experiments was to investigate carefully the neutrons from the reaction:

$$H^2+H^2\rightarrow He^3+n^1+Q_1. \qquad (1)$$

A search was made for low energy neutrons and particular care was taken to determine Q_1 as accurately as possible. A precise value of Q_1 is important because it is from this reaction that the mass of He^3 is best determined. The exact masses of He^3 and H^3 are particularly important as they each are made up of three fundamental particles (neutrons and protons). From their masses the relative magnitude of neutron-neutron forces and proton-proton forces may be deduced.

Experimental Procedure

The accelerating tube and d.c. source of potential were the same as that previously described.[3] The neutron energies were determined from the ranges of the recoil protons which were observed in a cloud chamber. The cloud chamber was 17 cm in diameter and 4.8 cm deep. It was constructed from as small an amount of material as possible in order to reduce neutron scattering to a minimum. The chamber was of the rubber diaphragm type, thus eliminating the material otherwise used in a piston. The chamber proper was made of a Pyrex glass ring which was 3 mm thick. The plate glass top had a thickness of 3 mm and the brass bottom plate a thickness of 1 mm. The cloud chamber was connected to the operating mechanism, an electromagnetic air valve, by a brass tube which was 2.5 cm in diameter and 90 cm long. With this arrangement only about 5 percent of the neutrons which pass through the cloud chamber make collisions before entering the chamber. This reduction in the number of scattered neutrons reduces the low energy tail or background which is ordinarily found on neutron energy distribution curves.[2] Consequently the experimental arrangement described above is well adapted for observing neutron groups of low intensity which are present along with higher energy neutrons.

The nearest edge of the cloud chamber was placed at a distance of 13 cm from the ion spot on the target. The neutrons which entered the cloud chamber made an angle of $90\pm11°$ to the direction of the deuterons on the target. The target was a 1 mm layer of D_3PO_4 at the bottom of a thin walled brass cup. Under these experimental conditions very few neutrons were scattered by the target or target holder.

The cloud chamber was filled with a mixture of 85 percent CH_4 and 15 percent C_2H_6 with

[1] P. I. Dee, Proc. Roy. Soc. **A148**, 623 (1935).
[2] Bonner and Brubaker, Phys. Rev. **49**, 19 (1936).
[3] T. W. Bonner, Phys. Rev. **52**, 685 (1937).

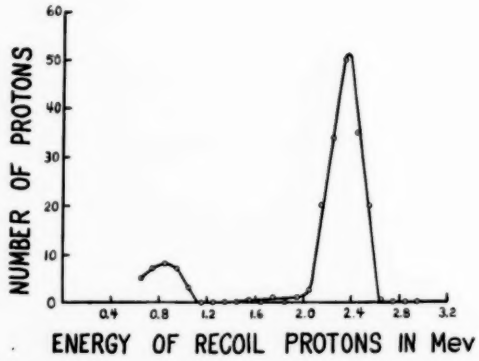

FIG. 1. The differential energy distribution curve of the recoil protons in the forward direction.

alcohol vapor. The expanded pressure in the chamber was slightly larger than atmospheric. The stopping power of the gas was found by measuring the mean length of polonium alpha-particles in the chamber. The stopping power for alpha-particles of range 3.805 cm was 1.07. This gas mixture has an appreciably different stopping power for polonium alpha-particles than for the highest energy protons which were observed. The stopping power for 10 cm protons was calculated from the data of Livingston and Bethe[4] and is 1.03.

EXPERIMENTAL RESULTS

Sixty-eight hundred pairs of stereoscopic pictures were taken of the cloud chamber when the deuterium target was bombarded with 0.11 Mev deuterons. On these photographs roughly 4000 recoil protons were observed and 205 of these were projected within the angular cone of 0–10° to the neutron's direction. The track lengths of these 205 acceptable tracks were measured and their ranges computed from the calculated stopping power of the gas in the chamber. Their energies were then computed from the range energy curve of Bethe and Livingston.[5] Fig. 1 shows the energy distribution of the recoil protons. There appear to be two definite proton groups with energies of about 1.1 and 2.6 Mev. These correspond to two neutron groups of very nearly the proton energies. The lower energy group has roughly 1/10 the intensity of the higher energy group. This ratio is complicated by the differing probability of observing tracks of

[4] Livingston and Bethe, Rev. Mod. Phys. 9, 275 (1937).
[5] Bethe and Livingston, private communication.

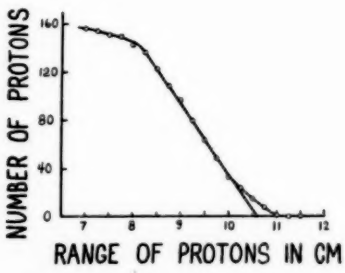

FIG. 2. The integral range number curve for long range recoil protons in the forward direction.

different lengths in the cloud chamber and the varying cross section for neutron-proton collisions.

A more accurate maximum energy of the neutrons was obtained from the integral range number curve of Fig. 2. The extrapolated range was 10.60 ± 0.30 cm. The calculation of the neutron disintegration energies was carried out by the method of Livingston and Bethe.[4] The experimental conditions correspond to their case of "good geometry." In their symbols, the range straggling s for 10.5 cm protons is 2.2 percent. The angular straggling γ/R was 4.55 percent and the total straggling s'' was 5.09 percent. For the thick target correction, β was calculated to be 11.9 and hence $x_{\text{extr}}=0.95$. Consequently the difference between extrapolated and mean range is $0.95\cdot5.09\cdot10.60/100=0.51$ cm. It follows that the mean range is 10.09 cm. This corresponds to a proton energy of 2.46 Mev. The correction for using recoils which made angles of 0–10° to the direction of the neutron is $\frac{1}{2}E_2\chi_0^2=2.5/2\cdot0.00306=0.04$ Mev. Therefore the energy of the neutrons coming from the top layer of the target at 90° is 2.50 ± 0.05 Mev. The disintegration energy is then calculated from the relation $Q_1=(4/3)En-(1/3)E_H$. The value of Q_1^0 is 3.29 ± 0.08 Mev. The corresponding value of Q_1^1, calculated from the low energy proton group, is 1.40 ± 0.11 Mev.

DISCUSSION OF RESULTS

The low energy neutron group corresponds to an excitation level in He^3 at 1.89 ± 0.11 Mev above the ground level. One should expect to find a gamma-ray with this energy with an intensity of about 1/10 that of the neutrons. In the experiments described above some high energy electron tracks were observed in the cloud chamber which probably were produced

by these gamma-rays. However their quantum energy must be determined before the correlation is made certain.

In view of the excitation level in He^3 at 1.89 Mev it seems reasonable to expect a similar level in H^3 of approximately the same energy of excitation. This follows since the level in He^3 should differ from that in H^3 only by the perturbation caused by the Coulomb field of the extra proton. This level in H^3 should be observed as a second lower energy group of protons from the reaction

$$H^2+H^2\rightarrow H^3+H^1+Q_2. \qquad (2)$$

One should expect a second proton group with a range of perhaps 5 cm. A careful search for such a group is planned, particularly since the results of Oliphant, Harteck and Rutherford[6] give some indication of such low energy protons.

The mass of He^3 can be most accurately found from the disintegration energy Q_1^0 together with Bainbridge and Jordan's spectrographic mass of $H^2=2.01473$ and a neutron mass[7] of 1.00893. The calculated mass of He^3 is 3.01700 ± 0.00010. Since the mass of H^3 is 3.01705, this indicates that H^3 may be unstable, disintegrating with a long half-life according to the reaction:

$$H^3\rightarrow He^3+e^-. \qquad (3)$$

This predicted instability of H^3 is consistent with the failure of recent attempts to concentrate H^3 from large samples of heavy water.[8]

The value of $Q_2^0-Q_1^0$ is just the difference between the binding energies of He^3 and H^3. For the value of Q_1^0 found above, this difference becomes $3.98-3.29=0.69$ Mev. Since the calculated value[9] of the Coulomb repulsion between the two protons in He^3 is very nearly equal to the experimental difference of 0.69 Mev, this shows that neutron-neutron forces must be very nearly equal to proton-proton forces.

[6] Oliphant, Harteck and Rutherford, Proc. Roy. Soc. **A144** 695 (1934).

[7] H. A. Bethe, Phys. Rev. **53**, 313 (1938).
[8] Lord Rutherford, Nature **140**, 303 (1937).
[9] Bethe and Bacher, Rev. Mod. Phys. **8**, 82 (1936); Share, Phys. Rev. **50**, 488 (1936); Rarita and Present, Phys. Rev. **51**, 788 (1937).

MAY 1, 1938 PHYSICAL REVIEW VOLUME 53

The Energy-Range Relations for Deuterons, Protons and Alpha-Particles

F. T. ROGERS, JR. AND MARGUERITE M. ROGERS
The Rice Institute, Houston, Texas

(Received March 16, 1938)

The complete deuteron, proton and α-particle energy-range relations as given by Livingston and Bethe and as subsequently revised by Bethe to include the latest data, are presented as a set of eleven equations. Given the range of a known particle, the corresponding kinetic energy of the particle can be computed easily and quickly from these equations.

IN 1937 Livingston and Bethe[1] published a very extensive set of kinetic energy *vs.* range relations for deuterons, protons and α-particles. These relations were in the form of graphs, in which the particle energies were plotted as functions of particle ranges. Later in 1937 these graphical energy-range relations were revised[2] to include the recent data of Parkinson, Herb, Bellamy and Hudson[3] on proton ranges and of Blewett and Blewett[2] on α-particle ranges. Now, to provide these latest revised energy-range relations in a complete and compact form suitable for the easy and rapid computation of energies, we present the following.

Let r be the mean range in cm of a particle in air at a temperature of 15°C and at a pressure of 760 mm Hg; let V be the corresponding energy of the particle expressed in millions of electron volts. Let the subscripts D, P, and α refer the symbols to which they are affixed to deuterons, protons and α-particles respectively. Then, given a value of r_D, r_P, or r_α (by observa-

[1] Livingston and Bethe, Rev. Mod. Phys. **9**, 266–269 (1937).
[2] See Bethe, Phys. Rev. **53**, 313 (1938).
[3] Parkinson, Herb, Bellamy and Hudson, Phys. Rev. **52**, 75 (1937).

TABLE I. *Precisions of Eqs. (1)–(11). Average deviations.*

Eq.	1	2	3	4	5	6	7	8	9	10	11
A	0.004	0.002	0.004	0.003	0.002	0.001	0.004	0.005	0.002	0.003	0.004

tion or otherwise), the corresponding value of V_D, V_P, or V_α can be obtained from the following equations:[4]

for deuterons having $r_D \leqslant 12$,

$$\log_{10} V_D = -0.0835+(0.595+0.45e^{-2r} +0.0025 \sin^2(\pi r/9)\cos(\pi r/6))\log_{10} r; \quad (1)$$

for protons having $r_P \leqslant 6$,

$$\log_{10} V_P = -0.3845+(0.595+0.45e^{-4r} +0.0025 \sin^2(2\pi r/9)\cos(\pi r/3))\log_{10} 2r: \quad (2)$$

for protons having $6 \leqslant r_P \leqslant 30$,

$$V_P = 1.819+0.16758(r-6) -0.003(r-6)^2+0.00004(r-6)^3; \quad (3)$$

for protons having $30 \leqslant r_P \leqslant 90$,

$$V_P = 4.661+0.08715(r-30) -0.000454(r-30)^2+0.00000217(r-30)^3; \quad (4)$$

for protons having $90 \leqslant r_P \leqslant 140$,

$$V_P = 8.714+0.054964(r-90) -0.00014(r-90)^2+0.00000047(r-90)^3; \quad (5)$$

for protons having $140 \leqslant r_P \leqslant 236$,

$$V_P = 11.174+0.044137(r-140) -0.0000429(r-140)^2 -0.000000108(r-140)^3; \quad (6)$$

for α-particles having $r_\alpha \leqslant 0.9$,

$$V_\alpha = 0.9851r+3.4958r^2-2.4681r^3 +0.03r \sin(2\pi r/0.9); \quad (7)$$

for α-particles having $0.9 \leqslant r_\alpha \leqslant 2.4$,

$$V_\alpha = 1.919+1.3167(r-0.9) +0.076 \sin(2\pi(r-0.9)/3); \quad (8)$$

TABLE II. *Estimated accuracies of Eqs. (1)–(11).*

PARTICLES	RANGE (cm)	POSSIBLE ERROR IN V	EQUATIONS INVOLVED
Deuterons	0 to 0.6	10%	1
Deuterons	0.6 to 12	0.06×10^6 ev	1
Protons	0 to 0.3	10%	2
Protons	0.3 to 236	0.03×10^6 ev	2–6
α-particles	0 to 0.35	10%	7
α-particles	0.35 to 1.05	0.05×10^6 ev	7–8
α-particles	1.05 to 3.5	0.03×10^6 ev	8–9
α-particles	3.5 to 10.5	0.01×10^6 ev	9–10
α-particles	10.5 to 21	0.03×10^6 ev	10–11

[4] In these equations the subscripts of the r's are, for simplicity, omitted.

for α-particles having $2.4 \leqslant r_\alpha \leqslant 7.2$,

$$V_\alpha = 3.894+1.0906(r-2.4) -0.07025(r-2.4)^2+0.00357(r-2.4)^3; \quad (9)$$

for α-particles having $7.2 \leqslant r_\alpha \leqslant 12$,

$$V_\alpha = 7.897+0.67375(r-7.2) -0.0108(r-7.2)^2-0.00082(r-7.2)^3; \quad (10)$$

for α-particles having $12 \leqslant r_\alpha \leqslant 20.8$,

$$V_\alpha = 10.799+0.50865(r-12) -0.000786(r-12)^2-0.000549(r-12)^3. \quad (11)$$

Each of Eqs. (1)–(6) and (9)–(11) is associated with only one of the graphs of Livingston and Bethe. Eqs. (7) and (8) are together associated with only one of the graphs.

The majority of the Eqs. (1)–(11) were obtained by fitting to the revised energy-range graphs, functions of suitable forms by a method of zero sums;[5] Eqs. (1) and (2) were obtained by a "trial and error" method, while Eq. (8) was obtained simply by inspection. As measures of the precisions with which Eqs. (1)–(11) represent these revised energy-range graphs of Livingston and Bethe, Table I shows for each equation the average deviation A (in millions of electron volts) of the computed energy-range graph from the corresponding revised energy-range graph. Obviously the representations afforded by Eqs. (1)–(11) are quite good.

As estimates of the accuracies with which Eqs. (1)–(11) give the appropriate energies, we may legitimately adopt the estimates by Livingston and Bethe[1] of the accuracies of their graphical energy-range relations. Accordingly in Table II we have tabulated as functions of ranges, the possible errors which (from Livingston's and Bethe's estimates) might be present in the energies computed from Eqs. (1)–(11). Table II should always be taken into consideration when Eqs. (1)–(11) are used, because it acts as a set of necessary restrictions which must be applied to computations made by Eqs. (1)–(11).

Finally, it is noteworthy that Eqs. (1)–(11) (of course restricted by Table II) are well suited for the simple and rapid numerical computation of V's when the corresponding r's are given, especially if tables of x^2, x^3, e^{-x}, $\log_{10} x$, and $\sin x$ are available.

[5] See, e.g., Campbell, Phil. Mag. **39**, 177 (1920).

Magnetic Field Corrections in the Cyclotron

M. E. Rose
Cornell University, Ithaca, New York
(Received March 15, 1938)

It is pointed out that in order to obtain magnetic fields which will allow the ions in the cyclotron to attain high energies it is first necessary to render the field homogeneous within an accuracy of about one part in a thousand. The correction (insertion of "shims") for the most important source of inhomogeneity, namely the decrease in the field near the edge of the pole pieces, is considered. A general method is given for determining the dimensions for any shape of these shims. Results are given for the dimensions of shims in the form of a ring of rectangular cross section placed at the edge of the cyclotron chamber. The magnetic field resulting from the use of such shims is determined and compared with the field of plane parallel pole faces. For the special case of a ring whose thickness is 1/16 the magnetic gap, the field is homogeneous within the required accuracy up to a distance from the edge of the poles of 0.4 of the magnetic gap. The uncorrected field is homogeneous only up to a distance from the edge equal to 0.9 of the magnetic gap.

I. Introduction

IT has been realized from the beginning of cyclotron technique that great homogeneity of the magnetic field is absolutely essential for the maintenance of resonance between the Larmor rotation of the ions and the oscillation of the accelerating electric field.[1] A deviation of one percent, e.g., will throw the ions completely out of resonance after 100 accelerations so that they will actually be decelerated instead of accelerated. Now the field produced by plane parallel magnetic poles is always inhomogeneous near the pole edges (cf. Fig. 4 below). Unless a great part of the area of the pole faces is to be sacrificed it is necessary to introduce "shims" near the edge which will have the effect of increasing the field in their neighborhood and thus render the field more homogeneous.

This shimming must be done rather accurately because over-correction must definitely be avoided. An over-correction, i.e., a magnetic field increasing with the distance r from the center of the cyclotron chamber, leads to strong magnetic defocusing of the ions, as was shown in a previous paper,[2] and therefore to enormous losses of intensity. The magnetic field must not increase radially at any point except possibly near the center where the electric field provides some focusing.

Even more exact design of the field is necessary if very high energy ions are to be obtained from the cyclotron. It was shown in I that the impossibility of simultaneously maintaining *exact* resonance and focusing of the ions imposes a limit on the energy obtainable. At the same time it was shown that magnetic fields can be devised which make this energy limit rather large.[3] In order to attain the highest energies, a field such as is given in Fig. 5 of I should be used. However, all such fields are somewhat critical in the sense that they necessarily do not differ by very much from a defocusing field. Hence the deviations from the prescribed field of the field finally obtained must be kept very small, of the order or less than one part in a thousand.

The success in attaining high energies will depend very much on the elimination of undesirable inhomogeneities in the field. The most important source of such inhomogeneity is the decreasing field due to the finite size of the pole pieces. In fact, since the desired field has been defined only inside the cyclotron chamber, the shims required to produce this field can be determined only if the effect of the pole edges is made negligible in the region where the ions move. The following section contains the calculation of the size of shims required to compensate for this edge effect as far out from the center of the chamber as is possible.[4]

[1] Of course, this is apart from the considerations of obtaining very high energies.

[2] M. E. Rose, Phys. Rev. **53**, 392 (1938); hereafter referred to as I.

[3] In the best case, field given in Fig. 5 of I, the energy is $E=2.12\ (V_0AZ)^{\frac{1}{3}}$ Mev where V_0 is the accelerating dee voltage in kilovolts, A and Z the atomic weight and atomic number of the ion.

[4] Of course, there will in general be some inhomogeneity due to the nonuniformity usually present in the large iron

II. Shims for Homogeneous Field

In the following we shall make two assumptions: The first is that the reluctance of the iron can be neglected so that the faces of the magnets (or lids of the cyclotron chamber) form equipotential surfaces.[5] The second assumption is that the shims may be placed on the inner surfaces of the lids of the cyclotron chamber rather than in the air-gap below and above the lids.

Since the magnets are supposed to be axially symmetrical we should introduce cylindrical coordinates with the origin at the center of the cyclotron chamber. Then the magnetic potential V is a solution of the Laplace equation written thus:

$$\partial^2 V/\partial r^2+(1/r)\partial V/\partial r+\partial^2 V/\partial z^2=0, \quad (1)$$

where z is the vertical coordinate. However for our present purpose, only the field near the edge where r is large is of importance. In this case the second term in (1) will be smaller than the other terms by a factor of order magnetic gap divided by diameter of magnetic poles[6] and hence may be neglected.

In this case we have a two-dimensional Cartesian problem to which we may apply the Schwarz transformation method.[7] We introduce a Cartesian coordinate system in a plane through the z axis, with origin at the edge and in the median plane. Denoting (radial) distances measured inward by x we have

$$\partial^2 V/\partial x^2+\partial^2 V/\partial z^2=0. \quad (2)$$

We introduce the complex variable

$$\zeta=x+iz \quad (3)$$

and the potential U conjugate to V (U=constant giving the magnetic lines of force). For our Cartesian problem we have the Cauchy-Riemann relations between the potentials:

$$\partial U/\partial x=-\partial V/\partial z, \quad \partial U/\partial z=\partial V/\partial x. \quad (4)$$

Hence the general solution of (2) is the imaginary part of the complex function W defined by

$$W(\zeta)=U(x, z)+iV(x, z). \quad (5)$$

The procedure now consists in the establishment of a connection by conformal mapping between an auxiliary variable t and W (potentials) on the one hand and between t and ζ (coordinates) on the other. By elimination of t the potentials or magnetic field can be obtained in terms of the coordinates. The variable t is to assume real values on the equipotential surfaces and particular values are to be assigned at all places where the slope of these surfaces changes i.e., at all the corners of the pole faces. Only three of these particular values (say 0, 1 and ∞) are independent, the remaining values being completely determined by the special geometry. If we regard the pole faces as forming the boundary of a polygon and if the particular value t_n is assigned to the nth corner where the internal angle of the polygon is α_n, then the connection between ζ and t is[8]

$$d\zeta/dt=C_1\prod_n(t-t_n)^{\alpha_n/\pi-1}, \quad (6)$$

where C_1 is a constant to be determined from the boundary conditions.

As an example we may consider the case of plane parallel poles. In the finite part of the ζ plane there is, of course, one corner on each pole to which the values $t_n=\pm 1$ may be assigned. At this corner the internal angle $\alpha_n=3\pi/2$. At $x=0$, $z=\pm\infty$ we can set $t_n=\pm\infty$ and at $x=\infty$, $t_n=0$, and $\alpha_n=0$. Then we have

$$d\zeta/dt=C_1(t^2-1)^{\frac{1}{2}}/t. \quad (6a)$$

Since in all cases there are only two equipotential surfaces we have, regardless of geometry, for the connection between W and t (cf. Fig. 1, also Fig. 73 reference 7).

$$dW/dt=C_2/t, \quad (7)$$

where again C_2 is a constant to be determined from the boundary conditions.

It is convenient to introduce as unit of potential the magnetic potential on the (lower) pole face so that we have as boundary conditions

$$W(t=1)=-i, \quad W(t=-1)=+i. \quad (8)$$

magnets, and possibly to irregularities arising from machining or assembling the magnets, etc. Obviously corrections for these inhomogeneities must be carried out empirically and it will be assumed that this can be done to the required degree of accuracy.

[5] No currents in the cyclotron chamber.

[6] Cf. the result (27) for the field obtained below and the remark preceding (15). The ratio of the second and first term of (1) is $1/2\pi$ times gap/diameter which for the usual dimensions is of the order of one percent.

[7] Cf. e.g., F. Kottler, *Handbuch der Physik*, Vol. 12, p. 480.

[8] The index n can assume a series of discrete or a continuous range of values. The latter case is pertinent when the slope of the shims varies continuously.

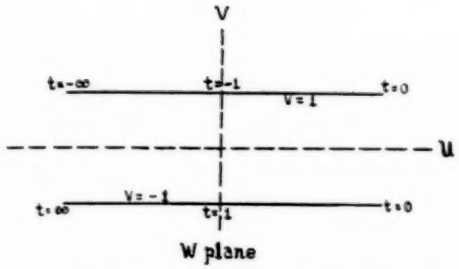

FIG. 1. Conformal mapping of the t plane on the W plane. The real t axis coincides with the equipotentials $V=\pm 1$.

Then we find from (7) and (8)

$$W=-(2/\pi)\log te^{\pi i/2}, \tag{9}$$

or by the use of (5)

$$t=\exp -\pi/2[U+i(1+V)]. \tag{10}$$

From the symmetry with respect to the median plane, the values t_n at corresponding corners of upper and lower pole faces are opposite in sign. At these corresponding corners the angles α_n will be the same. In addition, taking $t_n=0$ between the poles at $x=\infty$ at which point $\alpha_n=0$ we may write (6) in the form

$$d\zeta/dt=(C_1/t)\prod_n(t^2-t_n^2)^{\alpha_n/\pi-1}, \tag{11}$$

where the index n runs over the values on one pole face only.

Introducing the components of the magnetic field

$$H_x=-\partial V/\partial x, \quad H_z=-\partial V/\partial z \tag{12}$$

we find from (4) and (10)

$$H_z-iH_x=-(2/\pi)(td\zeta/dt)^{-1}, \tag{13}$$

or from (11)

$$H_z-iH_x=-(2/\pi C_1)\prod_n(t^2-t_n^2)^{1-\alpha_n/\pi}. \tag{14}$$

We use as unit of length half the magnetic gap so that for $x=\infty$, $t=0$ the magnetic field becomes

$$H_z=1, \quad H_x=0. \tag{15}$$

We may then determine the constant C_1 and obtain

$$H_z-iH_x=\prod_n(1-t^2/t_n^2)^{1-\alpha_n/\pi}. \tag{16}$$

Thus it is seen that the magnetic field may be obtained as a function of t or from (10) as a function of the potentials without integration.

From this result we see that the inhomogeneity of the field can be expressed as a power series in t^2. Further, since the field is in any case almost homogeneous inside the cyclotron chamber, U will be proportional to x within very small correction terms (cf. 24, 25 below). Hence from (10) the inhomogeneity is

$$1-H_z=k_1e^{-\pi z}\cos\pi z+k_2e^{-2\pi z}\cos 2\pi z+\cdots, \tag{17}$$

where $k_1, k_2\cdots$ are coefficients depending on the parameters t_n and hence on the geometry. In general the coefficient k_1 will not vanish and for plane parallel pole face $k_1\sim\frac{1}{4}$ so that the inhomogeneity at $x=1$ in this case is about one percent. To make the field more homogeneous the dimensions of the shims may be made such that k_1 vanishes. In this case the inhomogeneity $k_2e^{-2\pi z}\cos 2\pi z+\cdots$ decreases very rapidly and will be negligible for x larger than unity.

Application to ring shims

A great variety of shapes of shims would be equally suitable for accomplishing our purpose. In many cases it would be possible to make the main term in the inhomogeneity ($\sim e^{-\pi z}$) vanish. Of course, in the various cases, the size of the remaining inhomogeneity, i.e., the coefficient of $e^{-2\pi z}$ would depend on the geometry in different ways. However, since nothing is gained by complication, we consider here only the simplest case of a single ring shim of rectangular cross section on each pole face. The outer diameter of the ring is to be equal to the pole radius, the width of the ring a and its thickness b, cf. Fig. 2. The parameters t_n and internal angles α_n are:

ζ	t_n	α_n
$\pm i(1-b)$	± 1	$3\pi/2$
$a\pm i(1-b)$	$\pm t_1$	$3\pi/2$
$a\pm i$	$\pm t_2$	$\pi/2.$

(18)

In addition at $\zeta=\pm i\infty$, $t=\pm\infty$ and at $\zeta=\infty+iz$, $t_n=0$. From (16) we find

$$H_z-iH_x=(1-t^2/t_2^2)^{\frac{1}{2}}(1-t^2)^{-\frac{1}{2}}(1-t^2/t_1^2)^{-\frac{1}{2}}. \tag{19}$$

The coefficient of t^2 in the expansion of this expression vanishes if

$$t_2^2=t_1^2/(1+t_1^2) \tag{20}$$

and with this result we have

$$H_z-iH_x=1-t^4/2t_1^2+\cdots. \tag{21}$$

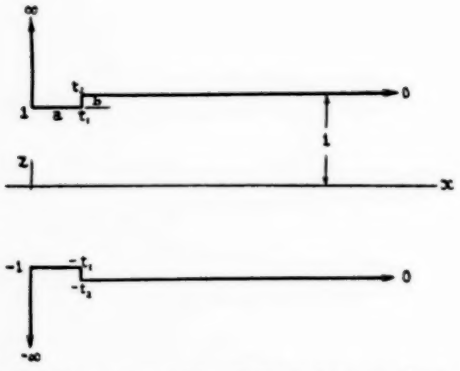

FIG. 2. Conformal mapping of the t plane on the ζ plane. The real t axis coincides with the surfaces of the magnets.

To make the inhomogeneity small, it is desirable that t_1 be not too small. This will mean as may be seen below that a should be small; e.g. $a \approx 0.1$ would be quite satisfactory.

For $d\zeta/dt$ we have from (13)

$$d\zeta/dt = -(2/\pi t)(1-t^2)^{\frac{1}{2}} \times (1-t^2/t_1^2)^{\frac{1}{2}}(1-t^2/t_2^2)^{-\frac{1}{2}}. \quad (22)$$

Upon integrating (22) from $t=1$ to $t=t_1$ we obtain a as a function of t_1. Again integrating (22) from $t=t_1$ to $t=t_2$ we obtain b as a function of t_1, using (20). Eliminating t_1 we have the thickness b in terms of the width a. This final result is given in Fig. 3.

The magnetic field on the median plane is obtained from (22), (13) and (10) with $V=0$.

$$H_z = (1+e^{-\pi U}/t_2^2)^{\frac{1}{2}}(1+e^{-\pi U})^{-\frac{1}{2}} \times (1+e^{-\pi U}/t_1^2)^{-\frac{1}{2}}. \quad (23)$$

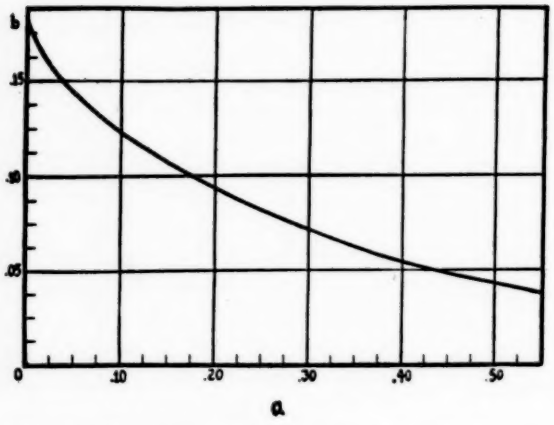

FIG. 3. Dimensions of ring shim for homogeneous magnetic field. Thickness of ring b, width a. The unit of length is half the magnetic gap.

To obtain the field in terms of x we have

$$x = U - U_0 - \int_U^\infty [f(U')-1]dU', \quad (24)$$

where $f(U)$ is the reciprocal of the expression given on the right-hand side of (23). The constant U_0 is given by

$$U_0 = -a + 2/\pi \log 1/t_2 + \int_0^{t_2} (2/\pi + t d\zeta/dt)dt/t, \quad (25)$$

the integration being taken along the surface of the magnet where t is real. This constant is only slightly geometry dependent and its value is in general about 0.2.

The field obtained in this way is given in Fig. 4 (upper curve) for a special case. In the same figure the field on the median plane for the case of plane parallel pole faces is given. It is seen that the homogeneity of the field is indeed very much improved. The curves also show that the approach to the asymptotic behavior (cf. (17), (24)) of the field is rather rapid. By retention of only the first term in the inhomogeneity ($\sim e^{-2\pi U}$) the error made at $x=1.0$ is only 3 percent of the total inhomogeneity. Thus for larger x we may write

$$U = x + U_0 \quad (26)$$

(cf. (24)) and

$$V = -z. \quad (26a)$$

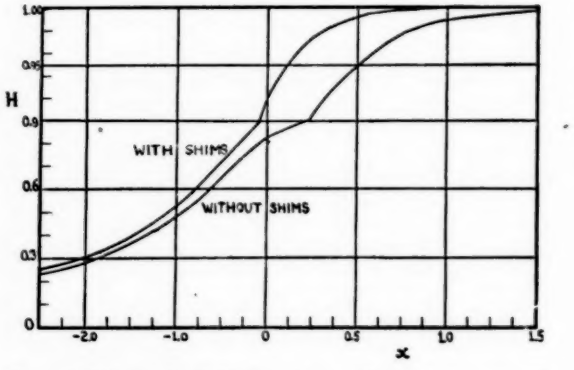

FIG. 4. Magnetic field on the median plane near the edge of the magnets. The unit of field strength is the difference of potential between the magnets divided by the magnetic gap. The field labeled "with shims" applies in the case of a ring shim of width $a=0.095$ and thickness $b=0.125$ in terms of half the magnetic gap as the unit of length. The field labeled "without shims" pertains to the case of plane parallel pole faces. Note the change in scale at $H=0.90$ and at $x=0$.

Then we obtain for the magnetic field in this region

$$H_z = 1 - \tfrac{1}{2}t_1^2 e^{-2\pi(x+U_0)} \cos 2\pi z,$$
$$H_x = \tfrac{1}{2}t_1^2 e^{-2\pi(x+U_0)} \sin 2\pi z. \quad (27)$$

For the uncorrected field of plane parallel pole faces the field inhomogeneity is one-tenth percent at $x=1.8$. For the field with ring shims in the case $b=0.125$, $a=0.095$ we find from Fig. 4 that this same inhomogeneity occurs at $x=0.80$. Thus if the exit slit is placed at this distance (0.4 the magnetic gap) from the edge, the magnetic field over the entire region of motion of the ions will be homogeneous within the required degree of accuracy.

Finally, we may return to a consideration of the assumptions made at the beginning of this section. First of all the assumption of low reluctance of the iron will in general be fulfilled rather well. Of course, it is sufficient if only the cyclotron lids and not the large magnets themselves be of low reluctance, high permeability iron. Secondly, the assumption that the shims be placed inside the chamber against the lids rather than in the air gap need not impose any restriction on the applicability of the results obtained here. Since the shims used to make the field homogeneous may be inserted at the time of construction it should perhaps be not inconvenient actually to place them inside the chamber.

MAY 1, 1938 PHYSICAL REVIEW VOLUME 53

Some Experiments on the Magnetic Properties of Free Neutrons

O. R. Frisch, H. von Halban, Jr.,* and Jørgen Koch
Institute of Theoretical Physics, University, Copenhagen

(Received February 5, 1938)

The behavior of partly polarized beams of slow neutrons as regards their precession on passing through homogeneous magnetic fields has been investigated. From the experiments it is concluded that the neutron has a magnetic moment not far from $2\times 1/1840$ Bohr magneton and that the sign is negative. Further, the precession of neutrons inside magnetized iron was investigated; it was found that the field accounting for the observed rate of precession is more than 100 times the actual field strength H and actually of the order of magnitude of the magnetic induction B.

1. Introduction

That a neutron should have a magnetic moment at all, seems somewhat surprising, on account of its being electrically neutral. On the other hand, from the magnetic moments of the proton[1,2] (2.5 to 2.8 n.m., 1 n.m. = 1 nuclear magneton = 1/1840 Bohr magneton); and the deuteron[2,3] (0.85 n.m.), a magnetic moment μ_n of the neutron, of about 2 n.m., can be deduced;[4] the sign of μ_n should be negative, that is, the relative position of spin and magnetic moment should be the same as in the (negative) electron. A tentative explanation of this moment, based on the Fermi theory of beta-decay, has been offered by Wick.[5]

A way of measuring, at least roughly, the magnetic moment of free neutrons has been pointed out by Bloch.[6] He showed that the magnetic interaction between neutrons and electrons must have a measurable influence on the scattering of slow neutrons by magnetic atoms or ions (provided the neutron has a magnetic moment of the order of 2 n.m.). Of special interest is the scattering of neutrons from a ferromagnetic substance in

* Now at the Institut de Chimie Nucléaire, Collège de France, Paris.

[1] O. R. Frisch, O. Stern, Zeits. f. Physik **85**, 4 (1933); I. Estermann, O. Stern, Zeits. f. Physik **85**, 17 (1933); I. Estermann, O. C. Simpson, O. Stern, Phys. Rev. **52**, 535 (1937).

[2] I. I. Rabi, J. M. B. Kellogg, J. R. Zacharias, Phys. Rev. **46**, 157, 163 (1934); **50**, 472 (1936).

[3] I. Estermann, O. Stern, Phys. Rev. **45**, 761 (1934).

[4] H. A. Bethe, R. F. Bacher, Rev. Mod. Phys. **8**, 91, 205 (1936).

[5] G. C. Wick, Att. Acad. Lincei **21**, 170 (1935); see also reference 4.

[6] F. Bloch, Phys. Rev. **50**, 259 (1936).

which, by means of a magnetic field, the magnetic momenta of a large number of electrons are adjusted parallel among themselves; then the scattering should depend on the spin orientation of the neutrons relative to that of the electrons. One should therefore be able to produce partly "polarized" beams of neutrons by sending them through a piece of magnetized iron; a second, similar piece might be used as an "analyzer."

The existence of such an effect was demonstrated by Hoffman, Livingston, and Bethe;[7] they found that the total transmission, for slow neutrons, of a system of two iron bars (of 1 cm thickness each) was 2.3 percent smaller when the bars were magnetized antiparallel instead of parallel. The amount of the difference was in fair agreement with a calculation[7] based on the assumption $\mu_n = 2$ n.m.; the agreement may be regarded as an argument for the correctness of this assumption. Similar results have been reported by Beyer, Carroll, Dunning and Powers.[8–10]

It was soon realized that the more or less irregular magnetic stray fields prevailing along the path of the neutrons would complicate the course of the phenomenon by causing frequent reorientation of the polarized neutrons. On the other hand, the systematic study of this reorientation might permit one to determine the magnitude and also the sign of the magnetic moment μ_n of the neutron. This was pointed out by Rabi,[11] who calculated the reorientation caused by a special type of an inhomogeneous magnetic field. Independently the author[12] also demonstrated the existence of this reorientation effect by using a homogeneous field perpendicular to the polarizing and analyzing fields, and showed that it behaves roughly as one would expect from the assumption $\mu_n = 2$ n.m.

Using a similar arrangement, the authors also proved[13] that the sign of μ_n is actually negative, as expected from the moments of proton and deuteron. The same result was found by Powers, Carroll, Beyer and Dunning[14] who used an arrangement similar to the one suggested by Rabi.[11]

A third paper of the authors[15] was devoted to the study of the precession of neutrons inside magnetized iron, where the question of some theoretical interest is, whether the magnetic field strength H or the magnetic induction B (or perhaps something in between) is responsible for the rate of precession.

In the following we shall give a more detailed account of the experiments the results of which have been published in the three preliminary notes,[12, 13, 15] and some considerations and calculations which have to do with the problem.

2. General Remarks

In the classical theory a particle possessing a magnetic moment μ and an angular momentum J precesses in a magnetic field H like a gyroscope, with an angular velocity $\omega = H\mu/J$. According to quantum mechanics, however, this picture cannot in general be used, and in particular fails entirely in cases like the Stern-Gerlach effect

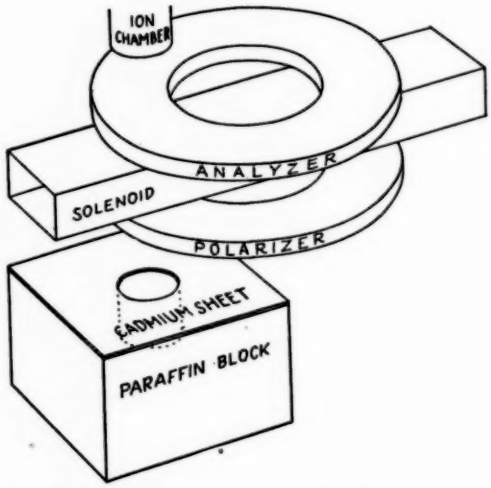

FIG. 1. Experimental arrangement for the demonstration of the precession of neutrons. The path of the neutrons from the hole in the paraffin block to the ionization chamber was almost entirely surrounded by boron and cadmium sheets (not shown in the figure) to suppress scattered neutrons.

[7] J. G. Hoffman, M. Stanley Livingston, H. A. Bethe, Phys. Rev. **51**, 214 (1937).
[8] J. R. Dunning, P. N. Powers, H. G. Beyer, Phys. Rev. **51**, 51 (1937).
[9] P. N. Powers, H. G. Beyer, J. R. Dunning, Phys. Rev. **51**, 371 (1937).
[10] P. N. Powers, H. Carroll, J. R. Dunning, Phys. Rev. **51**, 1112 (1937).
[11] I. I. Rabi, Phys. Rev. **51**, 652 (1937).
[12] O. R. Frisch, H. von Halban, J. Koch, Nature **139**, 756 (1937).
[13] O. R. Frisch, H. von Halban, J. Koch, Nature **139**, 1021 (1937).
[14] P. N. Powers, H. Carroll, H. Beyer, J. R. Dunning, Phys. Rev. **52**, 38 (1937).
[15] O. R. Frisch, H. von Halban, J. Koch, Nature **140**, 360 (1937).

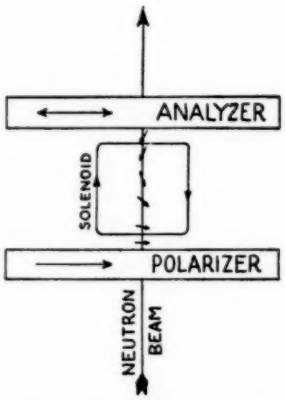

FIG. 2. Schematic diagram, illustrating principle of precession experiment.

where we have to do with a different motion of the particles in the separate stationary states corresponding to different orientations of the spin axes relative to the magnetic force. Still, as can be simply verified by a direct quantum-mechanical analysis,[16] the precession picture retains, in accordance with the correspondence argument, its validity in all such cases where, as in the phenomena considered below, the translative motion of the particles is not essentially influenced by their angular orientation in the field.

A particle with angular momentum $\frac{1}{2}\hbar$ and magnetic moment μ in a magnetic field H precesses with an angular velocity $\omega=2\mu H/\hbar$. If the velocity of the particle is v, then it moves a distance $l_R=v/\omega=v\hbar/2\mu H$, while rotating through one radian. Assuming $\mu=2$ n.m. $=1.10^{-23}$ c.g.s. units, we find $\omega=2\cdot 10^4\ H$; for an average "thermal" neutron with $v=2\cdot 10^5$ cm/sec. we get $l_R\cdot H=10$, where l_R is measured in cm and H in gauss.

This value of $l_R\cdot H$ is very much larger (about 10^4 times) than the values encountered in experiments on the reorientation of atoms.[17] In molecular beam experiments, unless special arrangements are made, the direction of the magnetic field changes only very slightly over a distance l_R along the path of the particles, and the spins therefore follow the magnetic field lines adiabatically, precessing within a very narrow cone around them. Only if the field is made very weak and at the same time strongly inhomogeneous at some point of the beam, are the spins "shaken off the field lines" and actual precessing occurs. Of course, all this may be expressed, as is usually done, in terms of space quantization and non-adiabatic transitions.

In analogous experiments with neutrons the field need be neither so weak nor so strongly inhomogeneous, because $l_R\cdot H$ is so much larger. Furthermore, it is possible, in the case of neutrons, to study the especially simple case of precession in a sharply limited homogeneous "precession field" which is e.g. perpendicular to the polarizing and analyzing fields; in order to separate the different fields, a layer of copper winding carrying a suitable current may be applied, since a thin layer of copper is almost transparent for neutrons.

3. Demonstration of the Precession of Neutrons

A. Experimental arrangement

Our first experiment[12] was designed to demonstrate the existence of the precession and to measure its rate in a rough way. The arrangement (Fig. 1) consisted of a paraffin block containing a neutron source (400 mg Ra+Be), the polarizer, the precession field solenoid, the analyzer, and the detecting boron-lined ionization chamber connected to an amplifier and mechanical counter. The principle of the method is shown in the schematic Fig. 2.

The polarizer was a flat iron ring (20 cm outer, 11 cm inner diameter, 0.8 cm thickness) which was wound all over with one layer of 1.5 mm copper wire (enameled). In such a symmetrical arrangement the magnetizing current should produce practically no field outside the iron (the fields in the neighborhood of the single wires can be neglected). Actually, when a current of 10 amp. was passed through the windings, irregular fields of several gauss were observed near the surface of the iron rings, presumably on account of slight local variations of the magnetic properties. We decided therefore to switch on the current of 10 amp. only for a few seconds every time the magnetization was reversed, and then to switch it off again, and use the remanent field only. In this case the stray fields were consider-

[16] Compare., e.g., C. G. Darwin, Proc. Roy. Soc. **117**, 258 (1927).

[17] O. R. Frisch, T. E. Phipps, E. Segrè, O. Stern, Nature **130**, 892 (1932); O. R. Frisch, E. Segrè, Zeits. f. Physik **80**, 610 (1933); J. M. B. Kellogg, I. I. Rabi, J. R. Zacharias, Phys. Rev. **50**. 472 (1936).

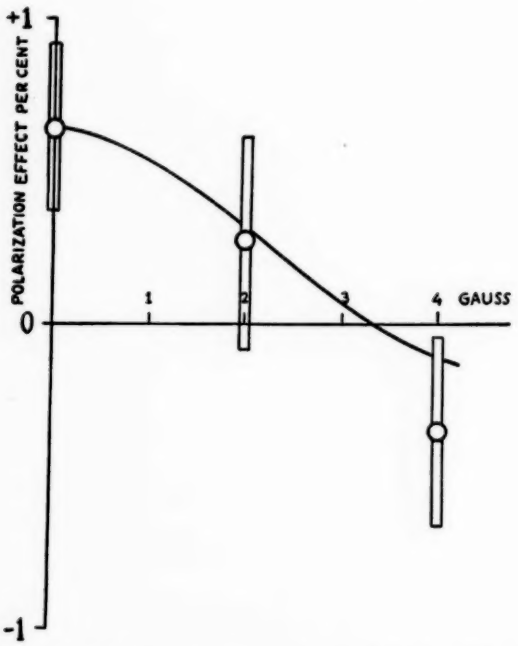

FIG. 3. Result of precession experiment. Polarization effect plotted as a function of precession field.

ably smaller and could not have caused appreciable precession.

The precession field coil was made with rectangular cross section, 3.5×5 cm, and 35 cm long, and consisted of a single layer of 0.65 mm copper wire, wound on a brass frame. The field was calculated from the formula for an infinitely long solenoid.

The analyzer was made identical with the polarizer.

The boron-lined ionization chamber was of the "double-decker" design, in order to get a large useful boron surface. It was connected to a transformer-coupled high gain amplifier acting on a mechanical counter; the resolving power of this arrangement was sufficient since only about 100 neutrons per minute were counted.

The experiment consisted in taking alternative counts, of 7 minutes each, with the magnetization of the polarizer reversed after each count; the analyzer was kept with the same magnetization all the time. Runs were made with three different currents through the precession field solenoid. Each run had to last about 50 hours in order to have a small statistical error. The whole experiment was carried through entirely automatically by means of an arrangement of relays and rotating switches, controlled by a clock. Every 7.5 minutes the counting was stopped during half a minute; within this time, a picture of the mechanical counter (and some control instruments) was taken on a motion-picture film, and the polarizer current was reversed and switched off again. Because of the short cycle of counting, slow variations of the sensitivity of the amplifier (which actually occurred) were practically eliminated.

B. Results and discussion

In the first run, with no current in the precession field solenoid, the number of neutrons recorded was 0.65 ± 0.28 percent larger with the fields in the polarizer and analyzer parallel than with antiparallel fields. In the second run, with a precession field of 2 gauss, a difference of 0.29 ± 0.36 percent was recorded, while in the third run, with 4 gauss precession field, the difference was -0.36 ± 0.31 percent; the negative sign indicates that the recorded number of neutrons was smaller with parallel than with antiparallel fields, in the third run. The errors have been calculated in the standard way from the square roots of the numbers of neutrons counted. It was found repeatedly that the fluctuations were not larger than those to be expected as purely statistical fluctuations. In this experiment, $1.2\cdot10^6$ neutrons were counted, on the whole.

Supposing, for the moment, that all the neutrons in the beam had the same velocity v_0, the polarization effect (difference in intensity, with parallel and antiparallel fields) would be proportional to the cosine of the angle $\varphi=2\mu Hl/\hbar v_0$ through which the neutrons precess on their way (of length l) through the field H. On account of the velocity distribution of the neutrons, the polarization effect as a function of H will be not a cosine but a superposition of cosines with different periods, which is roughly equivalent to a damping of the cosine function which corresponds to the mean velocity. We have calculated this function (see curve C, Fig. 5) making a number of assumptions which are discussed in §7.

In Fig. 3 the observed differences are plotted together with the theoretical curve, and it is seen that they agree within the very large experimental errors. Obviously it would be hopeless to

discuss these results any further and to try and enclose the magnetic moment of the neutron between definite limits. We started a new experiment with an improved arrangement, taking counts with five different values of the precession field, but from a fortnight's continuous counting we found differences showing the same general trend but still slightly smaller than those reported here, perhaps merely because of an adverse statistical fluctuation. Substantial improvement in the accuracy would have required such unreasonably long periods of counting that we decided to postpone a repetition of the experiment until a time when stronger sources should be available.

The maximum polarization effect found by us (0.65 percent) must be multiplied by 2 in order to take account of the fact that about half of the recorded neutrons were faster than one volt (went through 0.5 mm of cadmium) and, therefore, should not contribute to the polarization effect. The resulting figure, 1.3 percent, is smaller than the one found by Hoffman, Livingston, and Bethe,[7] (2.3 percent). This difference is understandable since we used a field of 10,000 gauss in polarizer and analyzer (the remanent field) while Hoffman, Livingston and Bethe used a field of 15,000 gauss.

4. Sign of the Magnetic Moment of the Neutron

A. Experimental arrangement

In order to determine the sign of the magnetic moment of the neutron it is necessary to find the direction of precession. This is obviously not possible with the symmetrical arrangement of our first experiment, and the arrangement was therefore changed in the following way (see Fig. 4): (1) the analyzing iron ring was rotated through an angle of 90°, with the beam as an axis, so that the polarizing and analyzing fields were perpendicular to each other (and to the neutron beam); (2) the precession field solenoid was removed and a short (2.2 cm long, 5 cm diameter) coil was inserted producing a field parallel to the beam; this field was found (by means of a small flip coil) to be fairly homogeneous, presumably on account of the iron below and above.

The experimental procedure this time was to reverse the precession field alternately while the rings were kept magnetized in the same direction all the time. The direction of precession changes with the precession field, and the neutron intensity recorded must be larger when the neutrons precess in the same direction as one would have to rotate the polarizer in order to make the polarizing and the analyzing fields parallel (see Fig. 4). From the direction of the precession field for which the transmitted neutron intensity is larger than for the opposite direction, one can deduce the sign of the magnetic moment of the neutron.

In order to get a large effect, the magnetizing current on the rings was left on (2 amp.) all the time. Consequently the stray fields were quite strong. By rotating the rings independently in their own plane, however, a position was found where the stray field was nearly homogeneous and parallel to the beam, and of the right magnitude (3 gauss) to turn the neutrons by 90°, on the average. This field could be reversed by passing a suitable current through the solenoid. A large number of counts (of 7 minutes each) were then taken with the solenoid current alternately on and off.

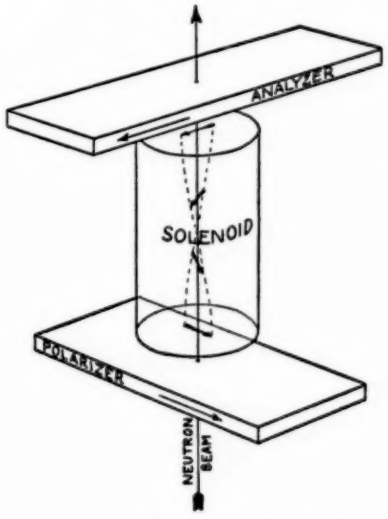

FIG. 4. Determination of the sign of the magnetic moment of the neutron, schematic diagram of the arrangement. If the neutrons precess in the way indicated, a larger fraction of them goes through the analyzer than when the current in the solenoid is reversed and the neutrons correspondingly precess in the opposite way. For the sake of clearness, the solenoid is made much longer in Fig. 4 than it was in the actual experiment.

B. Results

A difference of 1.05 ± 0.24 percent was recorded between the intensities observed with the two directions of the precession field. The amount of the difference is in accordance with the assumption $\mu_n = 2$ n.m., although the arrangement is not well suited for measuring the magnitude of μ_n. From the sign of the difference it followed that the neutrons precess in the direction of the (positive) current in the solenoid; from this again it follows that the sign of the magnetic moment of the neutron is negative, that is, the relative direction of spin and magnetic moment is the same as in the (negative) electron.

Shortly after our first publication, the same result was published by Powers, Carroll, Beyer and Dunning,[14] who had used a type of an unsymmetrical inhomogeneous field suggested by Rabi.[11] The negative sign had been generally expected on account of the moments of the proton and the deuteron (see §1).

5. Precession of Neutrons Inside Magnetized Iron

A. The problem

Rossi[18] and Mott-Smith[19] have tried to detect the deflection which cosmic-ray electrons undergo when passing through magnetized iron. For the interpretation of such experiments it is essential to know, whether the amount of deflection corresponds to the magnetic induction B (about 20,000 gauss at saturation) or the magnetic field strength H (in general only a few gauss). Weizsäcker[20] has examined the question with the help of Dirac's theory and found that the induction B is effective.

We have put to ourselves the analogous question: Is the rate of precession of neutrons inside magnetized iron determined by H or B? So far, no theoretical investigation of the problem as such has been published; but Bloch[21] made some interesting remarks from which it appears that the theoretical treatment of this and some similar problems would require a much more intimate knowledge of the interaction between electrons and neutrons than is available at present. In this state of affairs we thought that even a crude experiment might be of interest.

B. Experimental arrangement

The arrangement was in principle similar to our first one, but yet different in several respects. As polarizer and analyzer we used straight iron bars of cross section 1×5 cm, and 80 cm length, carrying a single layer of 0.65 mm copper wire; by means of iron pieces at the ends they were connected to form a single magnetic circuit. The magnetic induction in the bars was about 14,000 gauss. The space between them was investigated with a small flip coil, and the neutron beam was sent through at a point where the stray field was weak enough to cause no disturbance.

A long, flat solenoid (7×0.7 cm cross section, 15 cm long) was placed across the beam, similar to the first arrangement, and a strip of thin (0.15 mm) iron sheet inside the coil; the ends of the strip were connected by a strong iron yoke (made of round iron of 1 cm diameter) to close the magnetic circuit. The current through the solenoid was alternately set at two different values corresponding to magnetic fields of 2.8 gauss and 35 gauss, respectively; the polarizing and analyzing fields remained unchanged (they were bound to be antiparallel since they formed a magnetic circuit).

In order to enhance the polarization effect we used a low temperature source of neutrons,[10] consisting of an ice block at liquid-air temperature, of similar shape as the paraffin block used before.

C. Results

To check the whole arrangement, a run was made with the iron strip removed. With a precession field of 2.8 gauss, along a path of only 7 mm, the neutrons should hardly precess at all and the transmission of the system should have the low value corresponding to the polarizing and analyzing fields being antiparallel. With the precession field at 35 gauss, however, most of the neutrons precess by more than 360° and the beam should be practically depolarized, and consequently the

---

[18] B. Rossi, Rend. Lincei **11**, 478 (1930); Nature **128**, 300 (1931).
[19] L. M. Mott-Smith, Phys. Rev. **37**, 1001 (1931); **39**, 403 (1932).
[20] C. F. v. Weizsäcker, Ann. d. Physik **17**, 869 (1933).
[21] F. Bloch, Phys. Rev. **51**, 994 (1937).

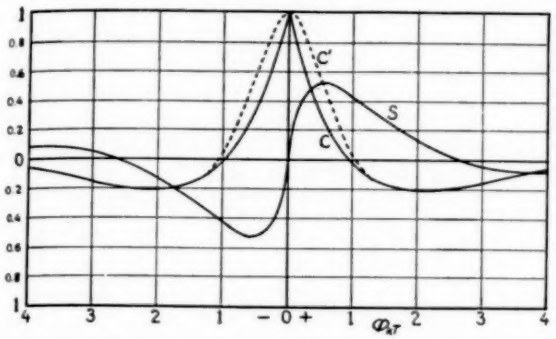

FIG. 5. Curves representing the precession of thermal neutrons.

transmission of the system should lie halfway between the values for parallel and antiparallel fields. Such a difference was actually observed; the intensity was 0.83 ± 0.26 percent larger with 35 gauss than with 2.8 gauss. This figure of 0.83 is to be compared with one-half of 0.65, the result in our first experiment (see §3B). It should be remembered that in this first experiment the polarizing field was alternately reversed. The improvement by a factor of 2 or 3 is to be attributed partly to the cooling, and partly to the larger magnetic induction in polarizer and analyzer (14,000 instead of 10,000 gauss).

The iron strip was now inserted (and closed by the yoke) and a second run, quite similar to the first one, was carried out. If the rate of precession in the iron was determined by the field strength H, then the iron strip should make no difference at all, because the field strength is the same within the iron as below and above it. If it is B that matters, however, then the neutrons should precess many times on their way through the iron sheet and be completely depolarized; since the iron is practically saturated even with the weak field of 2.8 gauss, the neutrons reaching the analyzer should be depolarized and the intensities transmitted the same both for 2.8 and 35 gauss. This is actually what we found: the difference was -0.05 ± 0.24 percent, that is, zero within the limits of error.

It is concluded that the field accounting for the rate of precession of neutrons inside magnetized iron is certainly much larger than H; a numerical discussion shows that it is probably larger than 500 gauss, or, in other words, larger than $0.03\cdot B$.

6. Calculation of the Precession of Neutrons with Maxwellian Velocity Distribution

We assume the velocity distribution by the neutron beam and the velocity dependence of the indicating system to be such that $f(v)dv$ is the number of neutrons with velocities between v and $v+dv$ counted per unit time, with polarizer and analyzer removed. With the polarizer (of thickness x) in place (and magnetized) the number of neutrons is reduced to

$$J_0(v)dv=\tfrac{1}{2}f(v)dv(e^{-x\mu_1(v)}+e^{-x\mu_2(v)}),$$

where μ_1 and μ_2 are the attenuation coefficients for parallel and antiparallel neutrons, respectively.

If now the analyzer (also of thickness x) is brought in place, the transmitted intensity depends on its position:

$$\text{parallel } J_1(v)dv=\tfrac{1}{2}f(v)dv(e^{-2x\mu_1(v)}+e^{-2x\mu_2(v)}), \quad (1)$$

$$\text{antiparallel } J_2(v)dv=f(v)dv\cdot e^{-x[\mu_1(v)+\mu_2(v)]}. \quad (2)$$

Introducing $\mu_1(v)=\mu+\beta(v)$ and $\mu_2(v)=\mu-\beta(v)$ (we may assume that μ does not depend on v) we find

$$[J_1(v)-J_2(v)]dv = 2f(v)dv\cdot e^{-2\mu x}\cdot\sinh^2[x\cdot\beta(v)]. \quad (3)$$

If the analyzer forms an angle φ with the direction of polarization, (3) must be multiplied with $\cos\varphi$. We assume that the analyzer forms an angle α with the polarizer, and that the neutrons pass through a magnetic field H (perpendicular to both polarizer and analyzer) and precess through an angle $\varphi_p=2\mu_n lH/\hbar v$. Then we have $\varphi=\varphi_p-\alpha$, and hence, if we integrate over v

$$J_1-J_2=\text{const.}\int f(v)dv\cdot\sinh^2[x\cdot\beta(v)]\cdot[\cos\alpha\cos\varphi_p(v)+\sin\alpha\sin\varphi_p(v)]$$

$$=\text{const.}\left[\cos\alpha\int f(v)dv\cdot\sinh^2[x\cdot\beta(v)]\cdot\cos\varphi_p(v)+\sin\alpha\int f(v)dv\cdot\sinh^2[x\cdot\beta(v)]\cdot\sin\varphi_p(v)\right]$$

$$=\text{const.}\,[\cos\alpha\cdot C+\sin\alpha\cdot S].$$

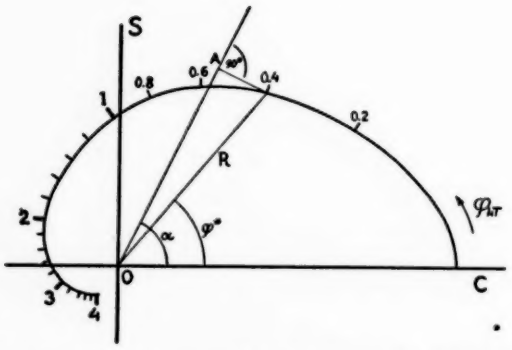

FIG. 6. Curve representing the precession of thermal neutrons. The distance OA indicates the polarization effect obtained for a given value (e.g., 0.4) of φ_{kT} and an angle α between polarizer and analyzer.

The functions C and S have been calculated (by numerical integration) and are plotted in Fig. 5. The abscissa is $\varphi_{kT}=H\cdot l\cdot 2\mu_n/\hbar(2kT/m)^{\frac{1}{2}}$, the angle through which neutrons with an energy of kT precess on their way l through the field H. For neutrons with a magnetic moment of 2 n.m. and thermal energy distribution at room temperature we have $\varphi_{kT}=0.088\,lH$. The scale of ordinates is chosen so that $C(O)=1$.

In calculating the functions C and S, we have made the following assumptions:

(1) $f(v)dv=\text{const.}\ v^2e^{-mv^2/2kT}dv$, which means Maxwellian distribution of the neutrons and $1/v$ sensitivity of the boron chamber. The integrations were carried from zero to infinity.

(2) $\sinh[x\beta(v)]\sim x\beta(v)$, which is correct for the larger part of the velocity spectrum where $x\beta(v)\ll 1$ (with $x\sim 1$ cm).

(3) $\beta(v)=\text{const.}/v$. This assumption[7] should be correct for the mean part of the spectrum, but tends to overemphasize the importance of the slowest neutrons. We have therefore recalculated a part of the function C for neutrons of room temperature, using for $\beta(v)$ the more accurate expression[7]

$$\text{const.}\,[K+1-(2K+1)^{\frac{1}{2}}]/K^2\,(K=0.43\cdot 10^{-10}\cdot v^2).$$

It is seen (Fig. 5, curve C′) that the initial slope is less steep, but the intersection with the axis of abscissae is not considerably shifted. It should be remembered, however, that the expression for $\beta(v)$ depends on the density distribution of those electrons which are responsible for the ferromagnetism of the polarizer material. Since this density distribution is not too well known, any determination of μ_n from the precession of neutrons with a wide velocity band would be somewhat uncertain. For high accuracy, experiments with neutrons of homogeneous velocity will be required.

In Fig. 6 a somewhat different representation of the functions C and S is given. Corresponding values of C and S are plotted as abscissae and ordinates, respectively, and the parameter φ_{kT} is noted along the curve. The polarization effect for any angle α between polarizer and analyzer and for any value of φ_{kT} may then be obtained in the way indicated in the figure. For a given value of φ_{kT} the largest polarization effect is obtained when the analyzer is placed in the direction of the vector R ($\alpha=\varphi^*$). The vector R represents therefore the "mean spin direction" in the beam, and its length is proportional to the polarization effect. If all the neutrons in the beam had the same velocity $v=v_{kT}=(2kT/m)^{\frac{1}{2}}$, then φ^* would be equal to φ_{kT} and the corresponding vector R would rotate at a uniform rate without changing in length, and would represent directly the precession of the neutrons. The velocity distribution of the neutrons has the effect that, firstly, the amount of R decreases with increasing φ_{kT} ("depolarization") and, secondly, φ^* is not proportional to φ_{kT}, but increases more slowly at large values of φ_{kT}; this is because the slowest neutrons are the first to be depolarized, and the remaining faster ones require stronger fields for precessing through the same angle.

In conclusion we wish to thank Professor Dr. N. Bohr for his kind interest and for putting the experimental resources of the Institute of Theoretical Physics at our disposal. For many stimulating discussions we wish to thank Drs. C. Møller, G. Placzek and V. Weisskopf.

The Isotopic Constitution of Gadolinium, Dysprosium, Erbium and Ytterbium

A. J. DEMPSTER
Ryerson Physical Laboratory, University of Chicago, Chicago, Illinois
(Received February 24, 1938)

The mass spectra of four rare earth elements have been photographed, by the use of a spark source for the ions. New faint isotopes have been found in all four. The mass numbers of the new isotopes and rough estimates of their abundance in percent are: Gd, 154 (1.5), 152 (0.2); Dy, 160 (1.5), 158 (0.1); Er, 164 (2), 162 (0.25); Yb, 170 (2), 168 (0.06).

THE isotopic constitution of all the rare earth elements has been examined by Dr. Aston[1] with anode rays.[2] The author has also photographed the mass spectra of cerium[3] and neodymium[4] and found in each of these elements two new faint isotopes that had not been observed by Aston. In samarium[4] no new isotopes were found.

The source of the neodymium ions was a spark between electrodes of the metal itself, and for cerium ions the spark was passed between electrodes made by packing nickel tubes with a mixture of the oxide and magnesium and aluminium powder. It was suggested by Hönigschmid[5] that the existence of two new isotopes at 148 and 150 might remove the discrepancy between his value of the atomic weight of neodymium 144.27 and Aston's mean value 143.5, but a measurement of their intensity by Mattauch and Hauk[6] showed they could account for only a part of the discrepancy. The remainder is removed if we take new values determined by them for the abundance of the strong components in place of those obtained by Dr. Aston.

Recently the attention of the author has been called to the possible existence of faint isotopes in other rare earth elements by Dr. Pool. His experiments on the radioactivity induced in these elements by fast neutrons[7] show that at least three new stable rare earth nuclei should exist, and it was thought desirable to examine the even numbered rare earth elements for possible faint isotopes. The stable atomic nuclei now appear to be bounded by radioactive forms, and it is thus of greater interest to complete the list of stable isotopes.

The mass spectrograph has been previously described.[8, 9] Dr. Pool kindly supplied a few milligrams of the oxides of the three elements Gd, Er, Yb from the samples used by him in his experiments. The electrodes were made by packing nickel tubes about one millimeter in diameter with the oxide mixed with a reducing agent. In these experiments, the reducing agent was either calcium, lanthanum or neodymium metal in the form of small filings. The heats of combination[10] are, for La_2O_3, 457 calories; for Nd_2O_3, 435 calories; for 3CaO, 456 calories. For the other rare earths, the values are apparently unknown. It was found that with lanthanum or neodymium as reducers, the spectra were several times as intense as with calcium. It was found that the oxides of the reducing agents appeared faintly, and with Gd, Dy, and Er, the oxides of neodymium could have been confused with their isotopes. In these cases, lanthanum or calcium was also used to reduce the oxides.

GADOLINIUM

Gadolinium oxide was first reduced with neodymium metal. A new isotope at mass 154 was observed on four photographs with exposures of ten to seventy minutes, and an isotope at 152 on two plates with seventy minutes exposure. A second series was made in which the oxide was reduced by lanthanum metal. Here the mass

[1] F. W. Aston, Phil. Mag. **47**, 385 (1924); **49**, 1191 (1925).
[2] F. W. Aston, *Mass Spectra and Isotopes*, (1933) p. 65, 127.
[3] A. J. Dempster, Phys. Rev. **49**, 947 (1936).
[4] A. J. Dempster, Phys. Rev. **51**, 289 (1937).
[5] O. Hönigschmid, Naturwiss. **25**, 701 (1937).
[6] J. Mattauch and V. Hauk, Naturwiss. **25**, 781 (1937).
[7] M. L. Pool and L. L. Quill, Phys. Rev. **53**, 437 (1938).
[8] A. J. Dempster, Proc. Am. Phil. Soc. **75**, 762 (1935).
[9] A. J. Dempster, Rev. Sci. Inst. **7**, 46 (1936).
[10] Bichowsky and Rossini, *Thermochemistry* (1936).

FIG. 1. Mass spectrum of erbium showing two new isotopes at 164 and 162. The mass at 169 is ascribed to thulium present as an impurity (about ½ percent). The mass at 155 is due to lanthanum oxide. The lines due to the strong components are broadened because of excessive over-exposure.

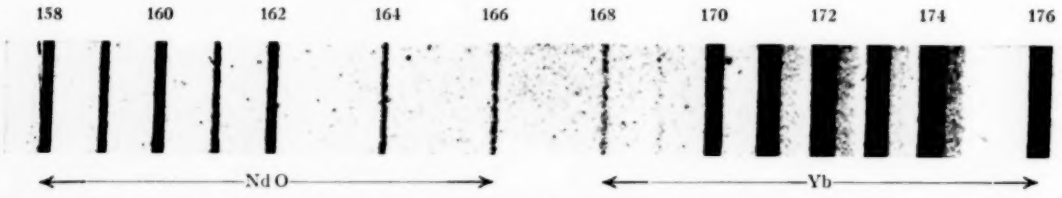

FIG. 2. Mass spectrum of ytterbium showing two new isotopes at 170 and 168. The lighter masses 166, 164, 162, etc. are due to neodymium oxide.

at 154 was observed on thirteen photographs with exposures ranging from half a minute to twenty minutes and the mass at 152 was observed on four with exposures of six to twenty minutes. From the series of photographs with different exposure times, it was estimated that the abundance of the new isotope at 154 was approximately 1.5 percent of the total and that the isotope at 152 was 0.2 percent of the total. The photographs also showed two europium lines at 151 and 153 with about the same intensity as the weakest gadolinium isotope at 152.

DYSPROSIUM

Two different samples of dysprosium oxide were used and reduced with lanthanum. In addition, one was reduced with calcium. Both samples showed two new isotopes at masses 160 and 158. One sample also showed strong lines at 165 and 159 due to holmium and terbium. With the second sample, these lines were much weaker. The isotope at 160 was found on 12 photographs with exposures from one-half to forty minutes, the one at 158 on 4 photographs. From the exposure times, it was estimated that the isotope at 160 makes up about 1.5 percent of the total, and the one at 158, 0.1 percent. In the second sample which was kindly supplied by Professor Quill, the holmium was estimated at 0.4 percent and the terbium at 0.2 percent. No line was observed at 166.

ERBIUM

Two new isotopes were also observed in erbium reduced with lanthanum at masses 164 and 162, the first on eleven photographs with exposures of ten seconds to twenty minutes and the second on four photographs with seven to twenty minutes' exposure. An example of the mass spectrum is given in Fig. 1. The abundances were estimated as approximately 2 percent for the mass at 164 and 0.25 percent for the mass at 162. The spectra also show a faint line at 169 (0.5 percent) which was ascribed to thulium. No other isotopes were observed as strong as 0.03 percent.

YTTERBIUM

The ytterbium oxide was reduced by neodymium and also showed two new isotopes at masses 170 and 168. The heaviest of the faint neodymium oxides came at 166. A spectrum is shown in Fig. 2. The mass at 170 was found on eight exposures of 20 seconds to 80 minutes, and the isotope at mass 168 on two exposures of 60 and 80 minutes. The abundances were estimated at 2.0 percent and 0.06 percent. Faint lines at 175 and 169 were ascribed to lutecium and thulium (<0.03 percent).

The thanks of the author are due to Professor M. L. Pool and Professor L. L. Quill for kindly supplying samples of the rare earth elements for use in the investigation, and to Dr. A. E. Shaw for assistance in preparing electrodes.

On the Sensitivity of the Balanced Space Charge Method for Detecting Ionization of Gases by Collision of Ions and Atoms

ANTONIO ROSTAGNI
Istituto di Fisica, R. Università di Messina, Italy

(Received November 30, 1937)

Factors which influence the balanced space charge method of detecting ionization are discussed. These factors are (1) the velocities of the ions, (2) the distances traveled by the ions before they are neutralized, (3) the effect of secondary electrons on the space charge. It is concluded that the reduced sensitivity in some experiments may account for the failure to observe ionization.

ONSET potentials for the ionization of gases by positive ions and atoms have been investigated in several papers by R. N. Varney,[1] who used a balanced space charge method. Last year he reported experiments on noble gases bombarded by their own accelerated atoms. His results for A and Ne agree quite well with those obtained previously by me.[2] With He atoms in He he does not observe any ionization up to 400 volts primary energy, while I have found a positive effect between 60 and 460 volts, and have measured the ionization efficiency, which is about ten percent that for A in A.[3]

Varney estimates, merely from the size of galvanometer readings, that his method would have revealed an ionization effect five percent that for A in A. For this reason and on account of the similitude of A and He curves, he is inclined to regard my results on He as having been due to some A impurities. Varney must implicitly have made some assumption about the relative effects of He and A on space charge, but on this very essential point no specification is given in his paper, and I shall show that, whatever the assumption may be, it must necessarily contain much that is arbitrary.

Neither does Varney stop to consider the *a priori* rather surprising fact that helium will behave so differently from argon and neon as his experiments indicate. We may remark by the way that a similar anomaly is shown also by previous experiments with the same method; for example Varney[4] does not observe any ionization of noble gases by the lightest alkali ions Li^+ and Na^+, with the exception of Ne by Na^+, while he has positive results with any other alkali ion noble gas combination.

It appears a legitimate question to ask whether the sensitivity of the space charge method has not been overestimated, in respect to its adaptation to the problem of ionization by massive particles. Investigations of this matter have not been published. I think they are necessary, because, as we shall see, the mechanism involved is quite different from all previous applications of the method.

The enormous efficiencies of positive ions in neutralizing electron space charge observed by Kingdon,[5] Foote and Mohler[6] and others are the result of two factors:

(1) The velocities of the ions are, for the same kinetic energy, i.e., for a given potential difference, some 10^2 times smaller than those of electrons (in inverse proportion to the square root of masses).

(2) Positive ions produced inside the diode with a small initial velocity component transverse to the filament must travel many times to and fro

[1] R. N. Varney, Phys. Rev. **47**, 483 (1935); **50**, 159 (1936); **50**, 1095 (1936). Varney, Gardner and Cole, Phys. Rev. **52**, 526 (1937).

[2] A. Rostagni, Nuovo Cimento **11**, 621 (1934); **13**, 389 (1936); Ricerca Scient. **7**, 511 (1936).

[3] My lowest measured point for He corresponds in the published diagram to 62 volts on the abscissa, and 0.01 cm^2/cm^3 on the ordinate (cross section for ionization); which represents, as explicitly stated in my paper, the sensitivity limit of the method. Direct extrapolation from the traced curves would point to an onset potential ranging between 50 and 60 volts. I therefore question Varney's statement that my results indicated ionization energies less than twice the electron ionization potential of He.

[4] R. N. Varney, Phys. Rev. **47**, 483 (1935). This partially negative result contradicts also Beeck and Mouzon's experiments by another method: Beeck and Mouzon, Ann. d. Physik **11**, 737, 858 (1931).

[5] Kingdon, Phys. Rev. **21**, 408 (1923).

[6] Foote and Mohler, Phys. Rev. **26**, 195 (1925).

across the inner space before they discharge themselves.

Under Kingdon's experimental conditions the average distance which an ion travels before reaching the filament is of the same order of magnitude as the kinetic mean free path. This may be some 10^2 times the cathode-anode distance at sufficiently low pressure. We thus obtain amplification factors of 10^4 to 10^6 for electron current with regard to positive ions as observed by different authors. Now the experimental conditions of Varney seem to me not very different from those of Kingdon, as regards the discriminating factor $V(r/R)^2$; but the pressure being of 10^{-2} mm of Hg, we should expect amplification factors of 10^3 both for A^+ and He^+ ions, with a ratio of about $\frac{3}{2}$ in favor of A. Varney gives much greater values; it is possible that he has determined them directly, by some method equivalent to those used by Kingdon, although no mention of that is made in his papers.

But there is an essential remark to be made. A necessary condition in order that factor (2) may be effective at all is that the initial energies of the ions should be less than the applied potential, so that if they will not hit the cathode they will be also unable to reach the anode. That is of course verified with ions produced by photoelectric effect or by electron collision as in the experiments of Foote and Mohler, Kingdon, etc; but in the present case, where the masses of colliding particles are of the same order of magnitude as the gas molecules, we must expect most of the secondary ions to receive a finite fraction of primary velocities. That is shown directly by my own experiments. And as the applied potential ranges between 1 and 2 volts (it must be less than the resonance potential of the gas) most of the ions will therefore reach the anode. Factor (2) then becomes inefficient. As the energy of many of the ions is large compared with that of electrons, also factor (1) will be affected.

Now the sensitivity of the space charge method is actually greater than it would appear from this remark, or the method would not have yielded any valuable result. The sensitivity may only arise from the partial neutralization of the secondary ions on the way to the anode, giving rise to slow tertiary ions for which both sensitivity factors may be efficient. This fact seems not to have been taken into consideration: the neutralization plays an essential part in the working of the ion detector and the mechanism is more complicated than in usual applications.[7] The efficiency must depend on the following quantities: (1) cross sections for neutralization; (2) cross sections for scattering; (3) velocities of slow ions arising from neutralization; all as functions of the velocity of secondary and eventually of tertiary ions. These quantities should be known for every ion velocity between primary and thermal velocity, but they are not completely known:[8] and in any case the problem will be much too complicated to allow a calculation either of absolute or of relative efficiency. To determine it by experiment, the ions under question must be produced under proper conditions.

Another effect which has been totally neglected in the discussion because of the relatively low sensitivity of the ion detector to electrons, is the secondary electron emission from metal surfaces. As it has been shown that the amplification factor measuring the ratio of sensitivities may be less than expected it seems advisable to examine whether secondary electrons may not sometimes influence the measurements and perhaps in extreme cases counterbalance the effect of positive ions on space charge, thus putting a practical limitation to the efficiency of the method.

The principal source of secondary electrons in the space charge cylinder would be of course the metal surface hit by the primary beam in front of the entrance hole. As a discriminating factor to the relative efficiency of the method in the investigation of various colliding particles in differents gases, we may of course adopt the quotient q_i/k of the cross section for ionization of the gas by the coefficient of electron liberation from the metal surface by the particles under question. These quotients have been measured by me[9] for both systems A gas A atoms, He gas He

[7] The part of neutralization in the working of the ion detector also in previous applications is probably more important than hitherto supposed, and ought to be taken into account for a complete theory of it; however it is not so essential as here.

[8] A. Rostagni, Nuovo Cimento **12**, 134 (1935); Atti di Torino **70**, 472 (1935). F. Wolf, Ann. d. Physik **29**, 33 (1935). For anomalies presented by both cross sections for ion velocities under 30 volts see also A. Rostagni, Atti del Congresso Galvani (Bologna, October, 1937) in press.

[9] A. Rostagni, Nuovo Cimento **11**, 621 (1934).

atoms and copper surfaces. For energies of the particles between 60 and 460 volts they are always about fifty times larger with A than with He.

We are forced to conclude that if secondary electron emission really can exert any limiting effect on the sensitivity of the method, that will be much stronger in He than in A.

In order to calculate the magnitude of the effect we may consider a particular case. With 200 volt He atoms in He at a pressure of 10^{-2} mm Hg q_i/k is 0.006 ions per electron-cm. Since the beam length in the space charge cylinder was 2 cm, and since the effective cross section for collision of He atoms of 200 volts energy in He gas at 10^{-2} mm is less than 0.1 cm^{-1}, it follows that more than 80 percent of the primary atoms will hit the top of the cylinder with full energy, and liberate there about 70 electrons per positive ion produced in the gas. As the wall is positive with respect to inner space, not all the electrons will be able to travel far from it, but, since the field is small and concentrated near the filament, there is no doubt that a large fraction of them will contribute to increase the negative space charge.

Besides, in the special arrangement for investigating ionization by atoms,[10] we may look for another possible source of secondary electrons at the back of aperture 3, where practically all primary ions stopped by the field between 3 and 4 fall with their full energy. Unless the cylinder is negative with respect to aperture 3 (no mention of that is made in Varney's paper), a large fraction of these secondaries will be conveyed by the same field, through aperture 4, into the cylinder.

The proportion of secondary electrons to the ions inside the space charge cylinder should then be of the order of 100 to 1, in the case of helium. This result seems to justify our doubts on the legitimacy of neglect of secondary electrons. Moreover, the coefficient k for He atoms is rapidly increasing between 50 and 100 volt (from 0.01 to 0.1), at a rate which is comparable with that of ionization;[11] therefore it seems possible that the augmentation of secondary emission has masked the onset of ionization. Above 100 volts the quotient q_i/k for He remains practically constant. Any further increase of the velocities of the atoms therefore will be of no use in making ionization detectable.

By way of conclusion: while the positive results of the balanced space charge method in determining onset potential are certainly the most reliable, in order to secure reliability of negative results the sensitivity of the method needs to be more thoroughly investigated. As regards the particular case of the ionization of helium I am of the opinion that Varney's published results do not prove anything against the consistency of mine. These are confirmed on the one side by independent measurements with two quite different arrangements, on ions as well as on atoms, and by the perfect agreement of part of them with Varney's positive results, on the other side. I do not see any specific reason why if my results on A and Ne are correct, those on He should be completely wrong, since I reject the too simplifying hypothesis that my He had been contaminated, and since the principal disturbing effect of collecting field methods, the secondary electron emission, has been directly accounted for. I have, however, pointed out two independent reasons why Varney's result on He could be inconsistent.

[10] See Fig. 1, in Phys. Rev. **50**, 159 (1935).

[11] A. Rostagni, Nuovo Cimento **11**, 99 (1934); Zeits. f. Physik **88**, 55 (1934).

The Sensitivity of the Balanced Space Charge Positive Ion Detector

ROBERT N. VARNEY
New York University, University Heights, New York, N. Y.

(Received February 19, 1938)

Additional information is given on the reaction of the balanced space charge detector to fast positive ions in the presence of gas in the tube. The sensitivity of the detector is analyzed, primarily in terms of experimental observations. Further notes on the mechanism of the detector are added.

IN view of the questions raised by Rostagni[1] on the sensitivity of the balanced space charge method of observing ionization of gases, used by the writer in several recent experiments,[2, 3] it is necessary to describe more in detail the observations which led to the estimated sensitivities reported for the method.

The basic features of the detector may be summarized:

1. A hot filament cathode emits a space charge limited electron current to an almost completely enclosing cylindrical anode.

2. A positive ion in the space charge region has the effect of neutralizing part of the space charge and thus allowing an increased electron flow to the anode.

3. This increased flow is measured in the balanced space charge method by a sensitive galvanometer connected in a balanced bridge circuit.

4. The size of the increased electron current per positive ion depends on the mean length of time a positive ion remains in the space compared with the same time for an electron.

5. The time a positive ion spends in the space depends on:

(a) Slow movement of the ion.
(b) A long free path for the ion.

Rostagni points out very accurately that neither of the conditions 5 (a) or 5 (b) are satisfied in the writer's experiments. (a) The positive ions all had high speeds. (b) The gas pressure was so high that free paths were short.

On the other hand, the writer did observe large effects by positive ions on the electron current, and this paper describes some experiments which indicate how Rostagni's proposed mechanisms actually operate.

The direct effect on the space charge electron current produced by a beam of positive alkali ions of various speeds was first observed. Gas pressures (A, Ne, N_2, He) ranging from less than 10^{-5} up to 10^{-2} mm of Hg were used. The results are summarized here:

1. From 0 to 10 volts ion speed, the ordinary positive ion effect on the space charge was observed. As predicted, it fell off rapidly with increasing speed.

2. Above 10 volts, the beam had a very nearly constant effect on the space charge current.

3. The size of the effect in 2 depended on the gas pressure. In vacuum the effect was very small. With gas pressures from 5×10^{-3} to 10^{-2} mm, the increase in electron current reached 250 to 300 times the actual positive ion current.

4. Helium pressures had to be higher than argon pressures to produce a given size of effect.

5. No conspicuous differences were observed among Li^+, Na^+, K^+, Rb^+, and Cs^+.

It is concluded from these experiments that scattering of ions in the gas plays an important role. The exchange of charge between alkali ions and atoms of the gases used is very small so can hardly influence the results. That scattering of fast ions from the anode cylinder walls may under favorable conditions influence the space charge current considerably is indicated in recent results of R. Kienzle[4] who tried similar experiments in vacuum.

Further analysis of the detector resulted from the failure to observe ionization in some cases, chiefly neon and helium, where Beeck and

[1] A. Rostagni, Phys. Rev. **53**, 729 (1938).
[2] R. Varney, Phys. Rev. **47**, 483 (1935).
[3] R. Varney, Phys. Rev. **50**, 159 (1936).
[4] R. Kienzle, Ann. d. Physik **30**, 401 (1937).

Mouzon[5] and Rostagni[6] were more successful. The writer attempted to set an upper limit on the ionization efficiencies which might escape detection by the balanced space charge method. A discussion of the effect in helium as compared with argon is given, as an example, below.

About 1/150 of the deflection produced by ionization of argon by 100 volt argon atoms could have been observed. The published figure, namely, that 1/20 (or 5 percent) of the ionization in argon could have been observed was based on the following:

(a) Helium ions of a given energy have over 3 times the speed of argon ions of the same energy. Since slow ions are more effective in space charge neutralization, this factor of 3 goes against the sensitivity to helium.

(b) It is more difficult to produce a beam of helium neutral atoms, as the charge exchange cross section for $(He^+ - He)$ is much less than for $(A^+ - A)$. It is the opinion of the writer that this factor far outweighs any considerations of space charge insensitivity. It is inapplicable to the results on ionization by positive ions, of course. To offset the difficulty, the initial intensity of the helium beam was enlarged by increasing the intensity of the preneutralization ion beam[3] by a factor of 2 of 3. The pressure of helium in the apparatus was varied over a range from 5×10^{-3} to 5×10^{-2} mm of Hg. (This figure was unfortunately omitted in the original report.) No trace of ionization was ever observed. The combination of factors (a) and (b) was set at 7.5 as a result. The sensitivity of the detector to helium must be reduced by this factor in comparison with argon. 1/150 of the deflection in argon could have been observed, so in helium 7.5 times this amount or 1/20 of the deflection in argon should have been detectable.

It may be pointed out here that Rostagni[1] has given an argument which the writer overlooked showing that helium ions will be more effective than argon ions in one respect. Since the collision cross section of argon is much greater than of helium (factor of at least 3), helium ions will travel much farther between collisions than argon ions. The sensitivity of the space charge detector depends on this distance between impacts, so a factor of 3 or more in favor of the sensitivity to helium results.

One experimental result, however, is probably more significant than all the complex analysis. The result is the following: The relative efficiencies for ionization of Ne by Na^+, A by K^+, etc., as observed, uncorrected, by the space charge method were of the same order of magnitude as Beeck[7] had observed by an absolute method. In fact they agreed as closely as 10 percent. No attempt at accurate comparisons of ionizations was made with the balanced space charge method, but the ion beam intensity and the gas pressures were kept practically constant for all ion sources. The galvanometer deflections in the balanced space charge circuit were thus roughly an indication of the combined efficiency of ionization and efficiency of detection. The close agreement with Beeck's measurements of ionization efficiency led to the conclusion that the efficiency of detection must have been nearly constant for different gases all the way from neon to xenon. The decreased sensitivity factor of 7.5 in going from argon to helium was thus believed to be by no means an underestimate.

Rostagni[1] has suggested a masking of the ionization in helium by secondary electrons. The use of more than one gas pressure should automatically eliminate this possible error, for a surface and a gas phenomenon can only coincide at one particular gas pressure. It would furthermore require that the coefficient of ionization and the coefficient of electron liberation be identical functions of voltage, and Rostagni's[6] results do not indicate this to be true in the important region near the onset voltage.

An error particularly to be feared was that secondary electrons ejected from the back of a slit might in some manner be accelerated into the detector and actually ionize the gas. We ruled this out quite certainly by intentionally placing an electron accelerating voltage between the last slit and the detector. It not only did not alter previous results, but ionization of such gases as He, N_2, and H_2 still did not appear. This same technique was used in all experiments including those on ionization by neutral atoms. Rostagni's[1] suggestion that secondary electrons might enter

[5] O. Beeck and C. Mouzon, Ann. d. Physik **11**, 737, 858 (1931).

[6] A. Rostagni, Nuovo Cimento **11**, 34 (1934).

[7] O. Beeck, Ann. d. Physik **6**, 1001 (1930).

from the back of the last slit seems to be definitely outlawed. The effect could at best be only of the second order of small quantities.

Just what mechanisms are involved in the space charge detector containing gas and used for fast ions is still difficult to conclude. Scattering from the walls and from gas atoms has already been advanced. I am indebted however to Professor L. B. Loeb[8] for an additional and important suggestion concerning the operation of the detector. If the filament of the detector is run at a very high temperature and the applied voltage is small, the space charge may be so heavy that an actual positive ion trap or potential trough of appreciable size exists between the filament and cylinder. If as the result of collisions or any other process, a positive ion finds itself in this trough with insufficient energy to escape, it may be extremely effective in neutralizing electron space charges. That this does occur is indicated by the frequent observations of the writer of an apparent increase in sensitivity of considerable magnitude with increase of filament temperature. Neither the space charge limited current nor the applied voltage was allowed to vary as the temperature was raised. The filament was already far into the space charge controlled region of emission at the start. The slight increase in potential drop down the filament was readily shown to be inadequate explanation of the sensitivity increase, for the plain variation of the applied potential gave no such effect.

Rostagni[1] has challenged the writer's negative results in some cases on the grounds that such results are surprising after all the positive ones with other noble gases. Without attempting to discuss what should or should not be expected, the writer feels obliged to point out that his statement that ionization efficiency in helium must be less than 5 percent of that in argon is hardly a denial of all ionization of helium by helium atoms. Rostagni's challenge could possibly be directed at the smallness of the result but not at its absence.

It has been pointed out previously, furthermore, that Beeck's data on the onset of ionization by positive ions fail to be even self-consistent in the cases (and only in those) where the writer has found no ionization by the balanced space charge method. Rostagni's[6] brilliant work on ionization by neutral atoms is clouded by a similar difficulty; the onset potential has been observed in every case to rise as the atomic weight decreases and as the ionization efficiency decreases. His result on He—He is the only one incompatible with this law.

[8] Private correspondence.

MAY 1, 1938 PHYSICAL REVIEW VOLUME 53

Quadrupole-Quadrupole Interatomic Forces

JULIAN K. KNIPP
Laboratory of Physics, University of Wisconsin, Madison, Wisconsin
(Received March 15, 1938)

Atoms the normal states of which are not S states experience quadrupole-quadrupole repulsive and attractive forces which vary as the inverse fifth power of the separation distance. At large distances, exchange being negligible, the expression for the interaction energy contains as factors two atomic coefficients and a root of a secular equation determined by the molecular state of the system. For a given atom the coefficient is determined by the nature of its lowest level. If one uses the Hartree-Fock approximation, it is proportional to the average of the square of the radial atomic distance for those electrons with orbital angular momentum not in complete shells. Atomic coefficients have been calculated for most of the atoms of the periodic table having incomplete p and d shells and the secular equations have been solved for a number of cases. At distances of twice the sum of the atomic radii, diatomic molecules resulting from the combination of such atoms of the first row of the periodic table have quadrupole-quadrupole energies of a few tenths of a volt, such energies becoming rapidly larger for smaller distances because of the inverse fifth power dependence.

1

WHEN two atoms are far enough apart that overlapping and consequent exchange effects are negligible, the interaction can be considered as being composed of mixed terms of different pole strengths. The terms are obtained from the expansion of the potential in a Taylor's

series in inverse powers of the interatomic distance. If the atoms are different, the dipole-dipole and dipole-quadrupole first-order interaction energies are zero because of the odd parity of the dipole portions of their potential terms. That is to say the expression for the energy is the sum of pairs of integrals, each referring to one atom alone. The integrand of each contains the product of two atomic functions, which product is even under inversion since the functions belong to the same atomic configuration. In addition each integrand contains a linear or quadratic function of the electron coordinates, referred to the nucleus of the atom in question. For first-order dipole-dipole or dipole-quadrupole interactions at least one of the any pair of such integrals contains a linear factor in its integrand, which being odd under inversion causes the integral to vanish. Moreover if either atom has spherical symmetry (S state), the first-order quadrupole-quadrupole energy is zero. Nonvanishing first-order dipole energies are obtained only if the atoms are the same and are in states with different parity. Second-order interaction energies do not in general vanish. They are sometimes referred to as polarization or induced energies. Since for two neutral atoms the expanded potential begins with the inverse third power of the interatomic distance, second-order energies vary with the inverse sixth and higher inverse powers of the distance. These interactions are those which produce van der Waals forces. They were first discussed extensively on the basis of quantum mechanics by London.[1] The most careful studies have been made for hydrogen and helium.[2]

Many atoms are not spherically symmetrical in the ground state; for these the quadrupole moment does not vanish. If we have two such atoms, there will be, in general, a nonvanishing first-order interaction. The quadrupole-quadrupole potential term varies with the inverse fifth power of the distance. London has noted in this connection that for two rotating molecules the quadrupole-quadrupole interaction energy will depend on the relative orientation of the two angular momenta.[3] The diagonal terms of the energy of interaction of two rotating neutral systems have in fact their dependence on orientation given by

$$(1/R^5)\{J(J+1)-3M^2\}\{J^*(J^*+1)-3M^{*2}\},$$

where J, M; J^*, M^* are the angular momentum and magnetic quantum numbers describing in part the states of the two systems and R is the separation distance. As London has pointed out, the interaction vanishes on the average over all orientations. However nondiagonal terms must be considered in an accurate treatment of the problem.

2

Let us introduce for the two atoms parallel sets of Cartesian axes, one with its origin in each nucleus, and let each have the z axis along the internuclear line. We shall use an asterisk to distinguish quantities referring specifically to the second atom. Thus coordinates, quantum numbers, wave functions (or states) are written, for example, x, M, Ψ when they refer to the first atom and x^*, M^*, Ψ^* when they refer to the second. If we have but two electrons, one near each nucleus, the expression for the quadrupole-quadrupole potential energy is

$$(3e^2/4R^5)\{r^2r^{*2}-5r^2z^{*2}-5r^{*2}z^2-15z^2z^{*2}+2(xx^*+yy^*-4zz^*)^2\}. \quad (1)$$

It is convenient to write this in terms of the following functions,

$$\begin{aligned} f(-2)&=\tfrac{1}{2}(\tfrac{3}{2})^{\frac{1}{2}}(x-iy)^2, \quad f(-1)=(\tfrac{3}{2})^{\frac{1}{2}}(x-iy)z, \\ f(0)&=\tfrac{1}{2}(3z^2-r^2), \quad f(1)=-(\tfrac{3}{2})^{\frac{1}{2}}(x+iy)z, \\ f(2)&=\tfrac{1}{2}(\tfrac{3}{2})^{\frac{1}{2}}(x+iy)^2. \end{aligned} \quad (2)$$

These functions have the property that they are partners belonging to the rows of the five-dimensional irreducible representation of the three-dimensional rotation group, which property

[1] F. London, Zeits. f. Physik **63**, 245 (1930).

[2] Slater and Kirkwood, Phys. Rev. **37**, 682 (1931); H. R. Hassé, Proc. Camb. Phil. Soc. **27**, 66 (1931); H. Margenau, Phys. Rev. **38**, 747 (1931); Pauling and Beach, Phys. Rev. **47**, 686 (1935).

[3] F. London, Zeits. f. physik Chemie **B11**, 222 (1931).

is helpful in evaluating matrix elements. Expression (1) becomes

$$(e^2/R^5)\{f(-2)f^*(2)+4f(-1)f^*(1)+6f(0)f^*(0)+4f(1)f^*(-1)+f(2)f^*(-2)\}. \quad (1a)$$

We define for a given atom the functions

$$F(m)=\sum f(m), \quad (2a)$$

where the summation is over all the electrons $1\cdots N$ of the atom. These atomic functions have the same rotational properties as the one electron functions. Summing (1a) over the electrons $1\cdots N$ of the first atom and $N+1\cdots N^*$ of the second atom, we obtain for the quadrupole-quadrupole interaction potential energy

$$e^2W/R^5\equiv(e^2/R^5)\sum_m a(m)F(m)F^*(-m),$$
$$a(-2)=a(2)=1, \quad (3)$$
$$a(-1)=a(1)=4, \quad a(0)=6.$$

3

The calculation of the energy of interaction of atoms at large separation distances is complicated by the fact that the atomic spin-orbit energy differences may be of the same order of magnitude. The doublet separation is only 0.0018 ev in the lowest term of boron but in the lowest term of thallium it is 0.94 ev. The limiting cases in which the energy differences are very small or very large compared to the interaction energy are most easily treated. For some atoms the atomic splitting is so small that it is negligible over a rather wide range of R. For other atoms it is at large distances much larger than the interaction; then at smaller distances the interaction becomes comparable to the splitting; at still smaller distances the molecular interaction is the dominant portion of the energy. We distinguish therefore the cases that the splitting in both of the atoms is negligible, the splitting in the first atom is large and in the second is negligible, and the splitting in both is large. Whether one of these cases is applicable to a pair of atoms depends of course on the value of R. Transition cases involve very complicated treatment except in the very simplest cases.

Let us suppose that Russell-Saunders coupling to exist in the states of the atoms. We restrict our attention to the states of an atom belonging to a definite term, distinguished by a symbol γ indicating the configuration of which it is a part and definite L and S indicating the total orbital and spin angular momenta.[4] Even or odd parity we distinguish by $\omega=\pm1$. If the spin-orbit splitting is neglected, all the levels of a term fall together and the atomic states are best described in the SLM_SM_L coupling scheme. On the other hand if the levels of a term are widely separated, we need consider only states of a given level, indicating the total angular momentum by J; under such circumstances the $SLJM$ coupling scheme is most suitable.

Let us now consider the case in which the atomic spin-orbit splitting is negligible. The characteristic values of the observables of the widely separated system are $\gamma\omega SLM_SM_L$; $\gamma^*\omega^*S^*L^*M^*_SM^*_L$. Let $\Psi(M_SM_L)$ be the Schrödinger representation of the state of the first atom and $\Psi^*(M^*_SM^*_L)$ be that of the second. We choose the relative phases so that the functions are partners belonging to the rows of the direct product of the Sth and Lth irreducible representations of the three-dimensional rotation-reflection group.[5] In neglecting exchange we we could very well use as our functions for the system simple products of the atomic functions. It is however almost as easy to use functions antisymmetrical in all the electrons. Such a presentation has the advantage that the correlation between atomic and molecular states is more apparent.

We first note that the original interaction energy was symmetrical in all $N+N^*$ electrons of the system while (3) is not. An unsymmetrical expression has been obtained from a symmetrical interaction by assuming particular electrons to belong to a given atom; a specific assignment is necessary if we are to expand the potential at this point of the treatment. If we use completely antisymmetrical wave functions, the expansion cannot be made until the functions have been substituted in the matrix integral and the latter reduced to expressions in which there are specific assignments of the electrons in each function. Those terms in which electrons are assigned to

[4] We use for the most part the atomic terminology of Condon and Shortley, *Theory of Atomic Spectra*.

[5] More accurately of the "unitary group" or the group of the two-dimensional unitary matrices of determinant 1; see, for instance, Wigner, *Gruppentheorie*.

different atoms will be small under the assumption of small overlapping. We therefore retain only terms in which the assignment is the same for each atom. It is then possible at this final stage to substitute expressions like (3) for the interaction.

It is simpler, however, to define from the start a function similar to (3) but having the desired property of symmetry and giving the same result for the energy as obtained by the process outlined above. We add to the definition of W the restriction that it vanish when the electrons $1\cdots N$ are not associated with the first atom and then sum over all exchanges Q, that is all permutations which lead to an ordered assignment in each atom. We obtain the symmetrical interaction

$$(e^2/R^5)T=(e^2/R^5)\sum_Q QW. \tag{3a}$$

As before, in computing energy matrices we finally obtain elements in which the electrons are assigned to specific atoms; we retain only those parts in which the assignment is the same for both functions for each atom. On introducing T there is only one term in the sum over Q which does not give zero, namely that which has the same assignment.

The symmetries of the system are those of rotations around the internuclear line, reflections in planes through this line, and in the case of like nuclei of inversion, that is reflections in the midpoint between the nuclei holding the nuclei fixed. The states of the system will, correspondingly, have quantum numbers Λ and Σ for the total orbital angular momentum and spin along the axis, be positive or negative (of importance only in Σ states), and for like nuclei be g or u. The possible molecular states and their relation to the states of the atoms when widely separated have been considered in detail by Wigner and Witmer.[6]

Let $\boldsymbol{S}$ be the total spin of the system. Its possible values are $S+S^*$, $S+S^*-1,\cdots,|S-S^*|$. We define the functions

$$\varphi(\boldsymbol{S}\Sigma M_L M^*_L)=\sum_{M_S}\Psi(M_S M_L)\times\Psi^*(\Sigma-M_S M^*_L)(SS^*M_S\Sigma-M_S|SS^*\boldsymbol{S}\Sigma), \tag{4}$$

which have been built up out of simple products by use of the vector model and belong to the $\boldsymbol{S}$th irreducible representation of the three-dimensional rotation group. The coefficients on the right are the elements of the usual transformation matrices for angular momenta.

Take first unlike atoms and $\Lambda\neq 0$. Let $c=\omega\omega^*(-)^{L+L^*}$. The two antisymmetrized functions

$$\psi(\boldsymbol{S}\Sigma\Lambda M_L)=A'\varphi(\boldsymbol{S}\Sigma M_L,\Lambda-M_L),\qquad c(-)^{\Lambda}\psi(\boldsymbol{S}\Sigma,-\Lambda,-M_L) \tag{5}$$

are partners belonging to the two rows of the Λth representation of the two-dimensional rotation-reflection group. The operator A' is defined as[7]

$$A'=(N!N^*!/(N+N^*)!)^{\frac{1}{2}}\sum_Q(-)^q Q,$$

where Q, as before, is a permutation which leads to an ordered assignment of electrons in each atom and q is the parity of Q. For a given Λ, M_L takes on the following values ($L\gtrless L^*$)

$$\begin{aligned}&L+L^*\gtrless\Lambda\gtrless L-L^*+1,\qquad M_L=L,L-1,\cdots,\Lambda-L^*;\\ &L-L^*\gtrless\Lambda>0,\qquad M_L=\Lambda+L^*,\Lambda+L^*-1,\cdots,\Lambda-L^*.\end{aligned} \tag{6}$$

This can be seen either by constructing a diagram or by calculating the character of the reducible representation. In addition we have for $\Lambda=0$

$$\psi\left(\boldsymbol{S}\Sigma\begin{matrix}a\\b\end{matrix}M_L\right)=\frac{1}{\sqrt{2}}A'\{\varphi(\boldsymbol{S}\Sigma M_L,-M_L)\mp\varphi(\boldsymbol{S}\Sigma,-M_L,M_L)\},\qquad M_L=L^*,L^*-1,\cdots>0, \tag{5a}$$

$$\psi(\boldsymbol{S}\Sigma\, b0)=A'\varphi(\boldsymbol{S}\Sigma\, 00).$$

The functions $\psi(a)$ are positive (Σ^+) if $c=-1$, negative (Σ^-) if $c=1$. On the other hand the functions $\psi(b)$ are positive if $c=1$, negative if $c=-1$. For a given c these functions belong to different irreducible representations. The matrix T is diagonal in $\boldsymbol{S}$, Σ, and Λ (also a and b) and moreover elements in which both states are replaced by partners will have the same values. The diagonality in $\boldsymbol{S}$ results from the fact that T is independent of the spin and therefore is

[6] Wigner and Witmer, Zeits. f. Physik **51**, 859 1928; also R. S. Mulliken, Phys. Rev. **36**, 1440 (1930); F. Hund, Zeits. f. Physik **63**, 723 (1930). For a good discussion see H. Sponer, *Molekülspektrum*, II pp. 132–137.

[7] Condon and Shortley, reference 4, p. 215.

symmetrical under all rotations of the spin axes alone.

Let us compute the matrix of W using the functions (4). It is no longer necessary to carry the quantum numbers $S\Sigma$. We find, because of the unitary nature of the transformation coefficients and the fact that the spin is not contained in W,

$$(M_L'M^*{}_L'|W|M_LM^*{}_L) = \sum_m a(m)(LM_L'|F(m)|LM_L) \times (L^*M^*{}_L'|F^*(-m)|L^*M^*{}_L). \quad (7)$$

Now the functions F belong to the representation 2 of the three-dimensional rotation group. The product $F(m)\Psi(M_L)$ occurring in the first of the elements on the right can be resolved by the vector model into a sum of functions χ belonging to representations L' according to the relation

$$\Psi(M_L)F(m) = \Sigma\chi(L2L'M_L+m) \times (L2L'M_L+m|L2M_Lm), \quad (8)$$

where again we have as coefficients the transformation functions for angular momenta. The summation is over the values $L'=L+2, \cdots, |L-2|$. Except for the case $L=0$ (S state), there is a χ in the sum belonging to the Lth representation. We have

$$(LM_L'|F(m)|LM_L) = A(L)\delta(M_L', M_L+m) \times (L2M_Lm|L2LM_L'), \quad (9)$$

using the orthogonality theorems for the scalar product. $A(L)$ is the scalar product of $\Psi(M_L)$ and $\chi(M_L)$ and is therefore independent of M and m. In this way we obtain for (7)

$$(M_L'M^*{}_L'|W|M_LM^*{}_L) = A(L)A^*(L^*) \times \delta(M_L'+M^*{}_L', M_L+M^*{}_L)a(M_L'-M_L) \times (L2M_LM_L'-M_L|L2LM_L') \times (L^*2M^*{}_LM^*{}_L'-M^*{}_L|L^*2L^*M^*{}_L'). \quad (7a)$$

The non-zero elements of T for the states of (5) and (5a) (unlike atoms) are found to be

$$(\Lambda M_L'|T|\Lambda M_L) = (M_L', \Lambda-M_L'|W|M_L, \Lambda-M_L),$$
$$\left(\begin{matrix}a\\b\end{matrix} M_L'|T|\begin{matrix}a\\b\end{matrix} M_L\right) = (M_L', -M_L'|W|M_L, -M_L) \mp (M_L', -M_L'|W|-M_L, M_L), \quad (10)$$
$$(bM_L'|T|b0) = \sqrt{2}(M_L', -M_L'|W|00),$$
$$(b0|T|b0) = (00|W|00).$$

Take next like atoms. The additional symmetry gives a reduction of the energy determinant, for g and u states do not mix. We define the functions

$$\psi\left(S\Sigma \begin{matrix}e\\f\end{matrix} \Lambda M_L\right) = \frac{1}{\sqrt{2}}A'\{\varphi(S\Sigma M_L, \Lambda-M_L) \mp \varphi(S\Sigma, \Lambda-M_L, M_L)\}, \quad (11)$$
$$M_L = L, L-1, \cdots > \tfrac{1}{2}\Lambda,$$

and in addition if Λ is even

$$\psi(S\Sigma f\Lambda\tfrac{1}{2}\Lambda) = A'\varphi(S\Sigma\tfrac{1}{2}\Lambda\tfrac{1}{2}\Lambda). \quad (11a)$$

$\psi(e)$ is g if S is odd (molecular triplets, etc.), u if S is even (molecular singlets, quintets, etc.). On the other hand $\psi(f)$ is g if S is even, u if S is odd. Moreover the states $\psi(e0M_L)$ are negative and the states $\psi(f0M_L)$ are positive. We have then the correlation ($\Lambda=0$) that negative states are g if S is odd and u if S is even, while positive states are g if S is even and u if S is odd. These functions belong to different representations of the group of inversions in the midpoint between the atoms. When $\Lambda\neq 0$, they belong to the second row of the Λth representation of the two-dimensional rotation-reflection group, their partners being the functions obtained by changing the signs of Λ and M_L and multiplying by $(-)^\Lambda$. The non-zero elements of T for the states of (11) and (11a) are

$$\left(\begin{matrix}e\\f\end{matrix}\Lambda M_L'|T|\begin{matrix}e\\f\end{matrix}\Lambda M_L\right) = (M_L', \Lambda-M_L'|W|M_L, \Lambda-M_L) \mp (M_L', \Lambda-M_L'|W|\Lambda-M_L, M_L), \quad (12)$$
$$(f\Lambda M_L'|T|f\Lambda\tfrac{1}{2}\Lambda) = \sqrt{2}(M_L', \Lambda-M_L'|W|\tfrac{1}{2}\Lambda\tfrac{1}{2}\Lambda),$$
$$(f\Lambda\tfrac{1}{2}\Lambda|T|f\Lambda\tfrac{1}{2}\Lambda) = (\tfrac{1}{2}\Lambda\tfrac{1}{2}\Lambda|W|\tfrac{1}{2}\Lambda\tfrac{1}{2}\Lambda).$$

4

Let us next consider briefly the case of two different atoms in one of which the atomic spin-orbit splitting is large and in the other it is negligible. We describe the states of the first atom in the $SLJM$ coupling scheme, keeping the second in the SLM_SM_L scheme, and consider only molecular states arising from a given J level. Introducing the new function

$$\varphi(JS^*M^*_SMM^*_L)=\Psi(JM)\Psi^*(M^*_SM^*_L), \quad (13)$$

we have at large distances the molecular states represented by the functions

$$\psi(JS^*M^*_S\Gamma M)=A'\varphi(JS^*M^*_SM,\Gamma-M), \quad (14)$$

for $\Gamma\neq0$. If J is an integer, Γ can in addition have the value zero, for which value we define the functions

$$\psi\left(JS^*M^*_S\begin{matrix}a\\b\end{matrix}M\right)=\frac{1}{\sqrt{2}}A'\{\varphi(JS^*M^*_SM,-M) \mp\varphi(JS^*M^*_S,-M,M)\}, \quad M\neq0; \quad (14a)$$

$$\psi(JS^*M^*_S\,b\,0)=A'\varphi(JS^*M^*_S00).$$

The possible values of M in these expressions depend on whether L^* is larger or equal to or less than J. We shall not write down the detailed expressions, for they are quite similar to the corresponding restrictions of the last section in any given case. There is one peculiarity which we note. The simultaneous rotation of spin and position axes does not give us a transformation group that is particularly useful. Instead we might introduce an artificial type of spin transformation depending on the space state of the particle in question. This is not necessary however, for one readily sees that T is diagonal in Γ and M^*_S. We define the expression

$$\begin{aligned}(JM'M^*_L'|W|JMM^*_L)&=\sum_m a(m)(JM'|F(m)|JM)\\&\quad\times(L^*M^*_L'|F^*(-m)|L^*M^*_L)\\&=C(J)A^*(L^*)\delta(M'+M^*_L',M+M^*_L)\\&\quad\times a(M'-M)(J2MM'-M|J2JM')\\&\quad\times(L^*2M^*_LM^*_L'-M^*_L|L^*2L^*M^*_L'). \quad (15)\end{aligned}$$

$C(J)$ is a scalar product independent of M and is zero if J is zero or one-half. In terms of this expression the non-zero elements of T are

$$\begin{aligned}&(J\Gamma M'|T|J\Gamma M)=(JM',\Gamma-M'|W|JM,\Gamma-M),\\&\left(J\begin{matrix}a\\b\end{matrix}M'|T|J\begin{matrix}a\\b\end{matrix}M\right)=(JM',-M'|W|JM,-M)\mp(JM',-M'|W|J,-M,M),\\&(JbM'|T|Jb0)=\sqrt{2}(JM',-M'|W|J00),\\&(Jb0|T|Jb0)=(J00|W|J00).\end{aligned} \quad (16)$$

5

We come finally to the case in which the spin-orbit splitting of the atomic term energies is large in both atoms. All atomic states are represented in the $SLJM$ scheme. The molecule has a quantum number Ω for the total angular momentum along the internuclear line. The components of the orbital angular momentum and spin are not defined separately. We introduce the function

$$\varphi(JJ^*MM^*)=\Psi(JM)\Psi^*(J^*M^*). \quad (17)$$

Consider unlike atoms and $\Omega\neq0$. Let

$$d=\omega\omega^*(-)^{J+J^*}.$$

The two antisymmetrized functions

$$\begin{aligned}&\psi(JJ^*\Omega M)=A'\varphi(JJ^*M,\Omega-M),\\&d(-)^\Omega\psi(JJ^*,-\Omega,-M),\end{aligned} \quad (18)$$

are partners belonging to the two rows of the Ωth representation of the two-dimensional rotation-reflection group in which the rotation of the spin as well as the position axes is carried out. For a given Ω, M takes on the values ($J\geqslant J^*$)

$$\begin{aligned}&J+J^*\geqslant\Omega\geqslant J-J^*+1, \quad M=J,J-1,\cdots,\Omega-J^*;\\&J-J^*\geqslant\Omega>0, \quad M=\Omega+J^*,\Omega+J^*-1,\cdots,\Omega-J^*.\end{aligned} \quad (19)$$

If J and J^* are integers or are half-integers, Ω

can in addition have the value zero. We define in case $\Omega=0$ the two sets of functions

$$\psi\left(JJ^*\begin{matrix}a\\b\end{matrix}M\right)=\frac{1}{\sqrt{2}}A'\{\varphi(JJ^*M,-M)\mp\varphi(JJ^*,-M,M)\},\quad M=J^*,J^*-1,\cdots>0, \tag{18a}$$

including if J and J^* are integers,

$$\psi(JJ^*b0)=A'\psi(JJ^*00). \tag{18b}$$

The functions $\psi(a)$ are positive (0^+) if $d=-1$, negative (0^-) if $d=1$ while the functions $\psi(b)$ are positive if $d=1$, negative if $d=-1$. The matrix T is diagonal in Ω (and a and b). We can express the results in terms of the expression

$$\begin{aligned}(JJ^*M'M^{*\prime}|W|JJ^*MM^*)&=\sum_m a(m)(JM'|F(m)|JM)\\&\quad\times(J^*M^{*\prime}|F^*(-m)|J^*M^*)\\&=C(J)C^*(J^*)\delta(M'+M^{*\prime},M+M^*)\\&\quad\times a(M'-M)(J2MM'-M|J2JM')\\&\quad\times(J^*2M^*M^{*\prime}-M^*|J^*2J^*M^{*\prime}).\end{aligned} \tag{20}$$

The non-zero elements of T for unlike atoms are found to be

$$\begin{aligned}&(JJ^*\Omega M'|T|JJ^*\Omega M)=(JJ^*M',\Omega-M'|W|JJ^*M,\Omega-M),\\&\left(JJ^*\begin{matrix}a\\b\end{matrix}M'|T|JJ^*\begin{matrix}a\\b\end{matrix}M\right)=(JJ^*M',-M'|W|JJ^*M,-M)\mp(JJ^*M',-M'|W|JJ^*,-M,M),\\&(JJ^*bM'|T|JJ^*b0)=\sqrt{2}(JJ^*M',-M'|W|JJ^*00),\\&(JJ^*b0|T|JJ^*b0)=(JJ^*00|W|JJ^*00).\end{aligned} \tag{21}$$

For like atoms in states of the same configuration and term ($\gamma^*=\gamma$, $S^*=S$, $L^*=L$, $\omega^*=\omega$) and the same J values, we define the functions

$$\psi\left(JJ\begin{matrix}e\\f\end{matrix}\Omega M\right)=\frac{1}{\sqrt{2}}A'\{\varphi(JJM,\Omega-M)\mp\varphi(JJ\Omega-M,M)\},\quad M=J,J-1,\cdots>\tfrac{1}{2}\Omega. \tag{22}$$

If J is an integer and Ω is even or if J is an half-integer and Ω is odd, we have in addition the function

$$\psi(JJf\Omega_2^1\Omega)=A'\varphi(JJ_2^1\Omega_2^1\Omega). \tag{22a}$$

$\psi(e)$ is u if J is an integer, g if J is a half-integer. $\psi(f)$ is g if J is an integer, u if J is a half-integer. When $\Omega\neq0$, these functions belong to the second row of the Ωth representation of the two-dimensional rotation-reflection group, their partners being the functions obtained by changing the signs of Ω and M and multiplying by $(-)^{2J+\Omega}$. For $\Omega=0$, g functions are positive and u functions are negative. The non-zero elements of T for like atoms with $J^*=J$ are found to be

$$\begin{aligned}&\left(JJ\begin{matrix}e\\f\end{matrix}\Omega M'|T|JJ\begin{matrix}e\\f\end{matrix}\Omega M\right)=(JJM',\Omega-M'|W|JJM,\Omega-M)\mp(JJM',\Omega-M'|W|JJ\Omega-M,M),\\&(JJf\Omega M'|T|JJf\Omega_2^1\Omega)=\sqrt{2}(JJM',\Omega-M'|W|JJ_2^1\Omega_2^1\Omega),\\&(JJf\Omega_2^1\Omega|T|JJf\Omega_2^1\Omega)=(JJ_2^1\Omega_2^1\Omega|W|JJ_2^1\Omega_2^1\Omega).\end{aligned} \tag{23}$$

The remaining possibility of like atoms in states belonging to the same configuration and term but with different J values leads to expressions which are somewhat more complicated than those considered because the coefficients involve both J and J^*. Since we are primarily interested in the lowest states of the atoms, we shall not discuss this case.

6

The elements of the matrix T in the cases discussed have as a common factor the product of

TABLE I. $\lambda(hh^*\delta)$ *for integral* δ. *If* δ *is not zero there are two states for each number listed. If the atomic term splitting is negligible in both atoms* ($h=L$, $h^*=L^*$, $\delta=\Lambda$), *the letters mean the following: Let* $c=\omega\omega^*(-)^{L+L^*}$. *If the atoms are different, an a after a number means that the state is positive* (Σ^+) *if* $c=-1$, *negative* (Σ^-) *if* $c=1$, *while b means that the state is positive if* $c=1$, *negative if* $c=-1$. *If the atoms are the same, an e means the state is g if the molecular spin is odd, u if it is even. An f means that the state is g if the spin is even, u if it is odd. Also for* $\Lambda=0$ *states with e are negative and states with f are positive. For other cases see the text.*

δ	$h=1$ $h^*=1$	2 1	3 1	4 1	1.5 1.5	2 2
0	0 *ea*	−1.014 *a*	−1.225 *a*	−1.305 *a*	2.4 *ea* 0 *ea*	2.774 *ea* −1.060 *ea*
	3.6 *fb* 0 *fb*	2.324 *b* −0.295 *b*	2.096 *b* −0.382 *b*	2.013 *b* −0.418 *b*	3.2 *fb* −0.8 *fb*	3.261 *fb* 1.508 *fb* −0.484 *fb*
1	0 *e*	2.456 0.047 −1.489	2.061 −0.170 −1.401	1.972 −0.289 −1.392	−1.6 *e*	1.202 *e* −0.917 *e*
	−2.4 *f*				1.2 *f* −0.8 *f*	1.127 *f* −1.413 *f*
2		0.356 −2.891	2.199 0.230 −1.939	1.367 0.347 −1.424	0.4 *e*	−2.000 *e*
	0.6 *f*				−2.8 *f*	0.857 *f* −1.857 *f*
3		1.014	0.646 −3.096	2.032 −0.032 −1.710		0.857 *e*
					1.2	−2.571 *f*
4			1.225	0.853 −3.222		
						1.714 *f*
5				1.354		

two atomic coefficients. Dividing by this common factor we obtain the elements of a dimensionless determinant the roots of which are needed to describe the quadrupole-quadrupole interaction between atoms.

In general let h, h^* be a pair of numbers, integers or half-integers, corresponding to L, L^*; J, L^*; or J, J^*. Let δ stand for Λ, Γ, or Ω as the case may be. The range of the remaining parameter (M_L or M) is essentially the same in all three cases. A comparison of (7a), (15) and (20) shows that for the same numerical values h, h^* the elements of W are the same aside from the atomic coefficients. If h^* is numerically different from h, we see from (10), (16) and (21) that on dividing out the atomic coefficients the dimensionless determinants are the same. For unlike atoms with $h^*=h$ there is one further simple reduction of the determinant possible. In this case ($L^*=L$, $L^*=J$, or $J^*=J$) we can form linear combinations $\psi(e)$ and $\psi(f)$ which are formally the same as for like atoms. It can be shown that T has no cross terms between these two groups and that the determinant is the same as obtained from the expressions for like atoms, that is from (12) or (23) on dividing out the coefficients. Thus we have the simplifying result that the dimensionless determinant depends only on the numerical values of the pair of numbers h, h^*. We shall designate the roots of a subdeterminant by $\lambda(hh^*\delta)$. How many roots there are for a given δ depends in general on how many times the δth representation is contained in the reducible representation obtained from the transformation under two-dimensional rotations and reflections of all the possible simple product functions of the atomic states.

Roots of the dimensionless determinant for some values of h and h^* are given in Tables I and II.

7

The atomic coefficients $A(L)$ and $C(J)$ are defined by the relations

$$A(L)(L2M_L0\,|\,L2LM_L) = (LM_L\,|\,F(0)\,|\,LM_L), \quad (24)$$
$$C(J)(J2M0\,|\,J2JM) = (JM\,|\,F(0)\,|\,JM).$$

To obtain explicit expressions, we transform to the zero-order representation scheme characterized by the one-electron quantum numbers $a=nlm_sm_l$. If we let A stand for the collection of

TABLE II. $\lambda(hh^*\delta)$ *for half-integral* δ.

δ	$h=1.5$ $h^*=1$	2 1.5	4.5 1
0.5	2.746 0 −1.049	2.864 1.551 −0.377 −1.168	1.977 −0.399 −1.345
1.5	0.176 −2.722	0.916 −1.195 −1.872	1.916 −0.206 −1.476
2.5	0.848	0.619 −2.770	1.883 0.125 −1.774
3.5		1.434	2.054 0.518 −2.339
4.5			0.934 −3.270
5.5			1.401

such quantum numbers in a zero-order state of the atom, we have for $A(L)$ the relation

$$A(L)(L2M_L0|L2LM_L)=\sum_{A,B}(\gamma SLM_SM_L|A)\times(A|F|B)(B|\gamma SLM_SM_L). \quad (25)$$

But only $A=B$ terms occur or are different from zero. For $(A|F|B)$ vanishes if A differs from B by more than one individual electron quantum number set and has the value $\pm(a|f|b)$ if all sets but $a\neq b$ are the same. But even this term is ruled out since if all but one of the m_l are the same, they must all be the same because of the condition $\Sigma m_l=M_L$ for both A and B. We have therefore for (25) the expression

$$\sum_A\{(\gamma SLM_SM_L|A)^2\sum_a(a|f|a)\}. \quad (26)$$

But

$$(a|f|a)=(-)\left[\frac{l(l+1)}{(2l-1)(2l+3)}\right]^{\frac{1}{2}}\times(l2m_l0|l2lm_l)\langle r^2\rangle_{Av}, \quad (27)$$

where

$$\langle r^2\rangle_{Av}=\int_0^\infty drr^2R(nl)^2, \quad (28)$$

$R(nl)/r$ is the radial part of the wave function for an electron in an nl state. We note that since the coefficient

$$(l2m_l0|l2lm_l)=\frac{3m_l^2-l(l+1)}{[(2l-1)l(l+1)(2l+3)]^{\frac{1}{2}}} \quad (29)$$

when summed over the electrons in complete shells gives zero, contributions to $A(L)$ will come only from incomplete shells. All atoms whose normal states are not S states have one incomplete shell having angular momentum. We can write

$$A(L)=B(L)\langle r^2\rangle_{Av}, \quad C(J)=D(J)\langle r^2\rangle_{Av}. \quad (30)$$

The second factor in each case is the average value of r^2 for electrons in that shell. We have

$$B(L)=(-)\left[\frac{l(l+1)}{(2l-1)(2l+3)}\right]^{\frac{1}{2}}\sum_A\left\{(\gamma SLM_SM_L|A)^2\sum_{m_l}\frac{(l2m_l0|l2lm_l)}{(L2M_L0|L2LM_L)}\right\}. \quad (31)$$

Likewise if we start in the $SLJM$ scheme we obtain

$$D(J)=(-)\left[\frac{l(l+1)}{(2l-1)(2l+3)}\right]^{\frac{1}{2}}\sum_A\left\{(\gamma SLJM|A)^2\sum_{m_l}\frac{(l2m_l0|l2lm_l)}{(J2M0|J2JM)}\right\}. \quad (32)$$

TABLE III. *Atoms with incomplete p-shells. A star after an element means the spin-orbit splitting of the lowest energy term is less than 0.036 ev. Abbreviations (s.c) and (s.c.f) are used to distinguish numbers obtained using shielding constant and self-consistent field wave functions, respectively.*

Element	Ground Level		$B(L)$	$D(J)$	r_m in Bohr radii		$\langle r^2\rangle_{Av}$(np) in (Bohr radii)^2	
	np				(s.c)	(s.c.f)	(s.c)	(s.c.f)
B*	$2p$	$^2P^0_{1/2}$	-0.6325	0	1.54	1.80	4.4	9.12
Al*	$3p$	"	"	"	2.57		10	
Ga	$4p$	"	"	"	2.74		11	
In	$5p$	"	"	"	3.20		14	
Tl	$6p$	"	"	"	3.53		17	
C*	$2p^2$	$^3P_0$	$+0.6325$	0	1.23	1.26	2.8	4.882
Si*	$3p^2$	"	"	"	2.17		7.3	
Ge	$4p^2$	"	"	"	2.42		8.5	
Sn	$5p^2$	"	"	"	2.83		11	
Pb	$6p^2$	"	"	"	3.12		14	
O*	$2p^4$	$^3P_2$	-0.6325	-0.3743	0.88	0.85	1.4	2.440
S	$3p^4$	"	"	"	1.65		4.2	
Se	$4p^4$	"	"	"	1.97		5.6	
Te	$5p^4$	"	"	"	2.30		7.5	
F	$2p^5$	$^2P^0_{3/2}$	$+0.6325$	$+0.4472$	0.77	0.73	1.1	1.82
Cl	$3p^5$	"	"	"	1.48		3.4	
Br	$4p^5$	"	"	"	1.80		4.7	
I	$5p^5$	"	"	"	2.11		6.2	

The transformation coefficients to the zero-order scheme are usually simplest for extreme values of $M_S M_L$ or M. They can often be obtained for extreme values by inspection. Otherwise they are readily obtainable with the help of the angular momentum operators as used by Gray and Wills.[8]

8

We come now to the problem of obtaining the numerical values of $\langle r^2\rangle_{Av}$. In Tables III and IV we have listed most of the elements for which these considerations are of interest. The second column in the tables gives the nature of the lowest level of the atoms. We restrict our discussion to the lowest term or level.

The average value of r^2 has been estimated for each atomic valence l electron by using the shielding constants and effective principal quantum numbers of Slater.[9] Such a method gives unreliable values, however, especially for light atoms. This is because the major contribution to the average value comes in the expression (28) from values of r out beyond the maximum of the density function. In this range it is well known that simple functions with shielding constants are poor approximations. The error is presumably less for an electron with a large principal quantum number, n, since the peak of the density function is sharper and the value obtained more nearly the square of the radius at the maximum, r_m. The magnitude of the error for small n is shown by the values which we have calculated for B, C, O and F using wave functions obtained from the self-consistent field.[10] The numbers so obtained are approximately twice those calculated from shielding constants.

The self-consistent field probably gives wave functions which are too large at large distances. Electrons are kept away from the neighborhood of the nucleus because of the static nature of the electron field which the method uses. This tendency to favor a more diffuse distribution is more clearly the case when no account is taken of exchange. The value of $\langle r^2\rangle_{Av}$ is a very sensitive function of such effects. For the chlorine negative ion the value of $\langle r^2\rangle_{Av}(3p)$ has been calculated with exchange to be[11] $5.137a_0^2$ (a_0 = Bohr radius). The closely related diamagnetic susceptibility is calculated to be $-30.4\cdot10^{-6}$. Without exchange the diamagnetic susceptibility is calculated to be $-41.3\cdot10^{-6}$ which corresponds to a value of $\langle r^2\rangle_{Av}(3p)$ of about $7.4a_0^2$. The self-consistent field functions for oxygen and carbon were obtained without exchange and hence the values for $\langle r^2\rangle_{Av}$ obtained for these atoms are probably much too large, judging from the effect of exchange on Cl^-. The importance of exchange in neutral atoms may be slightly less however. The function for F (also Ne and F^-, Table V) was calculated with exchange between the $2p$ electrons. Boron has but one $2p$ electron. The values for these atoms are probably quite good.[12]

Additional information is obtainable from the diamagnetic susceptibility of closely related atoms. The diamagnetic susceptibility of a gas of atoms in singlet states is given by Van Vleck's expression, $-0.79\cdot10^{-6}\Sigma\langle r^2\rangle_{Av}$, where the sum is over all the electrons of an atom. In Table V we have some experimental values for Ne and A obtained by Havens and in addition some values

TABLE IV. *Atoms with incomplete d shells. Numbers in parentheses are positions of maximum radial density of the two electrons in the s shell lying outside the incomplete d shell, which electrons are most effective in determining the radius of the atoms.*

Element	Ground Level nd		$B(L)$	$D(J)$	r_m in Bohr Radii (s.c)	$\langle r^2\rangle_{Av}$(nd) in (Bohr Radii)^2 (s.c)
Sc*	$3d4s^2$	$^2D_{3/2}$	−0.5345	−0.4472	3.00(4.55)	14
Y	$4d5s^2$	"	"	"	4.55(5.33)	30
La	$5d6s^2$	"	"	"	5.33(5.88)	40
Ti	$3d^24s^2$	$^3F_2$	−0.2213	−0.1833	2.47(4.35)	9.5
Zr	$4d^25s^2$	"	"	"	3.75(5.08)	20
Hf	$5d^26s^2$	"	"	"	4.38(5.60)	27
V	$3d^34s^2$	$^4F_{3/2}$	+0.2213	+0.1533	2.09(4.15)	6.8
W	$5d^45s^2$	$^5D_0$	+0.5345	0	3.23(5.11)	15
Fe	$3d^64s^2$	$^5D_4$	−0.5345	−0.4006	1.44(3.65)	3.2
Co	$3d^74s^2$	$^4F_{9/2}$	−0.2213	−0.1935	1.32(3.51)	2.7
Ni	$3d^84s^2$	$^3F_4$	+0.2213	+0.2003	1.21(3.38)	2.3
Ir	$5d^9$	$^2D_{3/2}$	+0.5345	+0.4782	2.58	9.4

Additional information is obtainable from the diamagnetic susceptibility of closely related atoms. The diamagnetic susceptibility of a gas of atoms in singlet states is given by Van Vleck's expression, $-0.79\cdot10^{-6}\Sigma\langle r^2\rangle_{Av}$, where the sum is over all the electrons of an atom. In Table V we have some experimental values for Ne and A obtained by Havens and in addition some values

[8] Gray and Wills, Phys. Rev. **38**, 248 (1931).
[9] J. C. Slater, Phys. Rev. **36**, 57 (1930).
[10] Self-consistent field data have been calculated from functions given by the following: B, Brown, Bartlett and Dunn, Phys. Rev. **44**, 296 (1933); C, C. C. Torrance, Phys. Rev. **46**, 388 (1934); O, Hartree and Black, Proc. Roy. Soc. **139**, 311 (1933); F, F^-, and Ne, with exchange between p electrons, F. W. Brown, Phys. Rev. **44**, 214 (1933).
[11] Hartree and Hartree, Proc. Roy. Soc. **156**, 60 (1936); Cl^- with exchange. The value of 7.4 for $\langle r^2\rangle_{Av}(3p)$ without exchange is only approximate since the numbers for inner electrons without exchange are not given.
[12] Unfortunately some doubt as to the accuracy of the functions is cast by Brown's result for the electron affinity of fluorine. He obtained a negative number for the electron affinity when effects due to the change in the function on removal of the electron were included.

for the negative halogen ions obtained by Brindley and Hoare from salt crystals using the assumption of additivity of the susceptibilities of the two ions of the salts.[13] The magnetic susceptibility of Ne obtained from the self-consistent field with exchange between the $2p$ electrons is only five percent greater than the experimental value. If we calculate back from the experimental values using Slater values for the inner electrons, which contribute only a small fraction of the sum, we obtain the numbers for $\langle r^2\rangle_{Av}$ listed in the fifth column (the numbers in parentheses have been obtained from self-consistent field values for the inner electrons). We see that for Ne the difference is about ten percent. However with ions the agreement is not so good. The experimental values are much smaller than the values from the self-consistent field. This result is not surprising since each ion is in the disturbing field of its neighbors. The crystals are not completely ionic; Ewing and Seitz have shown by the application of the Hartree approximation to LiH and LiF crystals that there is considerable charge in the neighborhood of the metallic ion.[14] The picture of the valence electrons localized in a region about the electron-negative atoms is not a very accurate one.

We have a lower bound for $\langle r^2\rangle_{Av}$ for chlorine in the number 2.88 for argon and an upper bound in the number 5.137 for the chlorine negative ion.

9

If one of the three cases discussed in Sections 3, 4, and 5 is applicable, the quadrupole-quadrupole interaction energy between two atoms is given by one of the expressions

$$\begin{aligned}&(e^2/R^5)A(L)A^*(L^*)\lambda(LL^*\Lambda),\\&(e^2/R^5)C(J)A^*(L^*)\lambda(JL^*\Gamma),\\&(e^2/R^5)C(J)C^*(J^*)\lambda(JJ^*\Omega).\end{aligned}\tag{33}$$

The results would be of more significance if we knew at what distances other forces begin to be of equal strength. It is not easy to say however. At large distances the Heitler-London method gives the repulsive forces to a good approximation. From Sugiura's formula[15] we obtain for hydrogen at a separation distance of $4a_0$ for the lowest singlet and triplet states -0.27 ev and 0.20 ev, respectively. The induced polarization or van der Waals attraction is slightly smaller at this distance. Using the coefficients of Pauling and Beach,[2] we obtain for the first three terms (terms in the inverse sixth, eighth and tenth powers of R) the numbers of the expression $-(0.0429+0.0513+0.0293)$ ev $=-0.124$ ev.[16] For purposes of comparison let us find the distance at which the Heitler-London repulsion between two helium atoms is 0.2 ev. Slater has calculated this energy[17] and has obtained the expression $484\exp(-2.43R/a_0)$ ev. For 0.2 ev we find $R=3.2a_0$. At $R=4r_m\leqq 2.2a_0$ the repulsive energy is 2.3 ev (r_m is the position of the maximum of the radial density function). Using Margenau's coefficients we find for the van der Waals energy of two helium atoms $-(0.039+0.030+0.011)$ ev $=-0.080$ ev at $R=3.2a_0$. The Heitler-London energy, being essentially a penetration energy, builds up and falls off faster than an inverse power energy. As pointed out in the preceding section, for heavy atoms the electron distribution function dies off more rapidly beyond the last maximum than for light atoms. If for comparison we use a distance of twice the sum of the atomic radii, that is twice the sum of r_m, the exchange forces should be relatively smaller at such distances for heavy atoms than for light. For atoms with incomplete d shells the situation is complicated by the presence of an outside s shell.

TABLE V. *Data for some closely related atoms.*

	Magnetic Susceptibility 10^6			$\langle r^2\rangle_{Av}(np)$ in (Bohr Radii)^2		
	Expt.	(s.c)	(s.c.f)	From Expt.	(s.c)	(s.c.f)
Ne	-7.651 ± 0.008	-5.58	-8.08	1.20(1.23)	0.88	1.32
A	-19.23 ± 0.20	-18.5		2.88	2.77	
F^-	-9.4	-8.13	-17.1	1.48(1.50)	1.28	3.12
Cl^-	-24.2	-25.2	-30.4	3.64(3.82)	3.81	5.137
Br^-	-34.5	-39.3		4.38	5.14	
I^-	-50.6	-58.6		5.58	6.84	

[13] G. G. Havens, Phys. Rev. **43**, 992 (1933). Brindley and Hoare, Proc. Roy. Soc. **152**, 342 (1935).
[14] Ewing and Seitz, Phys. Rev. **50**, 760 (1936).
[15] Y. Sugiura, Zeits. f. Physik **45**, 484 (1927); see H. Bethe, *Handbuch der Physik*, Vol. 24, p. 537.
[16] In hydrogen the van der Waals energies are more important than exchange energies for R greater than about $7a_0$. For $R=7a_0$ the three van der Waals terms are in the proportion 1, 1/2, 1/8. The approximations made in calculating the coefficients are poor for smaller distances.
[17] J. C. Slater, Phys. Rev. **32**, 349 (1928).

TABLE VI. *Energies of attraction at distances of twice the sum of the atomic radii. The atomic radius is defined as the position of the last maximum in the electron density function. The spin-orbit coupling has been neglected and the values for* $\langle r^2 \rangle_{Av}$ *taken from the last column of Table III. The last four molecules have in addition attractive* Δ *states at this distance with energies one-sixth the energies of the* Σ *states and the same multiplicities (neglecting other forces). The known states listed are those which have been observed and which on dissociation go into normal states of the atoms.* $2r_e$ *is for the equilibrium position of the lowest observed state.*

	KNOWN STATES	$2r_e$ 10^8 cm	R 10^8 cm	E'EV	STATES
B_2			3.80	−0.112	$^1\Pi_g$, $^3\Pi_u$
BO	$^2\Sigma^+$, $^2\Pi$	2.4	2.80	−0.139	$^2\Pi$, $^4\Pi$
C_2	$^3\Pi_u$?	2.62	2.66	−0.190	$^1\Pi_g$, $^3\Pi_u$, $^5\Pi_g$
CF			2.10	−0.231	$^2\Pi$, $^4\Pi$
O_2	$^3\Sigma_g^-$, $^1\Sigma_g^+$, $^3\Sigma_u^+$	2.4	1.80	−0.341	$^1\Pi_g$, $^3\Pi_u$, $^5\Pi_g$
F_2	$^1\Pi$?		1.54	−0.406	$^1\Pi_g$, $^3\Pi_u$
BC			3.23	−0.202	$^2\Sigma^-$, $^4\Sigma^-$
BF			2.67	−0.195	$^1\Sigma^+$, $^3\Sigma^+$
CO	$^1\Sigma^+$, $^3\Pi$, $^1\Pi$	2.26	2.23	−0.347	$^1\Sigma^+$, $^3\Sigma^+$, $^5\Sigma^+$
OF			1.67	−0.549	$^2\Sigma^-$, $^4\Sigma^-$

If we have two atoms in P states and neglect the atomic multiplet splitting, we see from the first column of Table I that the states of the system fall into four energy levels due to the quadrupole-quadrupole interaction of the two atoms. In Table VI are given the energies for the lowest (attractive) levels at distances of twice the sum of the atomic radii for the molecular pairs obtainable from B, C, O and F. Consider B_2 and F_2. The atoms have spin $\frac{1}{2}$, which give $\boldsymbol{S}=0, 1$. Also $c=1$. From Table I we see that the lowest states ($\lambda=-2.4$) are f states. This means that $^1\Pi$ and $^3\Pi$ are g and u, respectively. Similarly we find that for the next level, which has zero energy, the states are $^1\Sigma_u^-$, $^3\Sigma_g^-$, $^1\Sigma_g^+$, $^3\Sigma_u^+$, $^1\Pi_u$, $^3\Pi_g$. The third level has the states $^1\Delta_g$, $^3\Delta_u$ and an energy $-\frac{1}{4}$ that given in Table VI, that is it is repulsive. The fourth level has the states $^1\Sigma_g^+$, $^3\Sigma_u^+$ and an energy -1.5 that of the lowest level.

For C_2 and O_2 since the spins are both 1, $\boldsymbol{S}=0, 1, 2$. The lowest level has the states $^1\Pi_g$, $^3\Pi_u$, $^5\Pi_g$ for which the energy is given in Table VI. The states $^1\Sigma_u^-$, $^3\Sigma_g^-$, $^5\Sigma_u^-$, $^1\Sigma_g^+$, $^3\Sigma_u^+$, $^5\Sigma_g^+$, $^1\Pi_u$, $^3\Pi_g$, $^5\Pi_u$ have zero energy. The states $^1\Delta_g$, $^3\Delta_u$, $^5\Delta_g$ are repulsive, the energy being $-\frac{1}{4}$ that of the lowest level, and the states $^1\Sigma_g^+$, $^3\Sigma_u^+$, $^5\Sigma_g^+$ are also repulsive, having energy -1.5 that of the lowest level. For BO and CF since the atomic spins are $\frac{1}{2}$, 1, $\boldsymbol{S}=\frac{1}{2}, \frac{3}{2}$. Also $c=-1$. AA^* is positive. The lowest level has the states $^2\Pi$, $^4\Pi$. The states $^2\Sigma^+$, $^4\Sigma^+$, $^2\Sigma^-$, $^4\Sigma^-$, $^2\Pi$, $^4\Pi$ have zero energy; the states $^2\Delta$, $^4\Delta$ have energy $-\frac{1}{4}$ that of the lowest level; the states $^2\Sigma^-$, $^4\Sigma^-$ have energy -1.5 that of the lowest level.

For BC and OF the atomic spins are $\frac{1}{2}$, 1 and therefore $\boldsymbol{S}=\frac{1}{2}, \frac{3}{2}$. We see that $c=-1$ and that AA^* is negative. The lowest level is therefore given by $\lambda=3.6$. Its states are $^2\Sigma^-$, $^4\Sigma^-$. The next energy is also attractive, $\frac{1}{6}$ that of the lowest level, and has the states $^2\Delta$, $^4\Delta$. The states $^2\Sigma^+$, $^4\Sigma^+$, $^2\Sigma^-$, $^4\Sigma^-$, $^2\Pi$, $^4\Pi$ have zero energy; the states $^2\Pi$, $^4\Pi$ are repulsive and have an energy $-\frac{2}{3}$ that of the lowest energy. For CO the spins are 1 and $\boldsymbol{S}=0, 1, 2$. $C=1$ and AA^* is negative. The lowest level has the states $^1\Sigma^+$, $^3\Sigma^+$, $^5\Sigma^+$. The next has $\frac{1}{6}$th the energy and the states $^1\Delta$, $^3\Delta$, $^5\Delta$. The states $^1\Sigma^-$, $^3\Sigma^-$, $^5\Sigma^-$, $^1\Sigma^+$, $^3\Sigma^+$, $^5\Sigma^+$, $^1\Pi$, $^3\Pi$, $^5\Pi$ have zero energy. The states $^1\Pi$, $^3\Pi$, $^5\Pi$ are repulsive with an energy $-\frac{2}{3}$ that of the lowest level. The level scheme of BF is the same as CO except that both spins are $\frac{1}{2}$ and therefore there are no molecular quintets.

The writer takes pleasure in acknowledging his indebtedness to Professor Wigner, who brought the problem to his attention, for advice and stimulating discussion. He wishes to thank the Wisconsin Alumni Research Foundation for its support of this work.

The Process of Diffusion in a Centrifugal Field of Force

WILLIAM J. ARCHIBALD
Rouss Physical Laboratory, University of Virginia, Charlottesville, Virginia
(Received January 11, 1938)

The general equation for the settling of particles and molecules in a liquid suspension or ideal solution in a centrifuge has been solved for the case of a sector-shaped cell extending to the center of the centrifuge. Curves are given which show the concentration at all points in the cell for different values of the time.

IF a liquid solution be placed in a gravitational field of force, the distribution of concentration changes from a uniform distribution initially to an exponential one after an infinite time. The differential equation which represents the concentration at a point in the solution at any time t has been completely solved by Mason and Weaver[1] for the case of a uniform gravitational field. It is the purpose of the present paper to consider the differential equation which applies to an ideal dilute solution placed in a centrifugal field of force. This equation has been derived by Lamm[2] and an approximate solution of it has been obtained by Faxen.[3] But the solution given by Faxen cannot be used conveniently for numerical computation and consequently has been of little use for comparing theory and experiment.

Consider a dilute solution in a sector-shaped cell in a centrifuge which is rotating with a constant angular velocity ω. In Fig. 1 OAB is a cross section of the cell in which the solution is confined. The distances of two cylindrical surfaces from the axis of rotation which passes through O, are r and $r+dr$. Let the concentration at the surface r be c, where c is understood to mean the number of dissolved molecules per cm³ of solution. The quantity of dissolved substance crossing the surface at r in an outward direction in unit time is

$$Q=(\omega^2rsc-D(\partial c/\partial r))r\theta h,$$

where h is the depth of the cell. In this expression s, which is the velocity of settling of the dissolved substance in unit gravitational field, is known as the sedimentation constant. D is the coefficient of diffusion which will be defined precisely below. The net accumulation of substance per second in the layer of thickness dr is $-(\partial Q/\partial r)dr$, which is also represented by $(\partial c/\partial t)r\theta hdr$. Thus the following relation holds

$$-\frac{\partial}{\partial r}\left\{\left(\omega^2rsc-D\frac{\partial c}{\partial r}\right)r\right\}\theta hdr=\frac{\partial c}{\partial t}r\theta hdr$$

$$\frac{1}{r}\frac{\partial}{\partial r}\left\{\left(D\frac{\partial c}{\partial r}-\omega^2rsc\right)r\right\}=\frac{\partial c}{\partial t}. \qquad (1)$$

The solution of (1) will give the concentration c as a function of r and t.

The diffusion constant D can be expressed in terms of other quantities as follows. In the final steady state the quantity of dissolved substance moving outward under the action of the centrifugal field is equal to the quantity diffusing inward under the action of the concentration gradient. Consider a single particle of the substance in solution. If a gravitational force X acts on it, it will acquire a terminal drift velocity v, since it is moving through a viscous medium, which is given by Stoke's law as $v=X/f$, where f is the frictional constant. In consequence of this velocity there will flow per second through an area $r\theta h$ a quantity of dissolved substance $vcr\theta h$ or

$$(X/f)cr\theta h. \qquad (2)$$

For the steady state it can be shown[4] that the concentration at any point r is given by

$$c=c_0'\exp\left[M(1-V\rho)\omega^2r^2/2RT\right], \qquad (3)$$

where c_0' is the concentration at $r=0$, M is the molecular weight of the dissolved substance, V its partial specific volume, ρ the density of the pure solvent, R the gas constant and T the

[1] Mason and Weaver, Phys. Rev. **23**, 412 (1924).
[2] Lamm, Arkiv Mat., Astro. Fysik **21B**, No. 2 (1929).
[3] Faxen, Arkiv. Mat., Astro. Fysik **21B**, No. 2 (1929).
[4] Svedberg, *Colloidal Chemistry*.

absolute temperature. From (3) one gets

$$\frac{\partial c}{\partial r}=\frac{Nm(1-V\rho)\omega^2 r}{RT}c, \tag{4}$$

where N is Avogadro's number and m the mass of a single molecule. But the quantity $m(1-V\rho)$ may be regarded as the effective mass of the molecule (i.e., the actual mass corrected for the effect of buoyancy) so that

$$m(1-V\rho)\omega^2 r=X. \tag{5}$$

Therefore, from (4) and (5)

$$\partial c/\partial r=NXc/RT. \tag{6}$$

The number of molecules which, as a result of the field, cross in one second a surface at r where the concentration is c is, from (2) and (6)

$$\frac{RT}{Nf}\frac{\partial c}{\partial r}r\theta h.$$

This is also equal to the number $Dr\theta h(\partial c/\partial r)$ of molecules crossing the same surface in the opposite direction as a result of the concentration gradient. Thus we have

$$D=RT/Nf. \tag{7}$$

But $m(1-V\rho)\omega^2 r=X=fv$ from Stoke's law and $v=\omega^2 rs$ from the definition of s. Therefore

$$sf=m(1-V\rho).$$

Substitution of this value of f in (7) gives

$$D=RTs/M(1-V\rho). \tag{8}$$

We return to Eq. (1) and try a solution of the form

$$c(r,t)=RT$$

where R is a function of r alone and T is a function of t alone. On substitution this gives

$$\frac{1}{rR}\frac{d}{dr}\left\{\left(D\frac{dR}{dr}-\omega^2 rsR\right)r\right\}=\frac{1}{T}\frac{dT}{dt}.$$

In this equation the variables are separated and the two equations

$$1/T(dT/dt)=-\beta \tag{9}$$

and

$$\frac{1}{rR}\frac{d}{dr}\left\{\left(D\frac{dR}{dr}-\omega^2 rsR\right)r\right\}=-\beta \tag{10}$$

are obtained, where β is a constant. From Eq. (9)

$$T=e^{-\beta t}.$$

Eq. (10) may be written in the form

$$d^2R/dr^2+(1/r-\delta r)(dR/dr)+\sigma R=0, \tag{11}$$

where $\delta=\omega^2 s/D$, $\sigma=(\beta-2\omega^2 s)/D$.

Assume $R(r)$ to be a solution of Eq. (11). Then a particular solution of (1) is

$$c(r,t)=R(r)e^{-\beta t}. \tag{12}$$

As yet there are no restrictions on β. However, from the nature of the problem certain boundary conditions must be satisfied by the function $c(r,t)$ which determine definite values of β.

The boundary conditions are as follows: (i) the net flow through the surface $r=l$ is zero; (ii) the function $c(r,t)$ is an even function in r; (iii) when $t=0$ the function $c(r,t)$ represents an arbitrary initial distribution of concentration which is assumed to be known. The first condition may be expressed mathematically by saying that

$$\partial c/\partial r-\delta rc=0 \quad \text{for } r=l. \tag{13}$$

It is now necessary to consider the solution of Eq. (11). Change the independent variable from r to x by the transformation

$$x=\delta r^2/2.$$

The equation which results is

$$\frac{d^2M}{dx^2}+\left(\frac{1}{x}-1\right)\frac{dM}{dx}-\frac{\alpha}{x}M=0, \tag{14}$$

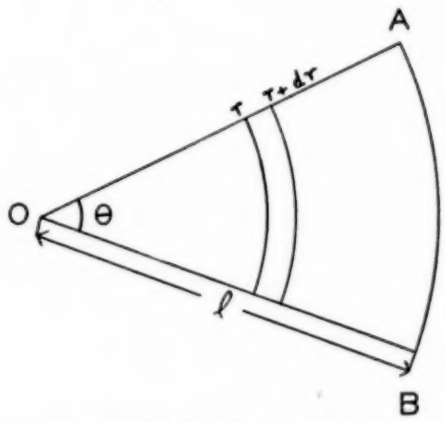

FIG. 1. Sector-shaped cell.

where M is the function of x which corresponds to R as a function of r and where

$$\beta = 2\omega^2 s(1-\alpha).$$

Thus the solution (12) may be written in the form

$$c(r, t) = M(\delta r^2/2)e^{(\alpha-1)\tau}, \tag{15}$$

where $\tau = 2\omega^2 st.$

Investigation of (14) for a series solution of the form

$$\sum_{n=0}^{\infty} a_n x^n$$

yields the single solution which follows:

$$M(x) = 1 + \frac{\alpha x}{1^2} + \frac{\alpha(\alpha+1)}{1^2 \cdot 2^2}x^2 + \cdots. \tag{16}$$

This solution is acceptable in that it is absolutely and uniformly convergent for all values of α and x and satisfies the second boundary condition automatically by being a series in r^2. Let this solution be denoted by $u(x)$. A second solution $v(x)$ may be found by the substitution[5] of

$$M = u(x)v(x)$$

in Eq. (14). On carrying through the substitution, the complete solution is found to be

$$Au(x) + B\Bigg[u(x)\log x + \frac{\alpha}{1^2}x\left(\frac{1}{\alpha} - \frac{2}{1}\right) + \frac{\alpha(\alpha+1)}{1^2 \cdot 2^2}x^2\left(\frac{1}{\alpha} + \frac{1}{\alpha+1} - \frac{2}{1} - \frac{2}{2}\right) + \frac{\alpha(\alpha+1)(\alpha+2)}{1^2 \cdot 2^2 \cdot 3^2}x^3 \times \left(\frac{1}{\alpha} + \frac{1}{\alpha+1} + \frac{1}{\alpha+2} - \frac{2}{1} - \frac{2}{2} - \frac{2}{3}\right) + \cdots\Bigg],$$

where A and B are constants.

This complete solution cannot be used because the factor $\log x$ becomes infinite at the origin: this requires that B be zero. Thus we are justified in accepting (16) as the required solution in this case.

If the expression for $c(r, t)$ given by Eq. (15) be substituted in the boundary condition (13), the following relation must hold

$$(d/dr)\{M(\delta r^2/2)\} - \delta r M(\delta r^2/2) = 0 \quad \text{for } r = l$$

or

$$(d/dx)\{M(x)\} - M(x) = 0 \quad \text{for } x = \delta l^2/2 = b. \tag{17}$$

On substituting the series expression for $M(x)$ in (17) and letting $x = b$ we arrive at the following equation

$$(\alpha-1)\left\{1 + \frac{2\alpha}{1^2 \cdot 2^2}b + \frac{3\alpha(\alpha+1)}{1^2 \cdot 2^2 \cdot 3^2}b^2 + \cdots\right\} = (\alpha-1)f(\alpha) = 0. \tag{18}$$

Thus one value which α may assume is $\alpha = 1$. The other values of α are those which satisfy the equation

$$f(\alpha) = 0,$$

which has an infinite number of real, negative roots.

Thus the complete solution of the problem is given by

$$c(x, t) = \sum_{n=0}^{\infty} a_n M_{\alpha_n}(x)e^{(\alpha_n-1)\tau}, \tag{19}$$

where $\alpha_0, \alpha_1, \alpha_2, \cdots$ denote all the values of α which satisfy Eq. (18); $M_{\alpha_0}(x), M_{\alpha_1}(x), M_{\alpha_2}(x) \cdots$ denote the values of $M(x)$ which correspond to these different roots; $a_0, a_1, a_2, \cdots$ are constant coefficients which are determined by the initial state of the solution in the cell.

It is now necessary to evaluate the coefficients of Eq. (19). For $t = 0$ we have

$$c(x, 0) = a_0 M_{\alpha_0} + a_1 M_{\alpha_1} + a_2 M_{\alpha_2} + \cdots. \tag{20}$$

Multiply each side of Eq. (20) by $\sigma_n dx$ and integrate from $x = 0$ to $x = b$. This gives

$$\int_0^b c(x, 0)\sigma_n dx = a_0 \int_0^b \sigma_n M_{\alpha_0} dx + a_1 \int_0^b \sigma_n M_{\alpha_1} dx + \cdots.$$

Each term of the right-hand side of this equation is an integral of the form

$$I = a_s \int_0^b \sigma_n M_{\alpha_s} dx.$$

If possible, the function σ_n is to be chosen such that $I = 0$, for $n \neq s$. If $I = 0$ except when $s = n$

[5] Whittaker and Watson, *Modern Analysis*.

then the coefficients $a_0, a_1, \cdots$ are given by

$$a_n = \int_0^b c(x, 0)\sigma_n dx \Big/ \int_0^b \sigma_n M_{\alpha_n} dx \qquad (21)$$

Since M_{α_s} is a solution of Eq. (14) we may write

$$a_s \int_0^b \sigma_n M_{\alpha_s} dx = \frac{a_s}{\alpha_s} \int_0^b \sigma_n \left\{ (1-x)\frac{dM_{\alpha_s}}{dx} + x\frac{d^2 M_{\alpha_s}}{dx^2} \right\} dx.$$

Integration by parts of the right-hand side of the above equation yields

$$\alpha_s \int_0^b \sigma_n M_{\alpha_s} dx = \left[\frac{dM_{\alpha_s}}{dx} x\sigma_n - M_{\alpha_s} \frac{d}{dx}(x\sigma_n) + \sigma_n (1-x) M_{\alpha_s} \right]_0^b + \int_0^b M_{\alpha_s} \left\{ \frac{d^2}{dx^2}(x\sigma_n) - \frac{d}{dx}[\sigma_n(1-x)] \right\} dx. \qquad (22)$$

If the quantity which multiplies M_{α_s} under the sign of integration be equated to $\alpha_n \sigma_n$ it is possible to get rid of the integral on the right-hand side of Eq. (22), and thus to have the integral

$$\int_0^b \sigma_n M_{\alpha_s} dx$$

given by functions which are not under any integration sign. Thus setting

$$(d^2/dx^2)(x\sigma_n) - (d/dx)\{\sigma_n(1-x)\} = \alpha_n \sigma_n \qquad (23)$$

in Eq. (22) we get

$$(\alpha_s - \alpha_n) \int_0^b \sigma_n M_{\alpha_s} dx = \left[\frac{dM_{\alpha_s}}{dx} x\sigma_n - M_{\alpha_s} \frac{d}{dx}(x\sigma_n) + \sigma_n (1-x) M_{\alpha_s} \right]_0^b. \qquad (24)$$

Suppose the factor σ_n to satisfy the differential Eq. (23) in the same manner as the function M_{α_s} satisfies the Eq. (14). A very simple relation between σ_n and M_{α_s} is discovered if in Eq. (23) we suppose

$$\sigma_n = e^{-x} s_n.$$

As a result of this substitution we get the equation for s_n as

$$d^2 s_n/dx^2 + (1/x - 1)(ds_n/dx) - (\alpha_n/x)s_n = 0,$$

which is the equation satisfied by M_{α_n}. Thus we obtain as the value of σ_n

$$\sigma_n = e^{-x} M_{\alpha_n}(x).$$

Introducing this value of σ_n into Eq. (24) gives

$$\int_0^b e^{-x} M_{\alpha_n} M_{\alpha_s} dx = \frac{1}{\alpha_s - \alpha_n} \left[xe^{-x} \left\{ M_{\alpha_n} \left(\frac{dM_{\alpha_s}}{dx} - M_{\alpha_s} \right) - M_{\alpha_s} \left(\frac{dM_{\alpha_n}}{dx} - M_{\alpha_n} \right) \right\} \right]_0^b. \qquad (25)$$

But at the point b

$$(dM_{\alpha_s}/dx) - M_{\alpha_s} = (dM_{\alpha_n}/dx) - M_{\alpha_n} = 0,$$

since α_n and α_s are values of α which satisfy Eq. (17). Thus for the allowed values of α we have

$$\int_0^b e^{-x} M_{\alpha_n} M_{\alpha_s} dx = 0, \quad n \neq s.$$

If $s = n$ the above expression gives for the integral an indeterminate form, which will be evaluated later.

From Eq. (21) it is now evident that the coefficient a_n is given by

$$a_n = \int_0^b c(x, 0) e^{-x} M_{\alpha_n}(x) dx \Big/ \int_0^b e^{-x} \{M_{\alpha_n}(x)\}^2 dx.$$

Thus the complete solution of Eq. (1) satisfying the boundary conditions is

$$c(x, t) = \sum_{n=0}^{\infty} \left[\frac{\int_0^b c(x, 0) e^{-x} M_{\alpha_n}(x) dx}{\int_0^b e^{-x} \{M_{\alpha_n}(x)\}^2 dx} e^{(\alpha_n - 1)\tau} M_{\alpha_n}(x) \right] = \sum_{n=0}^{\infty} T_{\alpha_n}. \qquad (26)$$

The symbol T_{α_n} is introduced for brevity: its definition is obvious. Usually the initial distribution $c(x, 0)$ is a constant c_0 at all points in the cell.

In the above summation suppose $\alpha_0=1$ as one value of α determined by the boundary conditions. It is also the largest value of α; all the others are negative as an inspection of Eq. (18) will easily show. Then we can write Eq. (26) in the following form, singling out the term for which $\alpha=1$.

$$c(x,t)=\frac{\int_0^b c_0 e^{-x}M_1(x)dx}{\int_0^b e^{-x}\{M_1(x)\}^2dx}M_1(x)+\sum_{n=1}^{\infty}T_{\alpha_n}.$$

But $M_1(x)=e^x$ and therefore

$$\frac{\int_0^b c_0 e^{-x}M_1(x)dx}{\int_0^b e^{-x}\{M_1(x)\}^2dx}=\frac{c_0 b}{e^b-1}.$$

Thus

$$c(x,t)=\frac{bc_0}{e^b-1}e^x+\sum_{n=1}^{\infty}T_n. \qquad (27)$$

In this final form

$$x=\frac{\delta r^2}{2}=\frac{M(1-V\rho)\omega^2}{2RT}r^2 \quad \text{and} \quad b=\frac{M(1-V\rho)\omega^2}{2RT}l^2.$$

It is to be noted that the complete solution consists of a series of terms, the first term of which is the only one independent of the time, and which represents the state of the solution when t is infinite. The other terms depend on the time exponentially and become less as time passes.

To complete the solution it is necessary to evaluate the integrals

$$I_1=\int_0^b e^{-x}M_{\alpha_n}(x)dx \text{ and } I_2=\int_0^b e^{-x}\{M_{\alpha_n}(x)\}^2dx.$$

Consider first I_1. In I_1, $M_{\alpha_n}(x)$ is a solution of Eq. (14). If $M_{\alpha_n}(x)=e^xS_{\alpha_n}$, S_{α_n} is found to satisfy the equation

$$xS_{\alpha_n}''+(1+x)S_{\alpha_n}'-(\alpha_n-1)S_{\alpha_n}=0, \qquad (28)$$

where the superscripts denote differentiation with respect to x.

Thus $$I_1=\int S_{\alpha_n}dx.$$

From (28)

$$(\alpha_n-1)\int S_{\alpha_n}dx=\int(xS_{\alpha_n}''+S_{\alpha_n}')dx+\int xS_{\alpha_n}'dx$$

$$=x(S_{\alpha_n}'+S_{\alpha_n})-\int S_{\alpha_n}dx.$$

Therefore $\int S_{\alpha_n}dx=(x/\alpha_n)(S_{\alpha_n}'+S_{\alpha_n})$

and $$I_1=\int_0^b e^{-x}M_{\alpha_n}dx=(b/\alpha_n)e^{-b}M_{\alpha_n}(b),$$

since $(d/dx)M_{\alpha_n}(x)=M_{\alpha_n}(x)$ when $x=b$. Now consider I_2. Here it is convenient to consider $M_{\alpha_n}(x)$ as a particular case of a more general class of functions which are defined as follows,[6]

$$M(\alpha,\gamma,x)=1+\frac{\alpha}{1\cdot\gamma}x+\frac{\alpha(\alpha+1)}{1\cdot2\cdot\gamma(\gamma+1)}x^2+\cdots. \qquad (29)$$

According to this definition the function $M_\alpha(x)$ which has been used all through the above discussion is equivalent to $M(\alpha,1,x)$. Two simple formulae[7] will be needed which may be verified easily from Eq. (29). These formulae are

$$(d/dx)M(\alpha,\gamma,x)=(\alpha/\gamma)M(\alpha+1,\gamma+1,x) \qquad (30)$$

and

$$\alpha M(\alpha+1,\gamma+1,x)$$
$$=(\alpha-\gamma)M(\alpha,\gamma+1,x)+\gamma M(\alpha,\gamma,x). \qquad (31)$$

To evaluate I_2 we refer back to Eq. (25). The expression

$$dM_{\alpha_s}/dx-M_{\alpha_s},$$

which occurs in this equation may be written as

$$(d/dx)M(\alpha_s,1,x)-M(\alpha_s,1,x). \qquad (32)$$

By the use of (30) and (31) it can be shown that (32) is also equal to

$$(\alpha_s-1)M(\alpha_s,2,x).$$

Thus (25) may be written as

$$\int_0^b e^{-x}M(\alpha_n,1,x)M(\alpha_s,1,x)dx=\frac{be^{-b}\{(\alpha_s-1)M(\alpha_n,1,b)M(\alpha_s,2,b)-(\alpha_n-1)M(\alpha_s,1,b)M(\alpha_n,2,b)\}}{\alpha_s-\alpha_n}.$$

[6] Bateman, *Partial Differential Equations of Mathematical Physics.*
[7] Webb and Airey, Phil. Mag. **36**, 129 (1919).

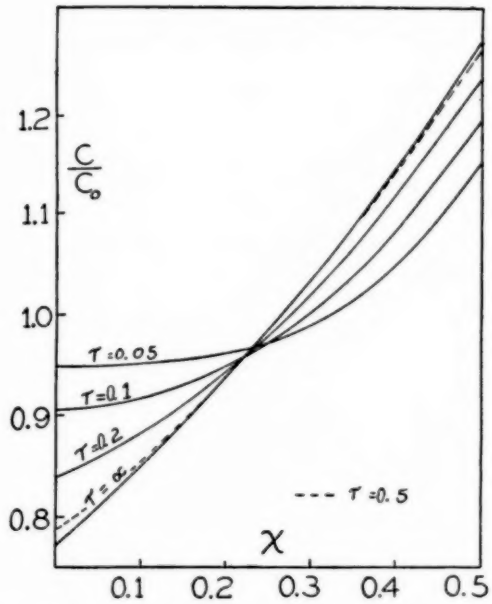

FIG. 2. Values of concentration change c/c_0 (c_0=initial constant concentration) as a function of position $X(=\omega^2 s r^2/2D)$ for various values of $\tau(=2\omega^2 s t)$ when $b=0.5$ $(=\omega^2 s l^2/2D)$.

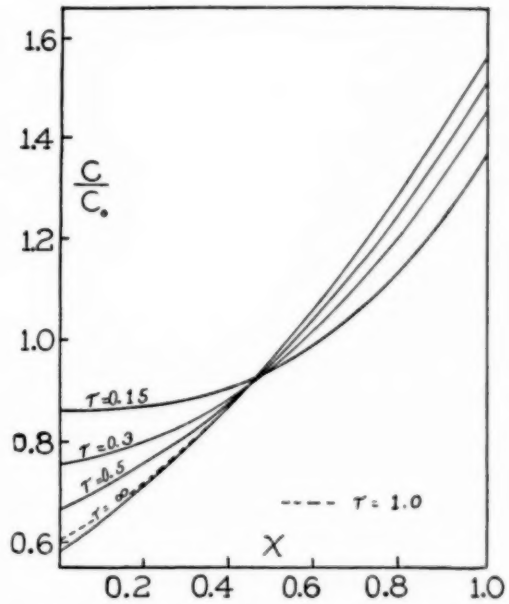

FIG. 3. Values of concentration change c/c_0 (c_0=initial constant concentration) as a function of position $X(=\omega^2 s r^2/2D)$ for various values of $\tau(=2\omega^2 s t)$ when $b=1.0$ $(=\omega^2 s l^2/2D)$.

When $s=n$ this gives as the value of the integral the indeterminate form 0/0. However the expression may be evaluated by differentiating both numerator and denominator with respect to α_s and then letting $\alpha_s=\alpha_n$. This gives (since $M(\alpha_n, 2, b)=0$)

$$I_2=\int_0^b e^{-x}\{M_{\alpha_n}(x)\}^2 dx$$
$$=be^{-b}(\alpha_n-1)M_{\alpha_n}(b)(d/d\alpha_n)[M(\alpha_n, 2, b)].$$

Introducing the values obtained for I_1 and I_2 into Eq. (27) we get the solution in a form which is free of definite integrals.

$$c(x, t)=\frac{bc_0}{e^b-1}e^x$$
$$+c_0\sum_{n=1}^{\infty}\frac{M_{\alpha_n}(x)}{\alpha_n(\alpha_n-1)(d/d\alpha_n)[M(\alpha_n, 2, b)]}e^{(\alpha_n-1)\tau}.$$

Recursion formulae as well as a short table of values for the functions used have been given by Webb and Airey[7] and are of considerable service for the purpose of computation.

The curves given in Figs. 2 and 3 represent the values of c/c_0 at all points in the cell for different values of the parameter $\tau(=2\omega^2 s t)$. Fig. 2 is for the case in which $b=0.5$, and Fig. 3 is for $b=1.0$. As an example of the sort of information which the curves yield, consider the case of carbon-monoxide hemoglobin for which Svedberg[8] gives the following data: molecular weight=68,000, partial specific volume=0.749 cm³/g. If a dilute aqueous solution of this substance were placed in a cell, such as has been discussed above, for which $l=0.5$ cm and rotated at a speed of 385 r.p.s., the value which b assumes is 0.5 approximately. Fig. 2 shows that for this case the equilibrium state has been reached to within one percent when $\tau=0.5$. That is when $2\omega^2 s t=0.5$. For hemoglobin $s=5.0\times10^{-13}$ approximately. Thus $\tau=0.5$ corresponds to a time of 23.4 hours.

The solution of the above equation for the case of a sector-shaped cell placed near the *periphery* of the rotor would be of great interest from an experimental point of view. The present discussion, although of interest in itself, has been given primarily as an introduction to the solution for the more general case which has been worked out and will appear in a separate article at a later date.

[8] Svedberg, article in *Colloid Chemistry, Theoretical and Applied*, edited by Alexander, Vol. 1, page 851.

The curves derived from this equation are of value for molecular weight determinations. One method[4] of determining molecular weights by the use of the ultracentrifuge depends upon the final equilibrium distribution of concentration having been established. As the solution of the equation shows, this final state is approached asymptotically, it is important to know how long a time must pass before it is approximated sufficiently accurately. The discussion given above of the case of hemoglobin shows that the solution of the equation readily yields this information if an approximate value of the molecular weight can be obtained.

Further, a comparison of the theoretical and experimental distribution curves would be useful for determining whether or not the liquid in the cell was free from stirring. If the liquid was found to be convection free (as in the case of the vacuum type ultracentrifuge[9] and Svedberg's ultracentrifuge[4]), the equation might make it possible to shorten the time of centrifuging by rendering it unnecessary to wait for the final equilibrium state. A knowledge of the sedimentation constant s should allow the molecular weight to be determined from the concentration curve for any time t.

The writer wishes to express his appreciation for the encouragement given him by Professors Beams, Snoddy, McShane and Hoxton in this work.

[9] Beams, J. App. Phys. **8**, 795 (1937).

MAY 1, 1938 PHYSICAL REVIEW VOLUME 53

Accidental Coincidences in Counter Circuits

CARL ECKART AND FRANCIS R. SHONKA
Ryerson Laboratory, University of Chicago, Chicago, Illinois

(Received February 24, 1938)

The accidental n-fold coincidences ($n>2$), are of various kinds. The first kind involves n events that accidentally occur nearly simultaneously. The second kind involves two events that are causally simultaneous, and $n-2$ events that are accidentally nearly simultaneous; etc. For theoretical purposes, it is sufficient to treat only accidentals of the first kind, since the theory of the other kinds is very similar. It is also possible, for theoretical purposes, to replace each of the various coincidence circuits in actual use by the same schematic circuit. This consists of three parts: the counting, relay, and recording circuits. For n-fold coincidences, the relay circuit will contain n relays (e.g. type 57 tubes). It is shown that the time constants (τ_i) of these relays determine the accidental counting rates. The time constants of the counting and recording circuits are not important in this connection. It is shown experimentally that each of the relays ordinarily has a different time constant, τ_i, even though it is constructed of commercially identical parts. By the use of these results, it is shown that when N_i particles per second traverse the ith counter, the rate at which accidentals of the first kind occur is given by

$$A_{1,2,\cdots n}=BC,$$
$$B=N_1\tau_1\cdot N_2\tau_2\cdots N_n\tau_n,$$
$$C=1/\tau_1+1/\tau_2+\cdots+1/\tau_n.$$

The rates of occurrence of the other kinds of accidentals are readily deduced from this result by slight modifications. This formula is verified by experiment.

1. Analysis of the Problem, and Schematization of the Circuit

THE increasing precision to which counter measurements are being carried makes it necessary to consider the statistical theory of accidental coincidences in greater detail than has hitherto been done. When n counters are connected in such a way that only n-fold coincidences are recorded, the recording rate is the sum of various contributions. Every coincidence consists of n events that occur simultaneously, or nearly so. If all n events are causally related, they form a true coincidence. If no two are causally related, they form an accidental of the first kind. If two are causally related to each other, but no other causal relations exist among the n events, they form an accidental of the second kind. The terminology may be extended because there is one kind of accidental for every partition of the number n into a sum of integers.

Fortunately, the theories of the various kinds

of accidentals are very similar, so that it is sufficient if the theory of the first kind is considered in detail. The theories of the other kinds require only that trivial complications be introduced. Consequently, the unmodified term "accidental" will be used to refer to accidentals of the first kind.

There is general agreement on the formula for twofold accidentals: if the rates of the two counters are N_1 and N_2 and the resolving time is τ, the rate at which accidentals occur is

$$A_{12}=2N_1N_2\tau. \tag{1}$$

For threefold accidentals, the rate is

$$A_{123}=\alpha N_1N_2N_3\tau^2, \tag{2}$$

but various values of α have been used. The correct value is $\alpha=3$, as was shown by Schiff,[1] but $\alpha=4$ and $\alpha=6$ have been used. Not much work has required higher values of n.

The validity of these equations depends on assumptions concerning the action of the counters and circuit. Although there are several circuits in use, it appears that all can be schematically represented[2] by Fig. 1. When one of the counters, C, is actuated, it furnishes a pulse of current to the corresponding relay. The relay thereupon closes and the duration of the contact is τ. The recorder is actuated only if all relays make contact simultaneously.

There is some question as to what will occur if the same counter is actuated twice within a time of length τ. It is also likely that different actual circuits will behave differently, and that σ, the duration of the pulse of current delivered by the counter, will be important in this connection. Schiff (p. 94) apparently assumes that $\sigma \ll \tau$ in order to avoid this question. This appears to be a very dubious assumption; in the following derivation, the question will be evaded by supposing that the counting rates are so low that the probability that one counter is actuated twice within a time τ is negligible. This makes the efficiency of the relay circuit 100 percent.

The duration of the pulse of current delivered by the relay circuit to the recorder will not be τ, but will vary from 0 to τ, depending on the timing of the events involved in the accidental. (For true coincidences, this duration will always be τ, unless there should be delays between the occurrence of the events in the counter and the closing of the relays.) The simplest assumption to make concerning the action of the recorder, is that all those pulses delivered by the relay, whose duration is greater than ρ, will be recorded. Pulses whose duration is less than ρ are not recorded. This limit, ρ, must be distinguished from the resolving time ρ' of the recorder: if the relay delivers two pulses whose separation in time is less than ρ', only one of these will be recorded. The influence of ρ' will again be ignored by assuming a sufficiently low counting rate. It will be seen that the influence of ρ is the same as if τ were diminished to $\tau-\rho$.

It is doubtful if any actual circuit corresponds exactly to the scheme of Fig. 1. The experimental investigation described below indicates that the idealization is not too great, provided only that each relay be supposed to have a different contact time, τ_i. This is found to be the case even when commercially identical parts are used in the construction of the relays.

2. Calculation of the Accidental Rates

Let the relays be numbered $i=1, 2, \cdots n$, and let N_i be the independent rate of relay i. That is, N_i is the probable number of events per second that close relay i, *and are not causally related to some event that closes some other relay.*

A coincidence is an interval of time during which all relays are closed. Such a concatenation of events is diagrammed in Fig. 2. The horizontal arrows, τ_i, extend from the instant at which relay i closes until the instant at which it opens again. The lengths, τ_i, of the arrows are thus the contact times of the various relays. The coinci-

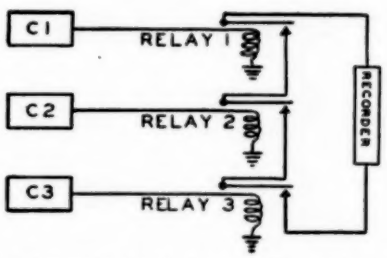

FIG. 1. Schematic circuit for recording coincidences.

[1] L. I. Schiff, Phys. Rev. **50**, 88 (1936).

[2] An alternative schematization would consist of relays in parallel, the recorder being actuated only when all relays are open simultaneously. The theory of such a circuit is identical with that of Fig. 1.

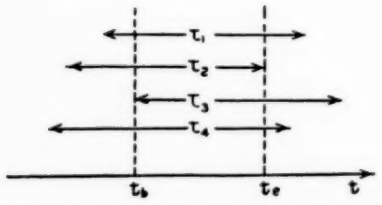

FIG. 2. Diagram illustrating a fourfold coincidence.

dence begins at t_b, the instant at which the last relay (No. 3 in the figure) closes, and ends at t_e, the instant at which the first relay (No. 2 in the figure) opens.

The problem is to calculate $P(t, t')dt$, the probability that n independent events fall together in such a way as to constitute a coincidence with $t<t_b<t+dt$ and $t'<t_e$. As a preliminary, it is convenient to calculate $Q(t, t')$, the probability that the accidental coincidence occurs so that $t_b<t$ and $t'<t_e$. The relation between P and Q is then clearly

$$P(t, t')=\partial Q(t, t')/\partial t. \tag{3}$$

If it is permissible to ignore the probability that the same relay is actuated twice during its contact time, then $Q(t, t')=0$ unless $t'-t>\tau_i$ for all relays i. The probability that relay i will close during the interval $t'-\tau_i \rightarrow t$ is $N_i(\tau_i-t'+t)$, so that

$$Q(t, t')=\Pi_{i=1}^{n} N_i(\tau_i-t'+t). \tag{4}$$

Because of the assumption concerning the action of the recorder, the rate at which accidentals are recorded will be $P(t, t+\rho)$. From (4) it is obvious that this is the same as $P(t, t)$, provided that τ_i is replaced by $\tau_i-\rho$. Hence, if the τ_i are determined empirically from the recorded counts, it is permissible to set $\rho=0$. Therefore the accidental rate of n-fold coincidences is

$$\begin{aligned} A_{12\ldots n}&=P(t, t)\\ &=BC, \end{aligned} \tag{5}$$

where

$$\begin{aligned} B&=N_1\tau_1\cdot N_2\tau_2\cdots N_n\tau_n,\\ C&=1/\tau_1+1/\tau_2+\cdots+1/\tau_n. \end{aligned} \tag{6}$$

For twofold circuits, this reduces to

$$A_{12}=N_1N_2(\tau_1+\tau_2), \tag{1'}$$

and for threefold, to

$$A_{123}=N_1N_2N_3(\tau_1\tau_2+\tau_2\tau_3+\tau_3\tau_1). \tag{2'}$$

If all the τ_i are equal, these reduce to (1) and (2), with $\alpha=3$.

As has been said, these formulae apply only to accidentals of the first kind. When threefold coincidences are recorded, accidentals of the second kind will also occur. The problem is then to calculate the total rate, N, at which coincidences are recorded, given that

(*a*) the independent rate of relay i is N_i;
(*b*) on the average, relays i and j are actuated N_{ij} times per second by two events that are causally related to each other, but are not causally related to an event that actuates counter k;
(*c*) on the average, true triple coincidences occur N_{123} times per second.

Let τ_{ij} be the smaller of τ_i and τ_j; then the probable number of accidentals of the second kind arising from causally related events in counters 1 and 2, and an unrelated event in counter 3 is easily seen to be

$$A_{12;\,3}=N_{12}N_3(\tau_{12}+\tau_3). \tag{7}$$

The total rate of recording will thus be

$$N=N_{123}+A_{12;\,3}+A_{23;\,1}+A_{31;\,2}+A_{123}. \tag{8}$$

If all the τ_i are equal, this reduces essentially to Schiff's Eq. (14).

3. Discussion of Actual Circuits

In order to show that the foregoing assumptions regarding the time constants apply to all circuits in use, the various types of circuits will be analyzed. It is most convenient to consider all these circuits (such as the Neher-Harper, the direct resistance coupled, and others) as composed of three separate circuits: the counting circuit, the relay circuit, and the recording circuit.

A typical onefold circuit is shown in Fig. 3. It consists of a Geiger-Müller tube, an applied voltage on the tube, and some arrangement for

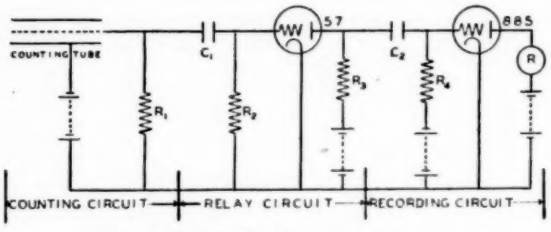

FIG. 3. Single-fold counting circuit.

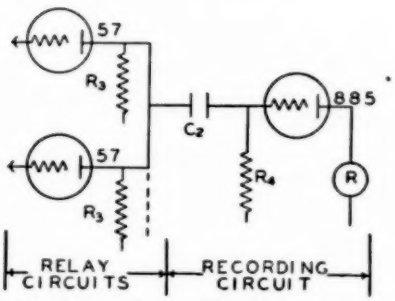

FIG. 4a. Older relay and recording circuit for coincidences.

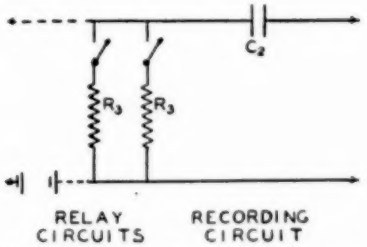

FIG. 4b. Schematization of the same.

quenching the glow in the tube when a discharge occurs. With an activation of the Geiger-Müller tube, a surge of current is produced in the counting circuit, resulting in the delivery of a pulse of duration σ to the relay circuit. This is true regardless of the type of circuit used for the quenching of this glow. σ depends on the characteristics and operating conditions of the Geiger-Müller tube, and the constants of the remainder of the counting circuit. σ is probably not only dependent on the constants of the circuit, and the characteristics of the Geiger-Müller tube, but also on the voltages, the counting rate of the tube, etc.

The relay circuit, consisting of an amplifier, acts as a switching device which sets off the recording circuit. The plate current is normally constant but is reduced nearly to zero by the pulse from the counting circuit. The effective time during which the current is zero is called τ. It is easily seen that the duration of the pulse in the relay circuit must be at least as great as the effective duration of the pulse in the counting circuit. (See Part 1.) Since the value of τ depends on the value of σ, τ will likewise be affected by the factors mentioned above.[3]

The recording circuit is controlled by the relay circuit. The pulse produced in the latter trips the recording mechanism, which in this case consists of a thyratron tube and a mechanical count recorder, R.

Two types of relay circuits have been in use for obtaining coincidence records. The first type is shown in Fig. 4a where each type 57 tube corresponds to one of the relays of Fig. 1. The pulse in the recording circuit is due to the individual pulses in the relay circuits and is equal to their sum. This may be represented schematically by an arrangement of switches and resistances, as shown in Fig. 4b, where the count recorder is so adjusted that it registers only the pulses occurring when all relay switches are closed simultaneously. Pulses of lesser magnitude do not affect the count recorder. This is in agreement with the schematization used above.

The type of circuit shown in Fig. 4a has been superceded by the one shown in Fig. 5a. In this arrangement the current in resistance R_3 is the sum of the currents in all the relays. If the current in some of the relays is reduced to zero, that in R_3 is not appreciably changed[4] because the remaining relays supply more current than before. This is due to the fact that there is a slight increase of voltage on the plates of the remaining type 57 amplifying tubes and the fact that the effective resistance of the tubes is not constant. This type of coincidence circuit is shown schematically in Fig. 5b. The counting mechanism is now so arranged that a count will be registered only when the current in R_3 is greatly reduced. Hence a coincidence will occur only when in an interval of time all the relay switches are opened. This too is in agreement with the schematic assumption made above.

4. EXPERIMENTAL VERIFICATION

The apparatus used in the experimental verification of formula (5) consisted of a threefold Geiger-Müller tube counting system as shown in

[3] In the course of the experiment τ was found to vary somewhat when the individual counting rate was varied. The dependence of τ on such factors is being studied at the present time.

[4] The following experiment was performed with a fourfold counting system: the current in R_3 was measured with a milliammeter, and the currents in the relays were successively reduced to zero by putting a negative bias on the control grids of the type 57 tubes. It was found that the current in R_3 did not vary by more than 3 percent, until all relays were biased, when it dropped to zero.

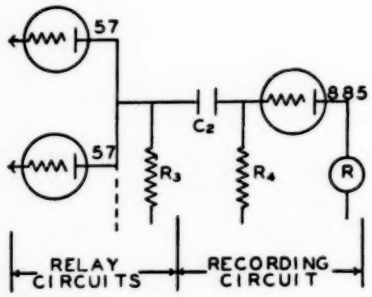

FIG. 5a. Newer relay and recording circuit for coincidences.

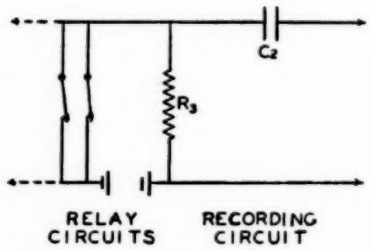

FIG. 5b. Schematization of the same.

Fig. 3 and Fig. 5a. Each of the three branches of this counting system was heavily shielded from electrostatic disturbances.

The Geiger-Müller tubes were made by a special technique developed in this laboratory.[5] They have a threshold voltage of about 1100, and a plateau width of about 800 volts and are filled with hydrogen. Their metal cylinder is 9/16 inch in diameter and $15\frac{1}{2}$ inches in length. Their efficiency is high, and the single counting rate, produced by cosmic rays and local radiation is about 150 per minute when the tubes are not shielded, and is decreased to about 60 per minute when they are heavily shielded with lead.

To verify the formula for accidental counts, it was necessary to have an experimental determination of A_{123}. To obtain this with the ordinary circuit constants would be difficult, since with the ordinary value of τ only one accidental in a few hours would be expected.

Furthermore, the cosmic rays would make the terms N_{123}, $A_{12;3}$, etc., in (8) much greater than A_{123}. It was therefore necessary to increase A_{123} by increasing the τ_i and N_i. This was done by using abnormally large resistances and capacities in the counting and relay circuits, and by artificial activation from radioactive sources. The quantities N_{123}, N_{12}, etc., were also decreased by shielding two of the Geiger-Müller tubes with 2.5 inches of lead, and by placing all three out of line in a horizontal plane, at distances of 12 feet from each other. In this way, the total number of recorded counts was made equal to A_{123}.

By means of suitable switches in the circuits, the quantities N_1, N_2, N_3, A_{12}, A_{23}, and A_{31} were also measured. From these and (1′), values of τ_1, τ_2, and τ_3 were calculated. These three numbers were not equal; a typical set of data is shown in Table I.

These data were obtained with a relay circuit whose homologous parts consisted of commercially identical resistors, condensers, and type 57 tubes. When these parts were interchanged, the values of τ_i altered. Thus the practical importance of the generalization of (1′) is demonstrated.

From the values of τ_i obtained above, one calculates $A_{123}=0.51\pm0.03$ min^{-1} from (2′). The value of A_{123} observed under these conditions was 0.513 ± 0.007. Several series of data similar to this were obtained; in no case was the difference between the calculated and observed values of A_{123} greater than 6 percent. Eq. (2′) was also checked by V. C. Wilson for the apparatus described by him in a recent paper.[6]

TABLE I. *Typical set of data. The A's and N's are in counts/min., the τ's in minutes.*

$N_1=182\pm1$	$A_{12}=16.1\pm0.2$	$\tau_1=12.0\pm0.3\times10^{-5}$
$N_2=435\pm2$	$A_{23}=21.0\pm0.2$	$\tau_2=8.3\pm0.2\times10^{-5}$
$N_3=481\pm2$	$A_{31}=12.0\pm0.1$	$\tau_3=1.7\pm0.02\times10^{-5}$

[5] J. B. Hoag, *Electron and Nuclear Physics* (D. Van Nostrand Company, 1938), p. 432.

[6] V. C. Wilson, Phys. Rev. **53**, 337 (1938).

The Magnetic Structure of Cobalt

W. C. ELMORE
Massachusetts Institute of Technology, Cambridge, Massachusetts

(Received March 7, 1938)

The magnetic powder method has been used to investigate the magnetic structure of cobalt crystals at room temperature. A stable colloid of gamma-ferric-oxide was deposited on suitable cuts of cobalt crystals by a magnetic field applied normal to the surface under observation. Smooth surfaces were prepared by metallurgical polishing followed by additional electrolytic polishing. (The latter method for polishing cobalt is described.) The surfaces chiefly studied approximated basal or prism planes. On all cuts three related patterns were found corresponding to no applied field or a normal field applied outward or inward. The two patterns with field were reciprocal in the sense that their spaces and deposits were interchanged. On basal planes the pattern appeared lace-like possessing considerable detail which was not easily modified by increasing the applied field. On prism planes the no-field pattern consisted of straight lines running parallel to the hexagonal axis. A small applied normal field spread the colloid in these lines into the alternate spaces between them. Further increase in field widened the resulting stripes in a somewhat erratic manner. Other interesting details of the patterns are described. In the discussion are listed the various energies involved in the demagnetization of an ideal crystal, i.e., one in which all energies concerned are reversible. The attempts of other authors to use these energies for devising magnetic structures are examined for their relation to magnetic powder patterns. It is concluded that the cobalt patterns do not accord with the structure demanded by simple theory which neglects irreversible energy changes accompanying demagnetization. The structure which seems best suited to explain the various patterns of cobalt is then proposed and discussed. To make this structure appear reasonable, the process by which a crystal goes from the fully magnetized to the demagnetized state (as suggested by various pattern observations) is described in terms of the dendritic growth of regions of reversed magnetization.

THE old magnetic powder method has recently been used with considerable success to establish new data concerning the magnetic structure of ferromagnetic crystals. Bitter[1] who first applied the method for this purpose published typical photomicrographs of patterns which he found on smooth (but unpolished) ingots of iron, nickel and cobalt. Other workers,[2,3] including the present writer, have improved the method and have extended the study of the iron and nickel patterns. No further investigation of the cobalt patterns has yet been reported.

Interpretation of the cobalt patterns in terms of a model should be easily made in view of the simplicity of the magnetic anisotropy of hexagonal cobalt which has but one direction of easy magnetization—the hexagonal axis. The present work shows that the structure is more complicated than that predicted by simple theory. It has been found possible, however, to propose a model which will account for the essential features of the various cobalt patterns.

[1] F. Bitter, Phys. Rev. **38**, 1903 (1931); **41**, 507 (1932).
[2] For a brief discussion with references see F. Bitter, *Introduction to Ferromagnetism* (McGraw-Hill Book Co., New York, 1937), p. 59.
[3] For more recent work see W. C. Elmore, Phys. Rev. **51**, 982 (1937) and T. Soller, Zeits. f. Physik **106**, 485 (1937).

Specimens and Experimental Details

Several cobalt specimens were kindly supplied by Professor P. W. Bridgman of Harvard who had earlier secured them from K. Honda in Japan. They were in the form of cylinders about one centimeter in diameter and several centimeters in length, containing a number of large crystal grains. Various cuts of selected grains were prepared by careful sawing followed by the usual metallurgical polishing. Many of the surfaces were then electrolytically polished by the method devised by Jacquet[4] for copper and brass. The orientation of exposed grains was determined by etch reflections. The surfaces chiefly studied were either approximately parallel or perpendicular to the hexagonal axis, the direction of easy magnetization in cobalt at room temperature.

To polish cobalt by Jacquet's method an electrolyte of orthophosphoric acid (specific gravity about 1.35) was used. A satisfactory polish resulted with 1.2 volts between a comparatively large cobalt cathode and the specimen anode. Lower voltages, or agitation at 1.2 volts, produced an excellent macroscopic etch useful in

[4] P. Jacquet, Comptes rendus **201**, 1473 (1935); **202** 403 (1936).

determining crystal orientations. Somewhat higher voltages were found to produce passivity. As with copper and brass, a black film appeared on the surface at the start of the polishing. For cobalt this film proved to be ferromagnetic, as will be made clear by the following observation.

The electrolytic polishing leaves a surface not completely flat. If there are parallel ridges these are found to coincide with no-field lines in colloid patterns (Fig. 3b). This variation in removal of surface material was at first interpreted as a "magneto-chemical" effect. However, a microscopic examination of the surface shortly after the appearance of the black film showed it to be distributed as in Fig. 1. The relief polish, therefore, was due to an interference of uniform electrolytic action by the magnetically held skin fragments (cobalt oxide?). To avoid this effect the black film was carefully wiped away with cotton as soon as it could be seen. Since this procedure temporarily destroyed in the electrolyte the concentration gradient necessary for the polishing action, but did not result in the formation of a new film, it seems probable that the film was formed during previous exposure to air and not in the electrolyte.

As in previous experiments, magnetic fields were applied by mounting the specimen, usually irregular in shape, on the pole of a vertical electromagnet attached to the movable stage of a metallurgical microscope with vertical axis. The applied field was thus approximately normal to the surface under observation. It was never more than a few thousand gauss. Details concerning the use of magnetic colloid remained essentially as described for earlier experiments.[5]

Patterns on Basal Plane

The patterns of colloid on the basal plane of cobalt or on cuts inclined at small angles to this plane were similar to those previously reported by Bitter.[1] However, considerable improvement in the detail of the patterns was found to result from the use of a stable colloid instead of coarser powder which permanently settles out. Upon reversing the applied normal field these patterns always exhibited a shifting effect similar to that of the "maze" patterns found on polished iron crystals. Fig. 2b illustrates the typical pattern found with no applied field. An applied normal field changed this pattern to that of Fig. 2a or Fig. 2c depending on its direction. Careful comparison of the latter two patterns reveals a complete reciprocity, i.e., a detailed interchange of deposits with spaces.

The colloid of the no-field pattern is spread out more evenly except in numerous small areas which are completely lacking in colloid. The position of these areas coincides with the centers of the meshes of the applied field patterns. The colloid of all cobalt patterns was found to be much more securely held by stray fields than that of patterns on polished iron or nickel crystals. Indeed, washing the surface with running tap water did not seem to disturb it. This procedure was found useful for removing excess colloid not yet congregated into the pattern.

In contrast to the "maze" patterns of iron crystals, none of the cobalt patterns required a cold-worked surface for their existence. In one experiment a mechanically polished surface was electrolytically polished to the extent of removing a layer 0.1 mm thick. The pattern on the new surface was very nearly identical with the old one. Patterns on other surfaces electrolytically polished to much greater depths possessed the same typical appearance. It was observed that the patterns on different grains and sometimes on different parts of the same grain varied considerably in scale.

Except for the shifting effect just described, the basal patterns proved to be very stable in the presence of the available normal field. This field, due to the large demagnetization factor of the specimen, was only sufficient to magnetize it to perhaps 25 percent of saturation. The stability of the basal patterns differs essentially from that of the line patterns on prism planes (see next section). The only change in basal patterns noticed was a sideward motion of some of the meshes near the edge of one grain. Bitter has shown (Figs. 7–9 of his second paper[1]) what happens to the basal patterns on applying intense fields parallel to the basal plane. No attempt has yet been made to investigate further these changes associated with intense fields. For purposes of discussion it seems correct to consider that the present patterns are produced by an

[5] For a discussion of technique see reference 2, p. 55.

FIG. 1. Distribution of film which was set free from the surface (a prism plane) early in the process of electrolytically polishing cobalt. No applied field. Magnification approx. 215×.

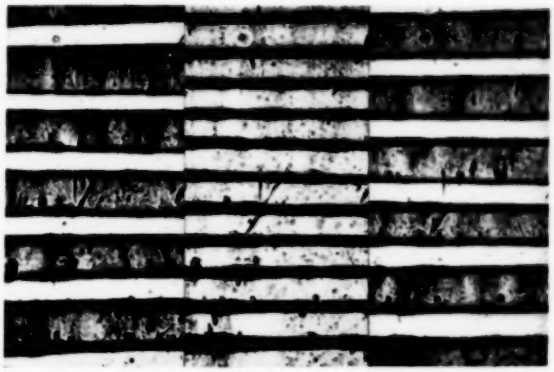

a b c

FIG. 3. Patterns of magnetic colloid on a cobalt surface approximately perpendicular to the basal plane with applied normal field (a) outward; (b) zero; (c) inward. The lines run parallel to the hexagonal axis. Magnification approx. 65×.

unchanging, or but slightly changing pattern of local fields with or without the superposition of an applied normal field.

PATTERNS ON PRISM PLANES

The patterns on planes approximately normal to the basal plane are illustrated in Figs. 3a, 3b and 3c. These patterns, whose general appearance does not depend on the angle between their plane and a type $\{10\bar{1}0\}$ plane, were obtained, respectively, with plus, zero, and minus applied normal fields. The no-field pattern consists of narrow lines whose general direction is parallel to the hexagonal axis. In Fig. 3b the average spacing of the lines is about 60μ. On other grains different spacings were found varying from a few microns

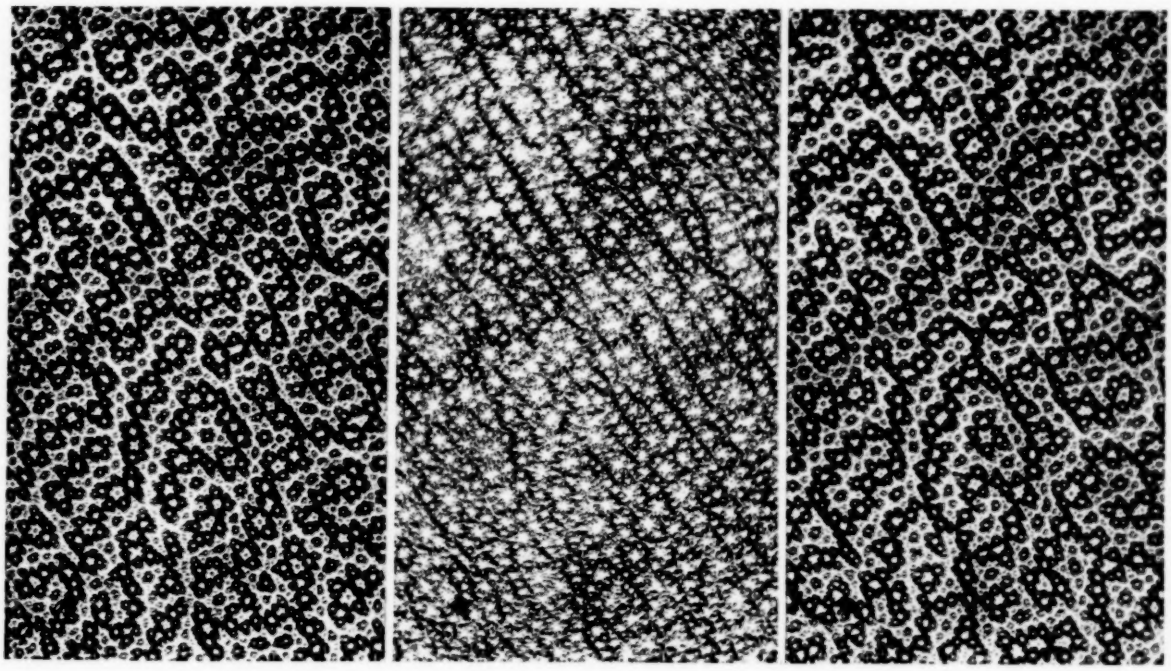

a b c

FIG. 2. Patterns of magnetic colloid on the basal plane of a cobalt crystal with applied normal field (a) outward; (b) zero; (c) inward. The spaces and deposits are interchanged in (a) and (c). Magnification approx. 75×.

FIG. 4. Line patterns on several crystal grains with no applied field. The lines are spaced closer together in the smaller grains. Lines on adjacent grains tend to join at the grain boundaries. The V shaped line deposits near these boundaries are especially to be noted. Magnification approx. 65×.

up to values slightly exceeding that of those shown. A variety of spacings can be observed in Fig. 4 which shows line patterns on several grains. The smaller grains exhibit the closer spacings.

The two patterns with applied field consist of bands of colloid located in alternate colloid-free stripes of the no-field pattern. They bear the now familiar reciprocal relation to each other. The width of these bands proved to be very sensitive to the magnitude of the applied field. For the patterns shown in Fig. 3 this field was the minimum necessary to spread some of the colloid into bands, though much of it, as can be seen, remained in the former no-field lines. The bands, however, are somewhat wider than the intervening spaces. When the field was gradually increased still further the bands continued to grow in width at the expense of the vacant spaces. At the same time the colloid spread itself out more evenly over the bands. The edges of the widening bands moved with a continuous motion punctuated locally by sudden jerks. It appeared as if a certain advancing edge would occasionally meet an obstacle which for a time prevented its progress. After other neighboring boundaries had advanced further the impeded boundary would abruptly jump into place, and then continue in its uniform motion. Two widening bands occasionally merged either by joining throughout their visible length, or quite often by first touching only at a point. In the latter case the apices

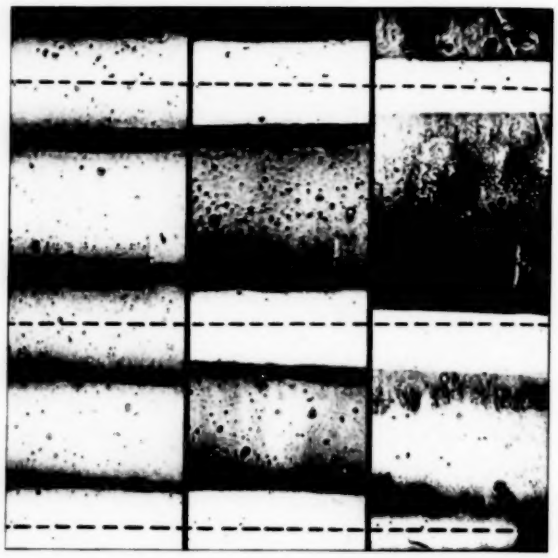

a b c

FIG. 5. Set of patterns which illustrate widening of bands when the applied normal field is increased. (a) No field; (b) small applied field; (c) applied field 5 times as intense as in (b). Magnification approx. 190×.

of the two V-shaped spaces receded from each other with a continued increase of the applied field.

If at any time the field was diminished, the motion of the boundaries reversed. Soon, however, discontinuities in motion of the sort just described would again be observed. Upon complete removal of the field the no-field pattern was similar in scale but in detail apparently unrelated to that first observed. Fig. 5 illustrates the

FIG. 6. Pattern of magnetic colloid associated with structure interpreted as a twin band. This pattern was found on the crystal grain which gave Fig. 3. Magnification approx. 215×.

widening of bands associated with increasing field.

The transition of a prism pattern to a basal pattern was studied at the rounded corner connecting the two planes. On approaching the corner V-shaped line deposits appeared which multiplied the number of lines at the edge of the prism pattern. These lines merged with a pattern resembling that of Fig. 2 when viewed at an oblique angle, the distortion decreasing further until the typical basal pattern appeared. The increase in the number of pattern lines was very similar to that found at the grain boundaries in Fig. 4. A somewhat similar group of V-shaped deposits was noticed near certain line markings found on many of the grains showing prism patterns as illustrated in Fig. 6. In this figure the narrow band, possessing a fine magnetic structure and crossing the black no-field lines, was also revealed by etching. This structure may therefore be identified as the trace of a twin band.[6] The plane of such a twinned lamina will in general approach the surface making an acute angle with it on one side of the trace, thus accounting for the unsymmetrical occurrence of the V-structures which according to this analysis depend for their existence upon large demagnetizing fields.

Discussion

Before discussing the experimental results the basic facts of ferromagnetism will be reviewed briefly. In this review the attempts of other authors to explain the nature of magnetic secondary structure will be considered. According to the Weiss-Heisenberg theory,[7] a ferromagnetic crystal will be at all times spontaneously magnetized to a saturation value which depends on the temperature and becomes zero at the Curie point. Actual crystals, however, possess little or no net magnetic moment unless placed in a magnetic field. To resolve this apparent contradiction the crystal has long been considered to be subdivided into numerous small domains each saturated, so that the crystal as a whole appears unmagnetized. This division into domains can be most simply dealt with by considering the various energies involved in the absence of applied fields.

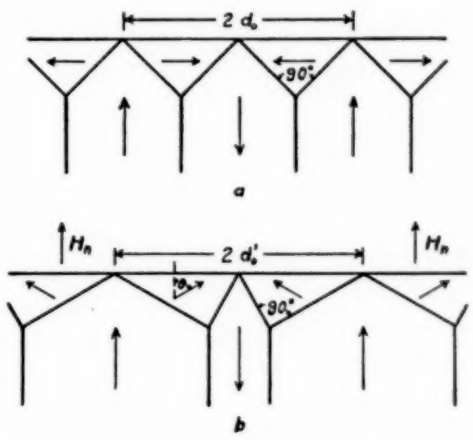

FIG. 7. (a) Schematic diagram (according to Landau and Lifshitz) showing arrangement of magnetization in plane perpendicular to a surface which is perpendicular to direction of easy magnetization. (b) Previous diagram so modified as to include the presence of an applied normal field H_n. Neither of these arrangements of magnetization demanded by minimum total energy of the crystal gives rise to superficial stray fields which can produce magnetic powder patterns.

(1) An energy density E_w associated with the Weiss field (exchange interaction)

E_w is increased by changes in direction of the local magnetization $\mathbf{I}_s$. Explicitly

$$E_w = -\tfrac{1}{2}NI_s^2 + \tfrac{1}{6}Na^2\{(\nabla I_{sx})^2 + (\nabla I_{sy})^2 + (\nabla I_{sz})^2\},$$

where N is the Weiss field constant, "a" is the lattice separation of nearest neighbors and $\mathbf{I}_s$ is the intensity of magnetization (varying only in direction). The first term is well known.[7] The second term, used by Landau and Lifshitz[8] in a manner to be mentioned presently, may be obtained readily by averaging the energy of interaction of a particular elementary magnet with its nearest neighbors. This interaction is assumed for each pair to be of the form $-c\mathbf{I}_s \cdot \mathbf{I}_s'$ where

$$\mathbf{I}_s' = \mathbf{I}_s + (\Delta\mathbf{r}\cdot\nabla)\mathbf{I}_s + \tfrac{1}{2}(\Delta\mathbf{r}\cdot\nabla)^2\mathbf{I}_s,$$

in which $\Delta\mathbf{r}$ gives the position of the selected neighbor. Here $c = \frac{1}{2}N$ since $E_w = -\frac{1}{2}NI_s^2$ when $\mathbf{I}_s$ does not vary in direction. In what follows E_w will be taken to stand for the second term alone.

[6] The twinning of cobalt has apparently not been reported. The present twinned regions are tentatively identified as occurring on the $\{10\bar{1}2\}$ pyramidal planes, as found for other close-packed hexagonal crystals.

[7] E. C. Stoner, *Magnetism and Matter* (Methuen and Co., London, 1934), Ch. XI.

[8] L. Landau and E. Lifshitz, Physik. Zeits. Sowjetunion **8**, 153 (1935).

(2) An energy density E_θ associated with the magnetic anisotropy of the crystal

This energy may include the effects of strain as well as the natural crystal anisotropy. E_θ for unstrained cobalt at room temperature is found empirically to be represented fairly well by $E_\theta = K' \sin^2\theta + K'' \sin^4\theta$ where θ is the angle between the hexagonal axis and $\mathbf{I}_s$, $K' = 5.1\times10^6$ and $K'' = 2.2\times10^6$.[9] The behavior of E_θ, therefore, depends essentially on the quadratic term, and the approximation $E_\theta \doteqdot \frac{1}{2}\beta I_s^2 \sin^2\theta$ may be conveniently used in discussing magnetic structure. In the simplified expression β may be taken to be $2(K'+K'')/I_s^2 = 7.2$ so that E_θ is correct for both $\theta = 0$ and $\theta = 90°$.

(3) An energy density $E_H = -\frac{1}{2}\mathbf{H}\cdot\mathbf{I}_s$ where H is the macroscopic field due to the entire crystal calculated from the potential

$$\phi = \int \frac{\mathbf{I}\cdot d\boldsymbol{\sigma}}{r} - \int \frac{\nabla\cdot\mathbf{I}}{r} d\tau.$$

Frenkel and Dorfman[10] seem to have made the first approximately correct estimate of the diameter d_0 of magnetic domains. By a simple argument (neglecting E_θ) they are able to estimate that $\int_0^V E_w d\tau = C_1/d$ and that $\int_0^V E_H d\tau = C_2 d$ for a space-filling array of disorientated domains of diameter d within a crystal of volume V. It follows that $do = (C_1/C_2)^{\frac{1}{2}}$ for minimum energy. They find for iron crystals of moderate volume V that $d_0 \doteqdot 100\mu$.

Bitter,[11] working with a torque equation equivalent to minimizing $\int (E_w + E_\theta) d\tau$, integrated over regions of the crystal remote from the surface, has discussed what he terms the "elastic deformation of ferromagnetism." The particular cases which he studied are unfortunately chosen since in all of them $\nabla\cdot\mathbf{I}_s \neq 0$. The torques due to the resulting internal magnetic fields are sufficient to render his arrangements of $\mathbf{I}_s$ physically unstable. His attack on the problem, if carried far enough, should lead to the more detailed conclusions of Landau and Lifshitz[8] which will now be discussed.

Landau and Lifshitz minimize $\int (E_w + E_\theta) d\tau$ integrated over the entire crystal. They conclude that in the demagnetized state the magnetization should occur chiefly in plane layers magnetized alternately parallel and anti-parallel to the direction of easy magnetization. Near a surface perpendicular to this direction they propose the arrangement of $\mathbf{I}_s$ shown in Fig. 7a, for which $\int_0^V E_H d\tau = 0$ since $\nabla\cdot\mathbf{I}_s = 0$ and $I_n = 0$. The transition of $\mathbf{I}_s$ from one layer to the next is found to occur gradually, not abruptly. It takes place by a twisting of $\mathbf{I}_s$ about the normal to the boundary between layers, thus making $\nabla\cdot\mathbf{I}_s = 0$. Their equations indicate that the thickness of the transition layer for cobalt is about 45 lattice spacings. The thickness d_0 of the layers is found by minimizing the sum of the energy of the transition layers (of the form $E_i = C_1/d$) and the anisotropy energy in the regions of triangular cross section (of the form $E_a = C_2 d$). If l is the distance between two basal surfaces of a cobalt crystal they find that $d_0 = (8l)^{\frac{1}{2}}(\alpha/\beta)^{\frac{1}{4}}$ for minimum energy, where $\alpha = \frac{1}{3}a^2N = 8.3\times10^{-12}$ and $\beta = 7.2$. This gives $d_0 \doteqdot 15\mu$ for $l = 0.3$ cm, the approximate size of the larger crystal grains in the specimens here studied. This spacing is less than that of the parallel lines of the prims patterns. It is more nearly a measure of the scale of the finer structure in the basal patterns. The minimum energy $\int_0^V (E_w + E_\theta) d\tau$ is somewhat increased if instead of layers, prisms of square or triangular cross section are assumed, together with the arrangement of $\mathbf{I}_s$ near plane surfaces which makes $\int_0^V E_H d\tau = 0$. Hexagonal prisms cannot be arranged so that $\int_0^V E_H d\tau$ vanishes, hence a model with these units would have a still greater minimum energy.

Landau and Lifshitz have also considered crystals with surfaces inclined to the basal plane. By suitable arrangements of $\mathbf{I}_s$ they retain the condition that $\int_0^V E_H d\tau = 0$ and calculate for the layer model the dependence of d_0 upon the inclinations of the exposed surfaces. If their condition that $\nabla\cdot\mathbf{I}_s = 0$ within the crystal be applied to the arrangement of Fig. 7a when an applied normal field is present, the situation becomes that depicted by Fig. 7b. For this arrangement

$$\nabla\cdot\mathbf{I}_s = 0, \quad I_n = I_s \cos\theta = H_n/4\pi,$$

and

$$d_0' = d_0[1 - (I_n/I_s)^2]^{-\frac{1}{2}}.$$

The change in scale of the structure indicated by the last equation results from the decrease in E_s

[9] J. H. Van Vleck, Phys. Rev. **52**, 1178 (1937). All energy densities are expressed in erg. cm^{-3}.

[10] J. Frenkel and J. Dorfman, Nature **126**, 274 (1930).

[11] F. Bitter, Sci. Rep. Tôhoku Imp. Univ. (Honda Volume), 228 (1936); also reference 2, p. 186.

due to: (1) a decrease in volume of the triangular prisms seen end-on in Fig. 7; (2) a decrease in E_θ in these prisms resulting from the rotation of $\mathbf{I}_s$ therein. From the equation it appears that d_0' differs appreciably from d_0 only for large I_n. The difference in scale is important, however, in considering the regrowth of magnetic structure in a crystal which has been magnetized to saturation by an external field.

It is a characteristic of the crystal internally divided into layers or into square or triangular prisms, that $\int_0^V E_H d\tau = 0$. Hence, in the absence of an applied field, a crystal possessing one of these structures should give no pattern. Even an applied normal field should produce no pattern if Fig. 7b is correct, for the field above the specimen is uniform although the magnetization beneath possesses a definite structure. In most cases, however, some stray field will be present; the result of an effect neglected in the Landau-Lifshitz model. $\mathbf{I}_s$ in the surface prisms of triangular section will in general rotate so as to diminish $(E_\theta + E_H)$. This requires $E_H > 0$. This effect can be estimated for the arrangement of $\mathbf{I}_s$ in Fig. 7b, as follows: replace the triangular prisms by an extensive parallel slab of crystal initially magnetized parallel to its surface. By minimizing the energy $E = E_\theta + E_H - H_n I_s \cos\theta$ it is found that a normal field H_n will tilt $\mathbf{I}_s$ by an amount given by $\cos\theta = H_n/[(4\pi - \beta)I_s]$ rather than by $\cos\theta = H_n/4\pi I_s$. As $\beta \doteqdot 2\pi$ for cobalt, this effect is quite appreciable, hence in the event of a layer structure, some deposition of colloid should be expected.

For ideal crystals there seems little doubt that the treatment just outlined is essentially correct. The discrepancy between the ideal structure and the one indicated by the patterns probably arises during the process whereby the crystal goes from the magnetized to the demagnetized state. Irreversible energy losses accompanying this process dissipate some of the potential energy which would otherwise be available to establish the ideal structure. Nevertheless, the Landau-Lifshitz treatment is important since it justifies the description of magnetic structure in terms of geometrical models. Furthermore, it suggests arrangements of $\mathbf{I}_s$ likely to occur, such as that of Fig. 7a. For instance, if the layers should extend all the way to the surface, the resulting surface energy $(\int_0^V E_H d\tau)$ would be much greater than that when the triangular prisms lying in the surface afford a return path for lines of induction within the crystal. With this background the patterns can now be analyzed.

The prism patterns (parallel lines and bands) can be interpreted as indicating sections of regions magnetized alternately parallel and antiparallel to the hexagonal axis. The no-field patterns indicate that the surfaces so far observed have not been exactly parallel to the axis so that alternate strips have I_n plus and minus. This accounts satisfactorily for the observed patterns. The widening of the bands with increasing applied field is, of course, an additional feature. The component of the applied field parallel to the axis must be responsible for this. Thus by a suitable choice of field direction near the normal it should be possible to control independently the width of the bands and the particular set of strips preferred by the colloid.

Since the field $\mathbf{H}$ below the surface arising from the potential $\int \mathbf{I}_s \cdot d\boldsymbol{\sigma}/r$ is an image of the stray field above the surface, the magnetization near the surface will be rotated so as to decrease the stray field. This decrease amounts to perhaps 60 percent for surfaces slightly inclined to the hexagonal axis. It should not alter the essential features of the prism patterns.

The spacing of the parallel lines requires some comment. Its regularity is probably not typical of the magnetic structure existing before the surface was prepared. For surfaces not too oblique to the axis the number of regions should not be changed, but the energy will be minimized by making the areas of adjacent regions of opposite polarity more nearly equal.

A clear interpretation of the basal patterns is more difficult to achieve. As already pointed out none of the simple structures of layers, square or triangular prisms is adequate. A clue is found in the fact that the spacing of the parallel lines is about equal to the spacings of the irregular areas of light and heavy deposit in the basal patterns. It is suggested that the more or less definite boundaries between these distinguishable areas are traces of the boundaries separating regions of reversed magnetization deep in the crystal. The finer detail seems closely connected with dendrite-like reversed regions extending short

distances into the crystal and producing in cross section the V-shaped line deposits. This picture is probably further complicated by the occurrence of dendrites within dendrites, as some of these deposits in Fig. 4 suggest. The following analysis, suggested by the behavior of the cobalt patterns studied so far, is an attempt to make this magnetic structure appear a reasonable one.

Imagine a disk shaped crystal having basal planes as faces and magnetized to saturation by a field applied parallel to the disk axis. If H is reduced slightly below $4\pi I_s$ regions of reverse magnetization must form. Presumably many of them occur first at the two basal surfaces and then grow inward towards one another, finally meeting by pairs to form complete thread-like regions extending through the crystal. In their early stages of growth these regions resemble dendrites of a solid phase growing into the melt. The conditions are similar in respect to the gradual supply of energy necessary for the change occurring and in respect to the stability in space of the transformed regions.

As H is still further reduced, more dendrites form, those already present continue to grow inward and the completed threads (or prisms) increase in cross section. The surfaces of the disk will on the average be uniformly populated with reversed regions. The number of reversed regions will become greater as demagnetization proceeds. This corresponds to the change in scale of the ideal layer structure, previously pointed out. The requirement of finer scale at later stages necessitate that some of the new dendrites form within regions already anti-parallel to H, and hence be themselves parallel to H. Photographs have been taken of V-structures near the boundaries of prism patterns which, if one judges from the deposit on them, were magnetized parallel to H, and *which grew as H was decreased*. Finally, when H becomes zero, many of the dendrites started last will remain as such, there being insufficient energy available for them to grow far into the crystal. This is equivalent to stating that the residual magnetic field at the boundaries of the dendrites is insufficient to cause their further advance. The resulting magnetic structure near a basal surface is not one of plane parallel layers, but one more nearly described as consisting of hexagonal prisms of about the same size, arranged so that the energy $\int_0^V (E_w+E_\theta+E_H)d\tau$ is as small as possible. A short distance from the crystal surface many of these prisms pinch out leaving the much coarser structure responsible for the typical prism patterns.

Some of the hexagonal prisms will be completely surrounded at a basal surface by others of opposite magnetization. An arrangement of $\mathbf{I}_s$ corresponding to the layer model in Fig. 7a is demanded by minimum energy for such a grouping. Hence there will be locally no stray field above the surface. The absence of colloid in certain areas of the no-field basal patterns, and the very small amount appearing above these same areas in the normal field patterns may thus be accounted for. At other boundaries between oppositely magnetized prisms only a part of the lines of induction can return within the crystal. Indeed, the best possible arrangement of regular hexagonal prisms permits the return of but two-thirds of the lines of induction in this manner; the remainder give rise to the stray field which is chiefly responsible for the basal patterns.

In conclusion it should be pointed out that the erratic movement of the parallel lines is visual evidence of the Barkhausen effect. This effect in cobalt does not seem to consist of the sudden reversal of definite domains in the crystal, but may be ascribed to the uneven motion of boundaries between regions considerably larger than those usually assigned to account for Barkhausen discontinuities, containing about 10^{12} atoms. Local imperfections in the crystal are no doubt responsible for this effect. They also must be largely responsible for energy lost during the process of demagnetization.

The author is greatly indebted to Professor F. Bitter of the department of metallurgy for providing certain facilities for conducting this research, and to Professor L. W. McKeehan of Yale for reading and discussing the manuscript.

LETTERS TO THE EDITOR

Prompt publication of brief reports of important discoveries in physics may be secured by addressing them to this department. Closing dates for this department are, for the first issue of the month, the eighteenth of the preceding month, for the second issue, the third of the month. Because of the late closing dates for the section no proof can be shown to authors. The Board of Editors does not hold itself responsible for the opinions expressed by the correspondents.

Communications should not in general exceed 600 words in length.

Radio Isotopes of Nickel

2.6-hour Ni^{63}

The early observations[1, 2] of a radioactivity of a few hours half-life induced in nickel by slow neutrons has been rather definitely identified as due to Ni^{63} through the work of Oeser and Tuck[3] with slow neutrons and that of Heyn[4] with fast and slow neutrons. It has also been produced by the bombardment of copper with neutrons,[3, 4] and of zinc with neutrons.[4] Chemical identification has been made in all these cases. The half-life is quoted as 2.5 and 2.66 hours. It is rather surprising, therefore, that this period should not have been found by Thornton[5] after bombarding nickel with 5 Mev deuterons, since its presence is to be expected, if due to either Ni^{63} or Ni^{65}. Only a positron emitting isotope of copper was found, presumably Cu^{61}, with a half-life of 3.4 hours; the activities in the nickel and cobalt precipitates were disregarded, as their intensities were only 0.01 and 0.005 that of the copper.

This note is to point out that the deuteron bombardment of nickel does produce the nickel activity as well as that of the copper (and in addition a cobalt period of some months' half-life on which we shall report later). The exposure of nickel for four hours to 100 microamperes of 5.5 Mev deuterons yields a chemically identified nickel isotope of half-life 2.6 ± 0.03 hours; the emitted particles are negative electrons which are absorbed to half-value by 0.13 gram/cm² Al and which have a range of 0.90 ± 0.1 gram/cm² Al, indicating a maximum energy of 1.9 Mev, by Feather's relation.[6] The gamma-rays are absorbed to half-value by 10.8 grams/cm² Pb, equivalent to an energy of 1.1 Mev, according to the data of Gentner.[7] Heyn's value for the half-thickness of the electrons from the neutron-produced activity is 0.10 gram/cm². The identification with this previously known period seems to be complete.

We cannot give an exact estimate of the intensity ratio of the Ni^{63} and Cu^{61} activities, since only part (perhaps one-quarter) of the voluminous nickel dimethylglyoxime precipitate was followed. The extrapolated initial intensity of this fraction of the nickel was 3.4×10^5 times background, while that of the entire copper precipitate was 4.0×10^6 times background (approximately 4 millicuries).

The production of this 2.6-hour nickel through the reaction $Ni^{62}(d,p)Ni^{63}$ may alter the interpretation of the excitation function for Cu^{61} produced by $Ni^{60}(d,n)Cu^{61}$ as given by Thornton,[5] since a chemical separation was not performed on the stack of nickel foils used to determine the activation probability. It is difficult for us to understand why the gamma-ray from Ni^{63} was not observed by Richardson[8] in his examination of the gamma-rays from a deuteron-on-nickel bombardment, unless a chemical separation for copper and nickel was made, which is not so stated.

Our neutron bombardments of nickel have not disclosed any nickel periods shorter than the 2.6-hour activity; short periods from deuteron irradiations of nickel have not been looked for.

36-hour Ni^{57}

We wish to report a new radioactive isotope of nickel, formed as the result of the exposure of iron to several microampere hours of bombardment with helium ions at 12.6 Mev and also at 16 Mev. The chemically separated nickel emits positrons with a half-life of 36 ± 2 hours. Absorption measurements on the particles indicate a half-value thickness of 0.034 gram/cm² Al and a range of 0.25 ± 0.05 gram/cm² Al, corresponding to a maximum energy of 0.67 ± 0.1 Mev by Feather's relation.[6] A gamma-ray is also evident, probably annihilation radiation.

The only unstable nickel isotopes that could be formed from iron by the $Fe(\alpha,n)Ni$ reaction are Ni^{57} and Ni^{59}. The lightest stable nickel is Ni^{58} (abundance 68 percent), so that if the 36-hour period were due to Ni^{59}, it should be produced by slow neutrons or deuterons on nickel. We have not been able to detect this activity after strong irradiation of nickel with deuterons or slow neutrons, so we feel justified in ascribing the activity to Ni^{57} through $Fe^{54}(\alpha,n)Ni^{57}$, followed by positron decay to stable Co^{57}. With fast neutrons (from lithium plus deuterons) on nickel, we have found a weak and somewhat doubtful indication of the period, intermixed with some longer lived activities, so that possibly the reaction $Ni^{58}(n,2n)Ni^{57}$ has also been observed.

We are glad to acknowledge the continued assistance of the Chemical Foundation, the Research Corporation and the Josiah Macy, Jr. Foundation.

J. J. LIVINGOOD
G. T. SEABORG

Radiation Laboratory, Department of Physics, (J. J. L.)
Department of Chemistry, (G. T. S.)
University of California,
Berkeley, California,
April 14, 1938.

[1] Rotblat, Nature **136**, 515 (1935).
[2] Naidu, Nature **137**, 578 (1936).
[3] Oeser and Tuck, Nature **139**, 1110 (1937).
[4] Heyn, Physica **4**, 1224 (1937).
[5] Thornton, Phys. Rev. **51**, 893 (1937).
[6] Feather, Phys. Rev. **35**, 1559 (1930).
[7] Gentner, J. de phys. et rad. **6**, 274 (1935).
[8] Richardson, Phys. Rev. **53**, 610 (1938).

Drift of Adsorbed TH on W Filaments Heated with d.c.

A study (soon to be reported) of the surface structure produced on tungsten lamp filaments during long heating with direct current has suggested that W ions drift over the wire surface toward the negative terminal. Such migration can be demonstrated directly, for the case of Th adsorbed on W, in a simple electron-optical tube.

A loop of 1 mil thoriated wire 6 mm long is mounted on 30-mil leads at the center of a spherical bulb 3 inches in diameter coated inside with willemite. The anode, a wire ring near the mouth of the bulb, is made a few thousand volts positive, and the emitted electrons form on the screen a magnified orthogonal image of the loop; the screen is kept near anode potential by secondary emission. A 10-mil Ni wire, welded to one filament lead and projecting between the ends of the loop, casts an electrical shadow which permits distinguishing the emission from the two ends, and also prevents evaporation of Th from one end across to the other. With the anode floating, the filament is first flashed and then is heated, from a 2 v d.c. supply, for 20 or 30 minutes at a low activating temperature. The electron image, observed briefly at a low temperature where Th is immobile, is then brightest opposite the negative end of the loop, with a sharp cutoff toward the lead and a gradual decrease toward the center. The positive side of the screen is dark. With 60-cycle a.c. heating, the activation is always symmetrical about the center of the wire. These observations have been repeated in a similar tube, with a loop of 2 mil thoriated wire.

The processes involved in activation of a short filament are obviously manifold, but the net result, that Th accumulates preferentially at the negative end, strongly indicates a drift of ions in the electric field. Ionization in the space is ruled out by the low voltage of the heating supply, the shadow-caster stops evaporation from one end to the other, and thermionic emission from either end is at the worst limited by space charge to a value too low to give appreciable cooling.

This experimental arrangement is not adapted for yielding values for either the mobility or the activation energy for migration under the influence of a field. Deposit of Th on an isothermal length of smooth undoped filament (preferably a single crystal), by evaporation from an external source, at present seems a promising technique for future study of the effect.

R. P. JOHNSON

Research Laboratory,
General Electric Company,
Schenectady, New York,
April 6, 1938.

On the Form of the β-Spectrum of Ra E in the Vicinity of the Upper Limit and the Mass of the Neutrino

The spectrum of the β-particles emitted by Ra E has often been studied and at the present time[1] it is established that the form of the spectrum over a wide range may be accounted for satisfactorily by the formula of Uhlenbeck and Konopinski. However the spectrum in the immediate neighborhood of the upper limit has been studied in much less detail. Nevertheless the results of Lyman's[2] measurements and those described in this note indicate that the

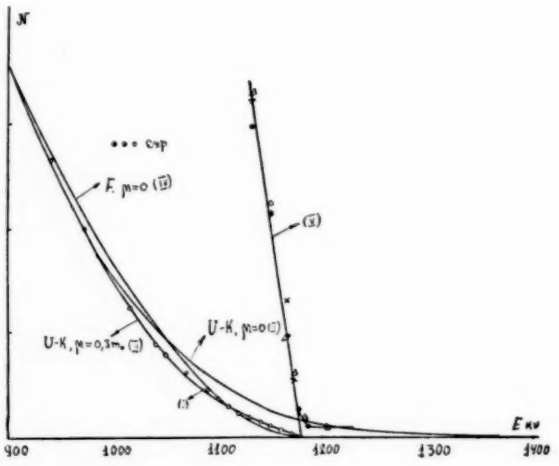

FIG. 1.

form of the spectrum in this region departs considerably from that predicted by theory. The study of the energy distribution of the electrons in the neighborhood of the spectral limit is for a number of reasons accompanied by considerable difficulty, chief of which is the low intensity of the radiation in this part of the spectrum. The choice of apparatus and the sensitivity of the method of registering the electrons are therefore of prime importance. In the experiments described below, the method of electron focusing in a uniform magnetic field has been used. The electrons were registered by the method of coincident discharges in Geiger-Müller counters. It was necessary to guard against electrons scattered from the walls of the apparatus and from the diaphragm entering the counters. This was attained by separating out a narrow beam of electrons ($\phi = 10°$) and by a special system of traps.

By placing the first counter with its narrow slit at the focus it was possible to eliminate almost completely the entry of scattered electrons. The source was a thin nickel strip on which 0.3−1.0 mC of Ra E were deposited. The spectrum was studied in detail from $E = 1030$ kv to $E_m = 1180$ kv. The results are represented in Fig. 1(I) and it will be seen that the energy intervals were very narrow. The random error of the individual points on the curve were very small and the measurements of the magnetic field constitute the main error. A noticeable feature in Fig. 1 is the sharp change in the curve at an energy of about 1120 kv after which the number of electrons decreases practically linearly. This part of the curve is reproduced on a larger scale in the same figure for the sake of clarity (V). The results of repeated experiments are indicated by different signs. The insignificant number of electrons observed at $E > E_m$ is undoubtedly due to scattered electrons and indicates that the experimental conditions were satisfactory.

The spectra computed according to the formula:

$$P \sim W \cdot (W^2-1)^{\frac{1}{2}} \cdot (W_0 - W)^3 \cdot [(W_0 - W)^2 - (\mu/m)^2]^{\frac{1}{2}} \cdot f(Z, W),$$

which follows from the theory of Konopinski and Uhlenbeck are given in Fig. 1. Curve II refers to the case $\mu = 0$

and $W_0=3.69m_0c^2$ and curve III to the case $\mu=0.3m_0$ and $W_0=3.69m_0c^2$. It is clear that curve III agrees excellently with the experimental results. It may be noted that the remainder of the experimental spectrum also fits the Uhlenbeck-Konopinski theory satisfactorily when $\mu=0.3m_0$. The curve IV of Fig. 1 has been computed according to Fermi's formula, from the experimental value of the spectral limit $(W_0)_{exp}=3.31m_0c^2$ while μ was taken equal to zero. This curve clearly does not agree with that found experimentally.

A. I. ALICHANIAN
A. I. ALICHANOW
B. S. DŽELEPOW

Physico-Technical Institute,
Leningrad, U.S.S.R.
March 16, 1938.

[1] A. Alichanian and A. Zavelsky, Comptes rendus d. Acad. d. L'URSS. **17**, 467 (1937).
[2] Lyman, Phys. Rev. **51**, 1 (1937).

The Shape of the β-Spectrum of Th C and the Mass of the Neutrino

In the preceding letter of A. I. Alichanian, A. I. Alichanow and B. S. Dželepow it was shown that the intensity curve of Ra E cuts the axis of abscissa at a certain angle.

It was of importance therefore to investigate whether the shape of the Ra E spectrum is typical for all radioactive elements. The end of the spectrum of Th C was accordingly studied by the magnetic focusing method with registration by means of coincidences. The apparatus was the same as that used for Ra E.[1] A narrow beam of electrons with an angle of spread $\phi=10°$ was focused onto the slit of the first counter ($d\sim0.8$ mm). A considerable number of diaphragms and traps prevented scattered electrons from entering the counting system. An active deposit of Th(B+C+C″) (1.0–1.5 mC) was deposited on an aluminum strip 0.3 mm wide and 5 mm long.

The end of the spectrum is represented in Fig. 1(I). There is a distinct break in the curve at $E=2130$ kv, similar to that observed in the spectrum of Ra E, after which the curve falls off practically linearly to the very limit. The small number of coincidences observed for $H>H_m$ is due partly to Compton electrons liberated from the walls of the vessel by γ-rays, and partly to scattered electrons and random coincidences. It is clear, however, that this background does not depend on the strength of the magnetic field. The remainder of the Th C spectrum down to $E=1275$ kv is given in the same figure (V). By constructing the Konopinski-Uhlenbeck plot from this spectrum (assuming the mass of the neutrino $\mu=0$) we found the extrapolated limit $W_0=6.18$ with the help of which the K−U spectrum for $\mu=0$ was constructed (curve II). Curve III was computed according to Fermi's theory with $\mu=0$ from the experimentally determined spectral limit for the total energy of disintegration. Finally curve IV has been computed according to the Konopinski-Uhlenbeck theory, for $\mu=0.8m_0$ from the formula

$$P\sim W(W^2-1)^{\frac{1}{2}}\cdot(W_0-W)^2\cdot[(W_0-W)^2-(\mu/m)^2]^{\frac{1}{2}}\cdot f(Z,\ W)$$

where $W_0=(W_0)_{exp}+0.8m_0c^2$. It is clear that none of the theoretical curves cited, with the exception of curve IV, agrees with the experimental spectrum. The satisfactory agreement between the latter and the Konopinski-Uhlenbeck curve for $\mu=0.8m_0$ was not confined to the immediate vicinity of the limit but extended to the rest of the spectrum. A similar analysis in the case of the Ra E spectrum showed that agreement between the theoretical and experimental curves is obtained when $\mu=0.3m_0$.

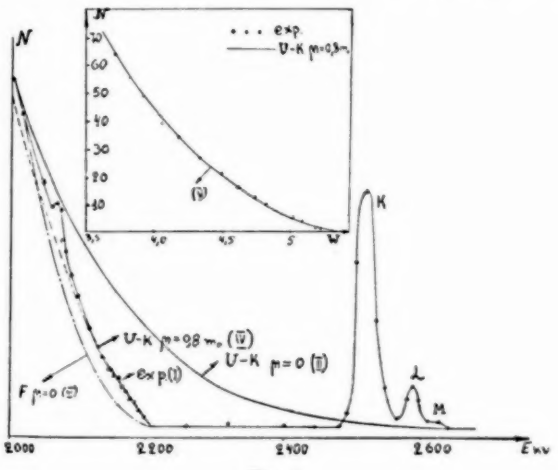

FIG. 1.

The following conclusions may be drawn from these results. The existing theory of Konopinski and Uhlenbeck describes the experimental results correctly when $\mu\neq0$. μ however is not a constant for all elements and varies with W_0.

It was found that the most suitable value of μ could be deduced from the equation:

$$(W_0)_{extr}-(W_0)_{exp}=\mu c^2$$

which gives $0.8m_0c^2$ for Th C and $0.3m_0c^2$ for Ra E. The fact, however, that μ varies from element to element means that no simple significance can be attached to this parameter.

Preliminary measurements of the end of the spectrum of Ra C showed that in this case also the shape is similar to that in the vicinity of the spectral limit of Ra E and Th C.

The three maxima observed in the figure at $E_1=2526$ kv, $E_2=2588$ kv and $E_3=2610$ kv are due to internal conversion of the γ-rays of Th C″ ($h\nu=2614$ kv) in the K, L and M levels of Th Pb. The sharpness of the lines bears witness to the high resolving power of the apparatus and the absence of disturbing factors. The relative intensities of the lines 5 : 1 : 0.2 give the relative probabilities of conversion of the γ-line 2614 kv in the K, L and M levels. The small maximum at $E=2070$ kv corresponds to the internal conversion of the γ-line $h\nu=2160$ kv found by Alichanow and W. Dželepow[2] in the positron spectrum of Th (C+C″). The present measurements yield a value of $\alpha=1.77\times10^{-3}$ for the coefficient of internal conversion of the γ-line 2614 kv whereas according to Taylor and Mott[3] the theoretical value is $\alpha=1.5\times10^{-3}$.

A. I. ALICHANIAN
S. J. NIKITIN

Physico-Technical Institute,
Leningrad, U.S.S.R.,
March 16, 1938.

[1] A. Alichanian, II Union Conference on Nuclear Physics, Moscow, Sept. 27, 1937.
[2] A. Alichanow and W. P. Dželepow, Physik. Zeits. Sowjetunion (in print).
[3] H. M. Taylor and N. F. Mott, Proc. Roy. Soc. **138**, 665 (1932).

Note on Atmospheric Absorption Caused by the Rotational Water Band

In a recent article[1] the writer computed the infra-red absorption of the atmosphere which is caused by the rotational water band. The work was based upon the analysis of the rotational spectrum given by Randall, Dennison, Ginsburg and Weber.[2] The average absorption for an interval containing many individual lines is proportional to the square root of the optical mass, a known result for the absorption of a line spectrum when the distance between the lines is large compared with the line width.

The black-body curve for $T=300°$ extends from about 4μ towards longer waves and has its maximum around 10μ. Thermal radiation of the atmosphere is mainly due to the vibrational water band at 6μ and to the rotational band. It appears from the above-mentioned calculations that the highest rotational lines are too weak to cause appreciable absorption and with an average water content of the atmosphere there should be practically complete transparency between about 8μ and 22μ. This result is not in agreement with the measurements of the heat radiation of the sky which give much higher values of the total radiation than one would expect on this basis. The discrepancy can be removed by taking into account the effect which is produced by the very intense rotational lines at a large distance from the line center. Although these lines are situated at the far infra-red side of the band (50μ), they produce absorption between 10 and 20μ. The absorption coefficient due to the line wings is readily seen to be

$$k=\sum_{\nu_0} i_0\alpha/\pi(\nu-\nu_0)^2,$$

where the summation extends over all lines of the band. The i_0 are the line intensities and α is the half-width for which, as previously,[1] a value of 0.25 cm^{-1} was assumed. Under atmospheric conditions line broadening is due to collisions and therefore α is proportional to the air pressure. The above value refers to standard pressure. Numerical calculations have been carried out for $T=220°$ (temperature of the stratosphere) and $T=300°$. They yield the results given in Table I, if the optical thickness of water

TABLE I. *Values of k at 200 and 300° Kelvin.*

$\nu(cm^{-1})$	400	450	500	600	700	800	900	1000
k_{220}	2.61	1.43	0.96	0.54	0.35	0.23	0.18	0.14
k_{300}	3.50	1.36	0.90	0.46	0.30	0.21	0.15	0.12

vapor is expressed in grams of water per cm^2. For $\nu>500$ cm^{-1} the following formula gives a good approximation

$$k=(78{,}000-240t)/(\nu-200)^2$$

where t is the temperature on the centigrade scale. It must be emphasized that this absorption is exponential, $J=J_0e^{-kx}$; it is therefore far more sensitive towards changes in the water content of the atmosphere than the absorption within the band itself which varies only with the square root of the water mass. This is in agreement with the observations of the thermal radiation of the sky which shows a very considerable dependence upon humidity. Under laboratory conditions the continuous absorption is too weak to be observed in moist air; it does however show up in the absorption of steam.[3] The absorption is proportional to the half-width of the lines and since the latter is not precisely known, the relative variation of the above figures is more significant than their absolute values.

A more detailed account of this work will be given later.

W. M. ELSASSER

California Institute of Technology.
Pasadena, California,
April 15, 1938.

[1] W. M. Elsasser, Astrophys. J. April, 1938.
[2] H. M. Randall, D. M. Dennison, N. Ginsburg and R. L. Weber, Phys. Rev. **52**, 160 (1937).
[3] G. Hettner, Ann. d. Physik **55**, 476 (1918).

Recalescence in Uranium

During the summer of 1937 the thermionic work function and the emissivity of well-outgassed uranium were investigated. The results will be published at a later date.

In the course of these experiments a striking double recalescence was observed, resembling the well-known phenomenon in iron at the β–γ transition just above 900°C. It is thought that there may be corresponding changes in the crystal structure of uranium at temperatures in the vicinity of 600 and 800°C. An attempt is being made to investigate the matter further by means of x-rays.

W. L. HOLE
R. WRIGHT
H. B. WAHLIN

Department of Physics,
University of Wisconsin,
Madison, Wisconsin,
April 12, 1938.

Cosmic Rays; Barometric Effect, Variations of Second Kind and Disturbances Produced by the Earth's Magnetic Field

Simultaneous records of the zenithal intensity of cosmic rays have been made during a period of nearly a year with large Geiger-Müller counters in two separated double coincidence arrangements. The new method of mutual control proved very reliable and rendered even semi-hourly values trustworthy as may be seen from the Figs. 1–3. In these the cosmic-ray intensity I reduced to 750 mm Hg together with the variations of the atmospheric pressure, the horizontal X (N–S) and vertical Z components of the earth's magnetic field are plotted separately for each arrangement for the month of January, 1938. I am very indebted to Professor Bartels and his staff for these magnetic data from the Adolf-Schmidt Observatorium Niemegk.

In the first half of January, 1938 the records run nearly undisturbed both for I, X and Z contrary to the second half of the month, during which three great magnetic storms, each of different behavior, occur. At once the cosmic-ray intensity diminishes simultaneously and almost in the same manner as X, and inversely as Z, but distinctly different each time as the magnetic storms themselves

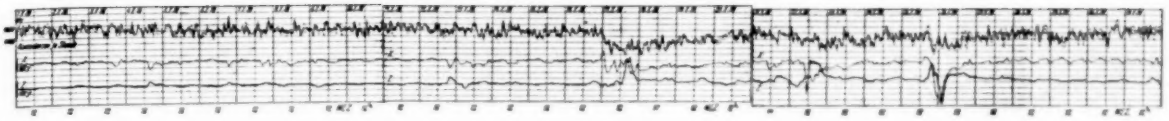

FIG. 1. Cosmic-ray intensity I, horizontal X (N–S) and vertical Z components of the earth's magnetic field.

vary. The first storm (Fig. 2) of January 16 exhibits a long perturbation of Störmer's toroidal stream and, in consequence of the large distance, a greater influence on cosmic-ray intensity; whereas the shorter storm (Fig. 3) with the extended aurora of January 25, occurring in lower regions, affected the rays not so much. Finally the second storm of January 22 brings only a relative small diminution of I; X, and Z changed at first inversely. It is to be hoped that closer investigation now in progress will reveal further details, also for the smaller variations of the earth's magnetic field. At any rate magnetic disturbances almost always seem to reduce cosmic-ray intensity contrary to the hitherto prevailing opinion.

For the so-called "variations of the second kind" of cosmic-ray intensity, especially the very fast decreases which are followed by more or less slow increases, are characteristic features. The magnetic influences here reported perform in essentially the same manner so that these variations of the second kind are really the consequences of magnetic disturbances.

The magnetic variations and their influence on cosmic-ray intensity reveals the variability of the barometric

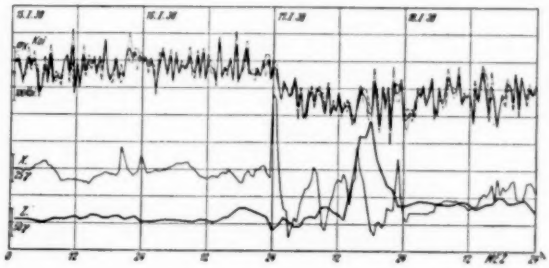

FIG. 2. Cosmic-ray intensity I, horizontal X (N–S) and vertical Z components of the earth's magnetic field.

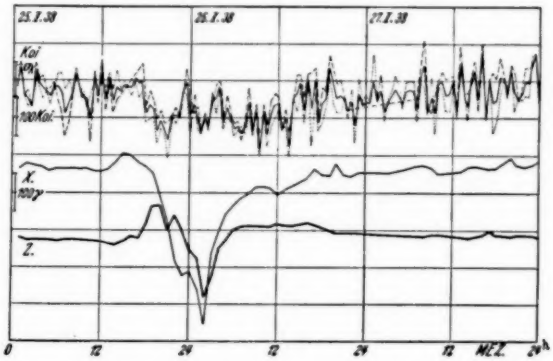

FIG. 3. Cosmic-ray intensity I, horizontal X (N–S) and vertical Z components of the earth's magnetic field.

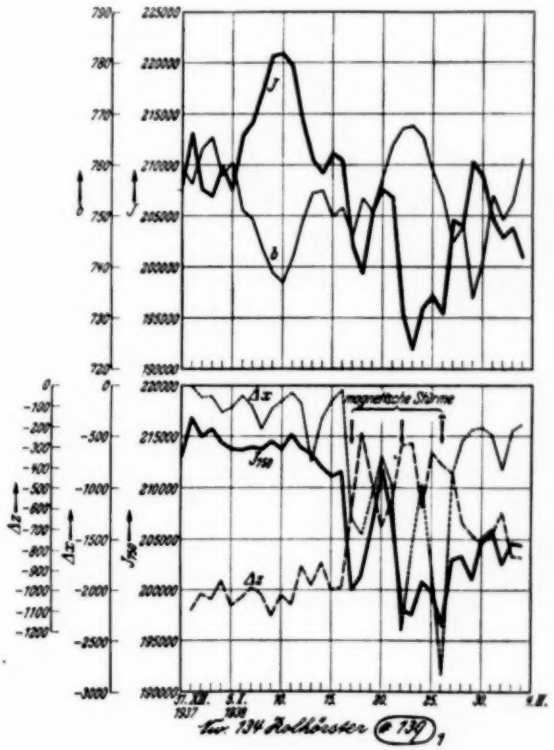

FIG. 4. Daily mean values of atmospheric pressure, cosmic-ray intensities and magnetic field values.

effect. Fig. 4 of the daily means both for intensity I (unreduced) and atmospheric pressure shows a perfect reciprocal behavior during the magnetic undisturbed period of January, 1938 contrary to the disturbed second half. If however the daily means of I are reduced with a constant barometric coefficient, derived from a long series, the intensity remains constant during magnetic undisturbed periods but changes at once when magnetic variations occur.

The real barometric effect is therefore a pure absorption effect with a nearly constant coefficient and has nothing to do with the observed variations of the usually so-called barometric effect, which result both from magnetic and absorption phenomena perhaps also from other but less important influences. However these absorption effects are somewhat complicated, since they originate from the different energies of the rays, as will be shown elsewhere.

W. KOLHÖRSTER

Institut für Höhenstrahlenforschung
der Universität Berlin,
Berlin, Germany,
April 4, 1938.

Artificial Radioactivity Produced by Protons

By the use of a beam of about one microampere of protons at an energy of 3.8 Mev, accelerated by the Princeton cyclotron,[1] we have found that Ni, Cu, Mg and Ag are strongly radioactive after bombardment. The following identifications are suggested for the radioelements formed.

Ni: Four periods are found in the decay of Ni bombarded with protons. The half-lives are 80 ± 2 seconds, 7.9 ± 0.6 minutes, 3.4 ± 0.1 hours, and 12.8 ± 0.3 hours. The relative initial intensities in a thick target, corrected to infinite bombardment time, are about 3 :1 :31 :35, respectively. The three shorter periods all emit positrons, while the 12.8-hour period has been found to emit both electrons and positrons. The last activity is then almost certainly to be identified[2] with Cu^{64}, formed here by the reaction $Ni^{64}(p, n)Cu^{64}$. The 3.4-hour period can also be identified with some certainty[3] as Cu^{61}, formed from the stable isotope Ni^{61} by the (p, n) reaction. Two radioelements of approximately these periods were reported as formed by proton bombardment of Ni in the preliminary data of DuBridge and his collaborators,[4] but were not mentioned in their recent paper.[5]

While chemical identification of the two short periods has not been carried out, the fact that positrons are emitted makes it seem very likely that the radioelements are Cu isotopes, formed by the (p, n) reaction. Our decay curves give no evidence for a half-life of 10 minutes, which is that[6] of Cu^{62}, so that one of the short lived radioelements observed probably arises from Ni^{60}, and the other from Ni^{58}. We may tentatively assign the 80-second period to Cu^{58} and the 7.9-minute period to Cu^{60}, on the doubtful basis of relating the activity ratio of these two radioelements with the abundance ratio of Ni^{58} to Ni^{60}.

Cu: Copper bombarded with protons displays a moderately strong activity in which positrons are emitted. The half-life is 38 ± 1 minutes. This radioelement may be identified[7] as Zn^{63}, formed here by the reaction $Cu^{63}(p, n)Zn^{63}$.

Mg: Measurement of the activity of this element was not begun soon enough after bombardment to detect the presence of Al^{26}, which has a 7-second half-life[8] and could be formed here by the (p, n) reaction. The decay curves of activated Mg showed a fairly strong period of 20 ± 2 minutes, together with a much weaker activity of some hours half-life. The short period radioelement emits positrons and has been chemically identified as an Al isotope. It is presumably either Al^{24} or Al^{25}.

Ag: The decay curves in this element show a weak activity of a few minutes half-life, which has not been investigated, and a very strong activity of half-life 6.67 ± 0.06 hours. Chemical identification of the long lived radioelement shows that it is an isotope of Cd, presumably either Cd^{107} or Cd^{109}. The particles emitted are negative electrons, as has been shown by deflecting them in a magnetic field, and their energies, as measured by absorption in Al, are not greater than about 250 Kev. A very much weaker radiation with greater penetrating power (see Fig. 1) has a mass absorption coefficient in Al which is that of the $K\alpha$ radiation of Ag. There is some indication of a harder radiation still which is of such small intensity that we have not been able to investigate its absorption with the Lauritsen electroscope used in these measurements.

Since neither In^{109} nor In^{107} is a stable isotope, we tentatively regard the negative electrons emitted by this radioelement not as disintegration electrons, but as photoelectrons ejected by a gamma-radiation which follows extranuclear electron capture by the unstable Cd isotope. If the absorption measurements are correct in indicating that the K radiation of silver is also emitted, the production of this radiation is presumably accomplished in two ways; by the filling of the K shell in Ag after the capture by the unstable Cd nucleus of one of its own K electrons, and by the replacement of electrons which have been removed from the atom by the internal conversion process postulated to explain the negative electron emission from this radioelement. The harder radiation suggested by the absorption curve may be the unconverted fraction of the nuclear gamma-radiation postulated above. Rough considerations of intensity lead to the conclusion that the internal conversion coefficient for this gamma-radiation must be about 90 percent. The whole situation in this radioelement is similar to the case of Ga^{67} discussed by Alvarez.[9]

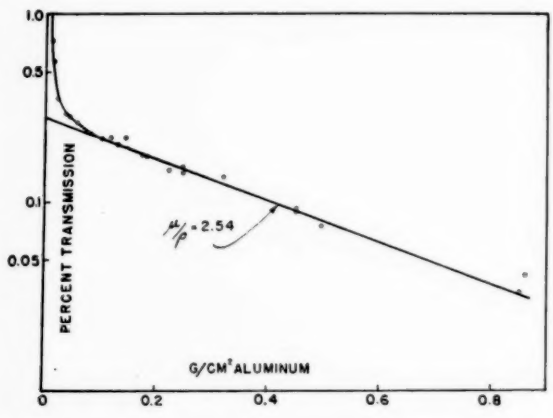

FIG. 1. Absorption in Al of the radiation from silver which has been bombarded with protons (6.67-hour period). The mass range of the electrons is seen to be about 70 mg/cm², while the mass absorption of the gamma-radiation is that of the $K\alpha$ radiation of Ag.

We are glad to be able to thank Mr. R. C. Newton, of the department of chemistry, for suggestions concerning the chemical separations, and Mr. John E. Walter for assistance in making the measurements.

LOUIS N. RIDENOUR
L. A. DELSASSO
M. G. WHITE
RUBBY SHERR

Palmer Physical Laboratory,
Princeton University,
Princeton, New Jersey,
April 15, 1938.

[1] M. G. Henderson and White, Rev. Sci. Inst. **9**, 19 (1938).
[2] Van Voorhis, Phys. Rev. **50**, 895 (1936).
[3] Thornton, Phys. Rev. **51**, 893 (1937); Ridenour and W. J. Henderson, Phys. Rev. **52**, 889 (1937).
[4] Livingston and Bethe, Rev. Mod. Phys. **9**, 245 (1937). See p. 317.
[5] DuBridge, Barnes, Buck, and Strain, Phys. Rev. **53**, 447 (1938).
[6] Heyn, Nature **138**, 723 (1936); Bothe and Gentner, Zeits. f. Physik **106**, 236 (1937); Ridenour and Henderson, reference 3.
[7] Pool, Cork and Thornton, Phys. Rev. **52**, 239 (1937). Also papers of reference 6.
[8] Frisch, Nature **133**, 721 (1934).
[9] Alvarez, Phys. Rev. **53**, 606 (1938).

Concentration of Radioactive Copper by Use of a High Speed Rotating Cathode*

Radioactive copper (period 12.8 hours), formed from zinc by neutron bombardment, has previously been concentrated in three ways: addition of inactive copper ion, followed by precipitation of CuS;[1] addition of inactive copper ion followed by deposition on a zinc plate;[1] and partial solution of zinc dust in acid, followed by electrochemical displacement on a lead plate.[2] This communication describes a fourth method, which may find wide general use in problems of concentrating minute quantities of such isotopes. The high speed rotating cathode,[3, 4] it has been found, will separate a considerable proportion of the radioactive copper from solution, without the addition of its nonradioactive isotope as a "carrier." It is thus possible to obtain extremely thin layers of radioactive copper on a variety of surfaces, including copper itself.

The procedure consists of irradiating overnight 90 grams of zinc dust with a radon-beryllium source (300 to 600 millicuries) of neutrons. The zinc is then treated with concentrated hydrochloric acid until all but five grams have dissolved, which undissolved part carries practically all the activity.[2] This is next dissolved in hydrochloric acid; 30 to 40 cc of concentrated sulphuric acid are added, and the mixture evaporated until fumes of SO_3 are given off. It is then diluted to 400 cc and filtered. This solution is then electrolyzed with the use of a rapidly rotating disk cathode of copper, platinum or other metal, of 3 cm diameter, 0.25 mm thickness. With a platinum anode, under these conditions, satisfactory operation was obtained with currents of 10 to 18 milliamperes and voltages ranging from 2.1 to 2.7 volts. The optimum speed of rotation of the cathode was about 4500 r.p.m.

Activities of various disks, sulphide precipitates, etc., were measured with a thin silvered-wall Geiger counter or with a pressure ion chamber electrometer system.

The following preliminary results are reported:

(a) The amount of radioactive copper ion deposited is approximately a linear function of the duration of the electrolysis in the initial period up to 30 minutes.

(b) The effect of the stirring rate on the removal of activity is such that there is a maximum between 2300 and 5000 r.p.m. The speeds tested ranged from 2300 to 12,000 r.p.m.

(c) The efficiency of cathode materials in the removal of radioactive copper decreased in the order: copper, molybdenum, platinum, tungsten, tantalum.

(d) It is estimated that a copper disk, running for 45 minutes, at 4500 r.p.m., 11 milliamperes and 2.1 volts, removed at least 50 percent of the activity in solution. The estimate is based upon a comparison of the activity of an aliquot of solution before electrolysis as CuS, and of the activity of the solution after electrolysis as CuS.

(e) The high speed rotating cathode gives very sharp separations. When a current of 10 to 11 milliamperes was used, it was found that the appearance of the disk after electrolysis was unchanged, and retained its mirrored finish, with no evidence of the deposition of other elements. At higher currents the appearance of the disks after electrolysis indicated that some impurities had plated out as well. They then presented a somewhat darkened appearance, although still retaining the mirrored surface which had been imparted to them by buffing.

This method permits a much higher concentration ratio of active to inactive isotope to be achieved than under ordinary conditions, since it eliminates the need for the addition of the inactive isotope to active solutions. It should be applicable to a large number of elements. It can facilitate the study of various diffusion and exchange phenomena and any researches which require high concentration and purity of the radioactive indicator.

The support of the Research Corporation in this work is gratefully acknowledged. I am also deeply indebted to Professors G. B. Pegram and J. R. Dunning of the physics department, and to Professor L. P. Hammett of the chemistry department for continued aid and guidance throughout the course of this research.

JOSEPH STEIGMAN

Departments of Physics and Chemistry,
Columbia University,
New York, N. Y.,
April 14, 1938.

* Publication assisted by the Ernest Kempton Adams Fund for Physical Research of Columbia University.

[1] Fermi, Amaldi *et al*, Proc. Roy. Soc. **A146**, 492 (1934).
[2] Haissinsky, Nature **136**, 141 (1935).
[3] Fink and Rohrman, Trans. Am. Electrochem. Soc. **58**, p. 403.
[4] Dunning and Pegram, Phys. Rev. **47**, 325 (1935).